DEVELOPMENT OF $Ti_3C_2T_x$ NANO MATERIAL AND ITS APPLICATION IN WASTEWATER REMEDIATION

THESIS SUBMITTED TO
JADAVPUR UNIVERSITY
FOR THE FULFILLMENT OF MASTER OF TECHNOLOGY IN
SCHOOL OF MATERIALS SCIENCE AND NANO TECHNOLOGY

Submitted by

Soumyadeep Garai

Registration No. 163810 of 2022-23

Roll. No. 002230701005

Under the guidance of

Prof. (Dr.) Kalyan Kumar Chattopadhyay

Department of Physics &

School of Materials Science and Nanotechnology Jadavpur University

Jadavpur University

88, Raja Subodh Chandra Mallick Rd, Jadavpur,

Kolkata, West Bengal 700032.

CERTIFICATE OF RECOMMENDATION

This is to clarify that the thesis entitled **"**Development of $Ti_3C_2T_x$ nano material and its application in Wastewater remediation'' is a bonafide work carried out by Soumyadeep Garai under our supervision and guidance for partial fulfilment of the requirement of Master of Technology (Nano Science and Technology) in School of Materials Science and Nano Technology, during the academic session 2022-2024.

SUPERVISOR
Prof. (Dr.) Kalyan Kumar Chattopadhyay
Department of Physics
Jadavpur University, Kolkata-700032

DIRECTOR
Dr. Mahua Ghosh Chaudhuri
School of Materials Science and Nanotechnology Jadavpur University, Kolkata-700032

DEAN
Faculty Council of Interdisciplinary Studies,
Law and Management (FISLM)
Jadavpur University, Kolkata-700032

CERTIFICATE OF APPROVAL

This forgoing thesis is hereby approved as a credible study of an engineering subject carried out and presented in a manner satisfactorily to warranty its acceptance as a prerequisite to the degree for which it has been submitted. It is understood that by this approval the undersigned do not endorse or approve any statement made or opinion expressed or conclusion drawn therein but approve the thesis only for purpose for which it has been submitted

_ _ _ _ _ _ _ _ _ _ _ _ _ _ _ _ _ _

_ _ _ _ _ _ _ _ _ _ _ _ _ _ _ _ _ _

Committee of final examination for evaluation of thesis

_ _ _ _ _ _ _ _ _ _ _ _ _ _ _ _ _ _

Contents

Sl. No.	Chapters	Page No.
1.	Certificate of Recommendation	2
2.	Certificate of Approval	3
3.	Acknowledgement	6
4.	List of Figures	7-12
5.	Abbreviation List	13-16
6.	Preface	17
7.	Introduction	18-22
8.	Literature Survey	23-63
	1. Introduction	24-26
	2. Structure, properties and synthesis of MXene	26-28
	3. Mass transfer of MXene-based materials and separation mechanism	28-32
	4. MXene based materials for water pollutant removal	32-45
	5. Adsorption mechanisms (dye, heavy metal, and pharmaceuticals)	45-50
	6. Factors affecting MXene efficiency for waste water treatment	50-53
	7. Environmental influence and toxicity	53-54
	8. MXene-based adsorbents regeneration evaluation	54-56
	9. Challenges and future prospects	56-60
	10. Practical applications of MXene-based membranes	60-62
	11. Conclusion	62-63
9	Objective and Scope	64-65
10.	Characterization Tools	66-75
	1. X-Ray Diffraction (XRD)	67-68
	2. Scanning Electron Microscopy	68-69
	3. Field emission scanning electron microscope (FESEM)	70-72
	4. Ultraviolet-Visible Spectroscopy (UV-Vis)	72-74
	5. High-resolution transmission electron microscope (HRTEM)	74-75

11.	Methodology	76-79
12.	Results and Observation	80-86
13.	Future Scope	87-89
14.	References	90-108

Acknowledgement

I would like to begin by acknowledging how this project has helped me in understanding the various processes and analyses that are involved in the development of $Ti_3C_2T_x$ nano materials and its application in wastewater remediation. The ideas, learnings and researches involved were backed by several people's collective efforts without whom this project would not have been possible.

I would like to extend my gratitude and thanks to Prof. Kalyan Kumar Chattopadhyay for allowing me to work under his humbled guidance and provide me with an opportunity worth remembering.

My gratitude and thanks extends to my senior colleagues, Miss Dimitra Das and Miss Nabanita Sen, who have intrinsically played a huge role in guiding as well as directing my course of action throughout the project.

I thank Dr. Mahua Ghosh Chaudhuri, Director of School of Material Science and Nano Technology, Jadavpur University, to provide me with this opportunity to do this project.

Lastly, I would like to thank my dear family members and well-wisher who helped by providing me with the required workspace and environment and constantly inspired me to thrive for the better.

List of Figures

Sl. No.	Figures	Page No.
1.	Achievement of MXene development.	26
2.	(a) Different structure of MXene (b)MXene synthesis (c) Classification of MXene (d) diverse properties of MXene	27
3.	(a) MXene membrane of varying thickness showing rate of water permeation and rejection, (b) MXene membrane of varying lateral size showing rate of water permeation and rejection.	28
4.	(a) Computational simulations depict preferred sites for water adsorption on MXene nanosheets, presented from both side and top views. (b) Recorded data showcases adsorption energies with and without negative charge on the MXene surface. (c, d) Analysis of noncovalent interactions assesses the bonding between MXene and water molecules, considering the presence or absence of charge. (e) Finite Element Method (FEM) measurements employ a 3D model comprising three MXene layers, with and without defects, denoted by '0' for no defects and '1' for one defect. (f) Illustration depicts velocity profiles of water flow within MXene slits with various defect configurations (0 0 0, 1 0 0, 0 1 0). (g) Water flow velocity is compared across different outlet lengths for varying defect formations, with inset images showing detailed velocity profiles near the outlet. (h, i) Snapshots of the system at the initial (t = 0 ps) and final stage (t = 500 ps), along with corresponding trends in Mean Squared Displacement (MSD) for both lubricating oil and water molecules over simulation time.	31
5.	(a) Procedure for synthesizing a composite of MoS_2 and 2D-MXene ($Ti_3C_2T_x$). (b) Scanning Electron Microscopy (SEM) images showing $Ti_3C_2T_x$ (left: scale bar = 5 μm), MoS_2/MX-I composite (middle: scale bar = 2 μm; right: enlarged view). (c) SEM image of the MoS_2/MX-II nanocomposite; scale bar = 2 μm. (d) Evaluation of adsorption kinetics for the MoS_2/MX-II composite for $Hg2^+$ removal. (e) Analysis of $Hg2^+$ adsorption onto MoS2/MX-II using the	34

	Langmuir adsorption fitting model. (f) Detailed procedure for 35synthesizing COOH− $Ti_3C_2T_x$. (g) Transmission Electron Microscopy (TEM) images showing $Ti_3C_2T_x$ (left) and COOH–$Ti_3C_2T_x$ sheets (right). (h) Percentage of mercury removal values for pristine MXene and COOH-MXene. (i) Mechanism of mercury ion adsorption over COOH– $Ti_3C_2T_x$.	
6.	(a) SEM images display the morphology of synthesized Ti_3AlC_2. (b) TEM images exhibit the morphology of monolayer $Ti_3C_2T_x$ at 100 nm, with an inset showing an SEM image of the same sample at 5 µm, along with corresponding AFM images and height scale. (e) Graph depicting adsorption capacity over time for the prepared sample at various concentrations, with an inset showing the time-dependent efficiency of Cr (VI) removal. A real photo confirms efficient Cr (VI) removal in approximately 10 minutes. (f) Schematic representation illustrating the mechanism of Cr (VI) adsorption on the monolayer $Ti_3C_2T_x$ surface. (g) Schematic diagram presenting the synthetic method for the hierarchical heterostructure of MXene/$ZnIn_2S_4$. (h) Evaluation of photocatalytic performance, (i) determination of 1st order kinetics, and (j) calculation of rate constants for Cr (VI) degradation of individual materials and heterostructures prepared at different percentages of MXene. (k) Illustration demonstrating the visible light illuminated photocatalytic mechanism for the prepared MXene/ZnIn2S_4 heterostructure.	36
7.	(a) Schematic depiction illustrating the utilization of $Ti_3C_2T_x$ MXene for the removal of methylene blue (MB) from wastewater. (b) Schematic view presenting TiO_2/ Ti_3C_2 heterostructures employed for the removal of Rhodamine B (RhB) from aqueous solutions. (c) Procedure for synthesizing self-assembled CTAB/MXene/BAC (CMAC) heterostructure. (d) SEM image displaying the morphology of BAC; scale bar = 5 µm. (e) SEM image displaying the morphology of MXene; scale bar = 1 µm. (f) SEM image displaying the morphology of CMAC; scale bar = 1 µm. (g-i) Kinetic study presenting experimental data for various dyes (AR, CR, SY) fitted	39

	using Pseudo-first order and pseudo-second order models. 40(j-l) Kinetic study displaying experimental data for various dyes (AR, CR, SY) fitted using the intraparticle diffusion model.	
8.	(a) Illustrative scheme depicting the membrane utilized for the dye removal process. (b) SEM image displaying the morphology of MXene, with a scale bar of 10 µm, and (c) an enlarged view of MXene with a scale bar of 1 µm. (d) SEM image showing the morphology of a pure nylon membrane, with a scale bar of 10 µm, and (e) an enlarged view of the pure nylon membrane with a scale bar of 1 µm. (f) SEM image displaying the morphology of a pure MXene membrane (sample: RPM-10). (g) SEM image showing the morphology of a pure GO membrane (sample: RPM-0). (h) SEM image displaying the morphology of a composite membrane (sample: RPM-8), and (i) an enlarged view of the RPM-8 membrane. (j) UV-Vis absorption data for MB dye before and after interaction with the composite membrane. (k) Values indicating the flux and interception of MB dye through the composite membrane. (l) UV-Vis absorption data for MB dye for six cycles using sample RPM-8. (m) Values indicating the flux and interception of MB dye through sample RPM-8 for six cycles. Column chart representation showing the flux and rejection rate of (n) Methyl Red, (o) Methyl orange, (p) Congo red, and (q) Evans blue.	41
9.	(a) Diagram illustrating the synthetic procedure for Au nanoparticle-decorated GCN/MXene (AGM) nanosheets. (b, c) SEM images depicting graphitic carbon nitride (GCN). (d, e) SEM images showing Au nanoparticles (NPs) decorated on GCN. (f, g) SEM images displaying Ti_3C_2 MXene. (h, i) SEM images revealing AGM03, which denotes Au NP GCN/MXene with 3 wt% of MXene. (j) Energy Dispersive X-ray (EDX) spectrum of $AGM0_3$ photocatalyst. (k, l) Results displaying the kinetic curve of cefixime decomposition. (m) Column bar chart illustrating the degradation rate (%) of all catalysts under visible light. (n) Column bar chart showing the rate constants of all catalysts under visible light. (o) Visual	45

	representation outlining the mechanism of photocatalytic degradation of cefixime using AGM nanocomposites under visible light irradiation.	
10.	(a) Illustrative diagram presenting the proposed mechanism for photocatalysis of Methyl Orange (MO) on a Ti_3C_2-TiO_2 heterostructure. (b) Step-by-step demonstration depicting the removal of Chromium (VI) using a Ti_3C_2/TiO_2 composite. (c) The adsorption mechanism of alkali-metal-intercalated MXene/LDH onto nickel under weak acidic conditions involves hydrolysis or exchange with sodium ions. Under weak alkaline conditions, it involves hydrolysis or exchange with sodium ions. Under strong alkaline conditions, the mechanism is characterized by direct precipitation. (d) Illustration demonstrating the adsorption of mercury chloride and mercury nitrate over the MXene surface.	47
11.	(a) Information regarding adsorption energy and adsorption percentage for cloxacillin interacting with MXenes. (b) A standard photocatalytic degradation mechanism of pharmaceuticals using MXene composite materials.	49
12.	(a) Data illustrating the adsorption of Methylene Blue (MB) on MXene@Fe_3O_4 composite with varying pH values.(b) Measurement of zeta potential for MXene@Fe_3O_4 composite at different pH values.Theoretical representations of:(c) The molecular structure of MB dye.(d) Hydrogen bonding between MXene and MB. (e) Electrostatic interaction between MXene and MB, with elements denoted by colors: S (yellow), N (blue), O (red), H (white), C (gray), and Ti (light gray).	52
13.	The mechanism of adsorption and regeneration of CPX using an SI-$Ti_3C_2T_x$ composite.	56
14.	(a) Diagram illustrating the synthesis of MXene.(b) Scheme demonstrating shelf-stable $Ti_3C_2T_x$ dispersed in water and antioxidant Sodium L-Ascorbate.(c, d) Real samples dispersed in water and NaAsc at fresh and after 21 days.(e) Corresponding SEM image of $Ti_3C_2T_x$ nanosheets stored for 21 days in 1 mg/mL NaAsc	59

	solution, displaying stable MXene nanosheet morphology.(f) SEM image of $Ti_3C_2T_x$ nanosheets stored for 21 days in DI water, showing dense and amorphous morphology of MXene nanosheets.(g) Graph depicting conductivity versus time, where improved conductivity for MXene treated with antioxidant is attributed to oxidation prevention.(h) Molecular dynamic simulation for prepared MXene in water.(i) Molecular dynamic simulation for prepared MXene in antioxidant. The attached groups of L-Ascorbate prevent further reaction among water and MXene nanosheets.	
15.	(a) Schematic diagram depicting the synthesis of an MXene h-$Ti_3C_2T_x$ membrane.(b) Scheme illustrating the filtration of microplastics (MPs).(c, d) Images captured from fluorescence microscopy before and after the filtration of wastewater.(e) Real photograph of the filtration setup utilized for wastewater treatment.(f-h) Initial photographs obtained using an optical microscope before the removal process.(i-k) Final photographs acquired using an optical microscope after the removal process, i.e., filtered wastewater (scale bar = 10 μm).	61
16.	(a) Schematic depiction of Bragg's law, (b) digital image of the experimental set-up of an XRD instrument.	67
17.	(a) Schematic depiction of working principle of FESEM, (b) digital image of the experimental set-up of an FESEM instrument.	70
18.	(a) Schematic depiction of working principle of UV-Vis, (b) digital image of the experimental set-up of an UV-Vis instrument.	72
19.	(a) Schematic depiction of working principle of HRTEM, (b) digital image of the experimental set-up of an HRTEM instrument.	75
20	(a) The schematic diagram for synthesis of $Ti_3C_2T_x$ MXene nano particles. From reference [192]. (b) SEM image of $Ti_3C_2T_x$ MXene nano particles (c) XRD spectra of $Ti_3C_2T_x$ MXene nano particles.	78
21.	Absorption spectra of pure 4-NP solution without $NaBH_4$ addition, absorption after addition of $NaBH_4$ in 4-NP solution, and absorption spectra of 4-aminophenol; digital images showing the gradual	81

	transformation of 4-NP to 4-AP in presence of $Ti_3C_2T_x$ MXene catalyst and $NaBH_4$.	
22.	Absorbance spectra of 4-Nitro phenol and $NaBH_4$ in absence of catalyst over a time of 20 minutes.	82
23.	Absorbance spectra of mixture of 4-Nitro phenol and $NaBH_4$ in presence of different dose of catalyst after a time of 5 minutes.	83
24.	Absorbance spectra of mixture of 4-Nitro phenol and $NaBH_4$ in constant concentration Ti_3C_2 of 2 mg.	84
25.	The catalytic activity of freshly prepared $Ti_3C_2T_x$ MXene was evaluated for its ability to degrade 4-Nitrophenol (4-NP) over four consecutive cycles. The efficiency of 4-NP degradation was assessed after each cycle to determine the stability and effectiveness of the $Ti_3C_2T_x$ catalyst over multiple cycles.	85
26.	The catalytic activity of $Ti_3C_2T_x$ prepared 60 days prior was assessed for its ability to degrade 4-Nitrophenol (4-NP) over four cycles. The efficiency of 4-NP degradation was evaluated after each cycle to determine the stability and effectiveness of the $Ti_3C_2T_x$ catalyst over time.	86

Abbreviation List

2,4-DNP = 2,4-Dinitrophenol

AOP = Advanced Oxidation Process

AP = Aminophenol

CB = Conduction Band

CBM = Conduction Band Minima

Cr(III) = Trivalent Chromium

Cr(VI) = Hexavalent Chromium

CsI = Caesium Iodide

CTF = Covalent Triazine Frameworks

CV = Crystal Violet

CVD = Chemical Vapour

Deposition

DFT = Density

Functional Theory

DI = Deionized

DMF =

Dimethylformamide

DRS = Diffuse

Reflectance Spectroscopy

EDS = Energy-Dispersive

X-ray Spectroscopy

EDTA = Ethylenediaminetetraacetic Acid Disodium Salt Dehydrate

EF = Fermi Energy Level

ELF = Electron

Localization Function

FA = Formic Acid

SEM= Scanning Electron Microscope

FESEM = Field Emission Scanning Electron Microscope

Fig. = Figure

FTIR = Fourier-Transform Infrared

GCN = Graphitic Carbon Nitride

GCNB = Bulk GCN

GCNX = Exfoliated GCN

GGA = Generalized Gradient Approximation

GPa = Giga Pascal

h = hour

HC = High Concentration

Hg(II)/$Hg2^{+}$= Mercury(II) cation

HOMO = Highest Occupied Molecular Orbital

HRTEM = High Resolution Transmission Electron Microscope

HSAB = Hard Soft Acid Base

ICDD = International Centre for Diffraction Data

IPA= Isopropyl Alcohol

IR = Infrared

JCPDS = Joint Committee on Powder Diffraction Standards

KBr = Potassium Bromide

LC = Low Concentration

LD/LOD = Limit of Detection

LMB = Leucomethylene Blue

LUMO = Lowest Unoccupied Molecular Orbital

M = Molar

M.W. = Molecular Weigh

MB = Methylene Blue

MG = Malachite Green

mg = milligram

mg/L = milligram/Litre

min = minute

mM = millimolar

MO = Methyl Orange

MPa = Mega Pascal

MR = Methyl Red

NHE = Normal Hydrogen Electrode

nm = nanometer

nM = nanomolar

NMP = N-Methyl-2-Pyrrolidone

NMR = Nuclear Magnetic Resonance

NNI = National Nanotechnology Initiative

NO = Nitric Oxide

NP = Nitrophenol

OA = Oxalic Acid

PAW = Projector Augmented Wave

PBE = Perdew–Burke–Ernzerhof

PDOS = Projected Density of States

PL = Photoluminescence Spectroscopy

PMMA = Poly(methyl methacrylate)

ppb = parts per billion

ppm = parts per million

RB = Rose Bengal

RhB = Rhodamine B

ROS = Reactive Oxygen Species

rpm = Revolutions per minute

RSM = Response Surface Methodology

s/sec = second

TA = Terephthalic Acid

TC = Tetracycline

TDOS = Total Density of States

Ti_3C_2 = Titanium Carbide

Ti_3AlC_2 = Titanium Aluminium Carbide

TGA = Thermogravimetric Analysis

UV = Ultraviolet

VASP = Vienna ab-initio Simulation Package

VB = Valence Band

VBM = Valence Band Maxima

Vis = Visible

WHO = World Health Organization

XPS = X-ray Photoelectron Spectroscopy

XRD = X-Ray Diffraction

$ZnCl_2$ = Zinc Chloride

ZnO = Zinc Oxide

Preface

The relentless pursuit of sustainable solutions to environmental challenges has led scientists and engineers to explore innovative materials and technologies. Among these, the development of $Ti_3C_2T_x$ MXene nanomaterials stands out as a promising avenue for addressing one of the most pressing issues of our time – wastewater pollution.

In this thesis, we delve into the fascinating realm of $Ti_3C_2T_x$ MXene nanomaterials and their transformative potential in wastewater remediation. With an interdisciplinary approach, we navigate through the intricacies of material synthesis, characterization, and application, offering a comprehensive understanding of their role in mitigating water pollution.

The journey begins with an exploration of the fundamental principles underlying the synthesis of $Ti_3C_2T_x$ MXene nanomaterials, unravelling the intricate mechanisms that govern their formation and properties. Through meticulous experimentation and analysis, researchers have harnessed the power of advanced techniques to tailor the structure and composition of these nanomaterials, unlocking their full potential for environmental applications.

As we venture further, we uncover the diverse array of applications where $Ti_3C_2T_x$ MXene nanomaterials shine brightest, with a particular focus on wastewater remediation. From adsorption to catalytic degradation, these nanomaterials exhibit remarkable efficacy in removing contaminants and purifying water, offering a beacon of hope in the quest for clean and safe drinking water worldwide.

However, this journey is not without its challenges and complexities. We confront the limitations and obstacles that must be overcome to realize the full-scale implementation of $Ti_3C_2T_x$ MXene nanomaterials in wastewater treatment plants. From scalability issues to environmental implications, we confront these hurdles head-on, paving the way for future advancements and innovations in the field.

The aim is to provide readers with a comprehensive overview of the latest developments and breakthroughs in the realm of $Ti_3C_2T_x$ MXene nanomaterials for wastewater remediation.

Let us embark on this journey together, as we explore the boundless potential of $Ti_3C_2T_x$ MXene nanomaterials to transform the landscape of wastewater remediation and pave the way towards a cleaner, healthier planet.

Introduction

Environmental scientists and engineers have a critical responsibility to ensure safe and clean water for the community by continually exploring new and appropriate technologies, as well as upgrading existing processes with cost-effectiveness. The goal is to provide water that is free from harmful contaminants such as toxic metals, organic pollutants and disease-causing organisms. For over 100 years, researchers have been working together through interdisciplinary approaches, using experiments and software tools combined with the application of technology, materials development, statistical modelling and process modifications, and knowledge of advanced levels of physics, chemistry, biology, and engineering. Various novel materials with the uptake of various pollutants that are usually unable to be removed by traditional processes are currently being used in water pollution modification fields. In order to achieve this, the use of nano-materials and their applications are now being widely discussed in various literature [1].

The term ‘nanotechnology’ has captured the world’s attention in recent years. This relatively new field of science has captivated scientists from around the world, to the point where it has been described as a ‘revolution in modern science’ and technology.

As defined by the NNI, nanotechnology involves the manipulation and engineering of nano-scale materials to modify their properties. Nano-scale materials have dimensions in the range of 1 to 100 nm [2], and at such small scales, they exhibit unique properties. These properties allow for novel applications in a wide range of scientific and technological fields.

The fundamental principles of nanoscience and nanotechnologies are at the core of this interdisciplinary field of science, which brings together scientists in the fields of materials science, physics, chemistry, biology, computer science, mechanical engineering, electrical engineering, and environmental engineering to modulate molecular properties at the nano-scale for contributions in their respective fields.

A nanomaterial is a material that can exist naturally or can be made from different precursors by different methods in research laboratories. There are two main synthesis methods: top-down and bottom-up. Top-down methods involve breaking down bulk materials into nano-dimensional materials step by step. Bottom-up methods involve rearranging and assembling atoms or molecules to form nano-structures. Compared to top-down methods, bottom-up materials have ordered structures, fewer defects, and are homogeneous in chemical composition. Nano-materials have very interesting optical, electrical, electronic, and quantum, as well as mechanical and magnetic properties. They also have some unique characteristics

compared to bulk equivalents. These characteristics include their large surface to volume ratio and the high proportion of surface atoms/molecules, their interesting scattering properties, the size and shape that determine their physiochemical properties, and their unique electronic band structure due to confined energy states. Surface-driving forces play a significant role in the modulation of their characteristics [3].

The tremendous potential of nanotechnology has led to its revolutionary applications in many areas of the contemporary world. Today, nanomaterial's applications are rapidly expanding in fields such as: medical science and health, environmental management, building and construction engineering, textile engineering, pharmaceutical industry, battery and fuel cells, flexible electronics, information and communication technology [4].

Nanomaterials researchers and technologists worldwide are constantly working to make the use of nano-materials more cost-effective and practical in various applications. Industries face several challenges in removing pollutants from the environment, some of which are listed below:

- A large number of pollutants are produced by industries. Clearing these pollutants requires a large amount of effort, manpower, profits and resources. Different pollutants have different chemical and physical properties, so different techniques are needed to remove them from the environment.
- Some pollutants require more complex treatment than others. The treatment and removal of these complex pollutants requires advanced techniques and instrumentation, which are costly to operate for small scale industries.
- For this reason, many industries are hesitant to use pollution control technologies due to economic considerations.
- Some pollution control techniques also produce secondary pollutants, which further contaminate natural resources and cause negative environmental impacts.
- The current state of environmental pollution is aggravated by the rapid growth of the pharmaceutical and textile industry, which not only threatens the aquatic ecosystem, but also threatens human health.

Bulk materials used to attenuate pollutants have several drawbacks that limit their effectiveness. In addition, traditional wastewater remediation methodologies have several drawbacks in terms of cost, treatment time, and competence. Mentioned below are some of the limitations of conventional bulk materials:

- Requirement of large amount of material for application
- Fewer surface-active sites for bulk materials
- Sludge generation and management problems
- High cost due to large requirements of material and costly processes
- Low removal efficiency of target pollutants
- It must be regenerated regularly and can't be recycled
- Material leaching into treated water can lead to secondary contamination
- Poor selectivity for target pollutants

From the above perspective, the need for nanotechnology using nanomaterials becomes clear in today's world. The disadvantages of conventional materials and methodologies have prompted the need for the search for nanomaterials that can effectively remove all types of pollutants from the water and wastewater environments [5].

There are several advantages of using nano materials for pollution control in industrial settings. Below are some of the key advantages:

- Efficiency: Nano materials have a higher surface area to volume ratio than bulk materials. This higher surface area, with abundant reactive sites, makes them more efficient at the capture of pollutants.
- Versatility: Nano materials can be tailored to specific pollutants, making them more suitable for environmental remediation than traditional pollution control technologies.
- Selectivity: Nano materials with high selectivity towards specific pollutants can additionally help in the efficient removal of pollutants.
- Lower cost: While the initial cost of nano materials may be high due to their synthetic strategies, their increased efficiency means less material is required during applications, resulting in a lower overall cost for pollution control.
- Environmental benefits: Nanomaterials are biodegradable and environmentally friendly, reducing the environmental impact of pollution control technologies.
- Improved safety: Unlike traditional pollution control materials, nanomaterials are less toxic, reducing the risk of injury to workers and to the environment.
- Recyclable properties: These materials can be recycled several times during catalytic activity for the decomposition of pollutants, and they do not lose efficiency after repeated use. This lowers the costs of materials and the treatment process.

Nano adsorbents or nano catalysts are specially designed nano-materials used to effectively treat industrial wastewater to remove harmful pollutants from water-bodies [6]. These nanomaterials are highly efficient in degrading pollutants to non-toxic end products, and in completely removing these pollutants from the water-body [7]. Compared to conventional bulk materials, the high efficiency of these nanomaterials is due to their large surface area and the large number of surface-active sites [8]. The common limitations of conventional bulk materials can be eliminated by selecting the right nanomaterial for practical implementation. The economic factors to consider include feasible synthesis process, large yield, abundant raw precursors and most importantly, non-toxic nature so as not to cause further contamination. Sustainable technologies using inexpensive and readily available materials should be employed instead of relying on costly and scarce resources [9].

Industrialization has resulted in a rapid and steady increase in environmental pollution. This has led to the development of materials that are highly effective in the fight against hazardous pollutants. These materials are MXenes, which come in the form of transition metal nitrate, carbide or carbonitride. MXenes have excellent conductivity, hydrating properties, structural stability and flexible surface chemistry, making them ideal candidates for water purification and clean environment applications [10].

In particular, MXenes have remarkable absorption properties and efficient reduction performances in the treatment of a wide variety of wastewater pollutants. In order to fully understand the mechanisms of the nano absorption of MXenes and their effectiveness in the removal of various pollutants from the water, it is necessary to have a thorough understanding of the elimination method using the specific physicochemical characteristics of the various contaminants.

Literature Survey

1. **Introduction**

The release of poorly treated wastewater into our aquatic realms wreaks havoc on ecosystems, inflicting severe harm on the living organisms within it [11]. Wastewater, a concoction of diverse contaminants, exhibits great variability in its composition, encompassing organic dyes, heavy metals, pesticides; aromatic rings like benzene and bisphenol A, volatile compounds, plastics, halogen-based substances, pharmaceuticals, and microorganisms [12-20]. It is thought-provoking that certain complex carbon-based pollutants, despite their toxicity, can be transformed into harmless forms through microbial action or catalytic processes [21-23]. The impact of these contaminants on the environment and biological systems hinges on their toxicity levels and their propensity for bioaccumulation [24, 25]. Therefore, developing and implementing robust treatment methods to eradicate these pollutants is crucial for ensuring an unpolluted environment.

A myriad of technological strategies is under investigation for wastewater treatment, including ion exchange, co-precipitation, adsorption, filtration, chemical oxidation, biological methods, and porous membrane separation. Advanced oxidation processes (AOPs) like ozonolysis [26], electrochemical oxidation [27], light-driven reactions and radiolysis [28], as well as the photo-Fenton [29] reaction, photocatalysis [30] and photochemical oxidation [31, 32], are gaining prominence for their potential large-scale industrial applications. Many of these processes are enhanced by adsorption using materials like biochar [33], activated carbon [34, 35], or innovative nanostructures [36]. Adsorption is widely favoured due to its efficiency in removing contaminants at minute concentrations, selective targeting, the possibility of regenerating adsorbents, and the availability of cost-effective adsorbents [37, 38]. Recent advancements in this field have focused on creating novel adsorbent materials.

Nanomaterials are increasingly recognized for their significant potential in water purification due to their exceptional physicochemical properties [39, 40]. MXenes, a family of two-dimensional transition metal carbides, nitrides, or carbonitrides, stand out as promising candidates for environmental remediation, sensing, catalysis, and energy storage [41]. MXenes boast unique attributes, such as simplistic functionalization, existence of active sites, biocompatibility, high porosity, hydrophilicity, substantial interlayer spacing, chemical stability, and impressive

adsorption-reduction capacity [42-44]. These characteristics make MXenes ideal for water treatment, enabling them to adsorb various contaminants through membrane formation and act as photocatalysts to detrimental pollutants [45-47]. Typically denoted by the formula $M_{n+1}X_nT_x$, where M represents a transition metal like titanium (Ti), molybdenum (Mo), scandium (Sc), tungsten (W), vanadium (V), or zirconium (Zr); 'X' signifies carbon or nitrogen; 'T' indicates surface termination groups like chlorine (–Cl), fluorine (–F), oxygen (–O), or hydroxyl (–OH); with 'n' ranging from 1 to 4[48].

The exploration of MXenes in wastewater treatment prompts several critical questions. The vital, most central, of these inquiries is understanding how MXenes can effectively adsorb different types of contaminants [49]. Equally important point is evaluating the cost-effectiveness and scalability of MXene synthesis for large-scale applications, enhancing selectivity for specific contaminants, and assessing the stability and durability of MXene materials in real-world conditions. Furthermore, integrating MXenes into membrane technologies and understanding their environmental impacts are vital areas of study. Other crucial considerations include the energy efficiency of MXene-based electrochemical processes and navigating the regulatory surrounding environment [50, 51]. Addressing these questions will be key to unlocking MXenes' potential to provide long-lasting, cost-effective solutions to water contamination challenges.

Despite the limited number of review articles on MXene-derived composites in water treatment [42, 52-57], there is a pressing need for a comprehensive and systematic evaluation of the chemical properties of various pollutants and their interactions with different MXene nanomaterials. This review endeavours to fill that gap, providing a thorough and current assessment of existing studies in this rapidly advancing field. Initially, it offers a concise overview of common techniques for designing MXene-based materials and their features [Fig. 1]. Subsequently, it delves into the application of MXenes and MXene-based composites in adsorbing heavy metal ions, dyes, and pharmaceuticals, and discusses the photocatalytic degradation of organic compounds. The review also addresses the toxicity of MXenes, their potential environmental contamination issues, and future prospects. This study underscores the critical importance of exploring MXene nanoparticles' burgeoning applications in environmental management, shaping future policies for water pollution mitigation, and

guiding the development of MXene-derived products for effective environmental remediation.

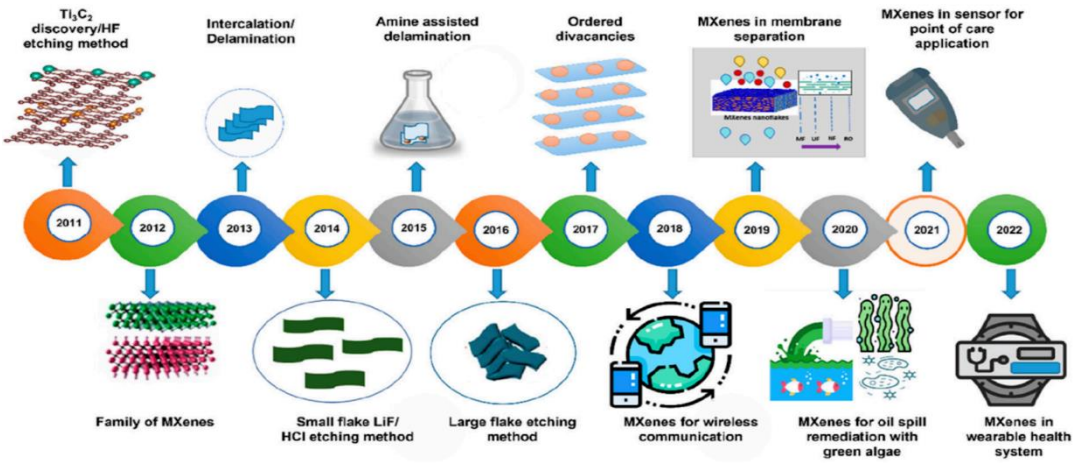


Figure 1. Achievement of MXene development. From reference [58].

2. Structure, properties and synthesis of MXene

Liable to the diverse potential applications of MXenes, advancing this field necessitates refining their intrinsic compositional characteristics. The properties of the final MXene product are influenced by several factors, including the starting MAX phase material, reaction time, etchant type, and temperature, all of which are determined during the synthesis process. However, controlling these parameters to achieve MXenes with the desired properties remains a significant challenge [59]. MXenes come in various types, including “conventional” MXenes, “o-MXenes”, and “i-MXenes” [60]. Typically, MXenes are synthesized through selective etching in suitable solvents or solutions, most commonly acidic ones [61]. This etching process creates surface terminations and introduces functional groups that are crucial for future applications [62]. MXenes have garnered interest in fields such as environmental pollutant remediation [63], energy storage [64], medicine [65], and diagnostics [66] due to their remarkable adsorption, optical, mechanical, and electrical properties[67].

Structurally, MXenes are composed of (n + 1) layers of transition metal "M" stacked on n sheets of X. Verified MXene formulas include M_2X, M_4X_3, and M_3X_2. The general formula for MXenes is $M_{n+1}X_nT_x$ [68], where M represents a group III or IV element (e.g., Nb, Cr, V, Ti), X can be either nitrogen or carbon, T denotes surface terminal groups (e.g., –F, –OH, –O), and n ranges from 1 to 3[69-71]. Parihar et al. [66], conducted an in-depth study of MXene's structure [Fig. 2(a)], demonstrating that intercalation of multilayer MXenes can yield exfoliable and delaminatable intercalated MXenes by removing "A" components from the MAX phase [Fig. 2(b)]. Recent research has exploited all dimensionalities of MXenes (0D, 1D, 2D, and 3D) [Fig. 2(c, d)] for various applications.

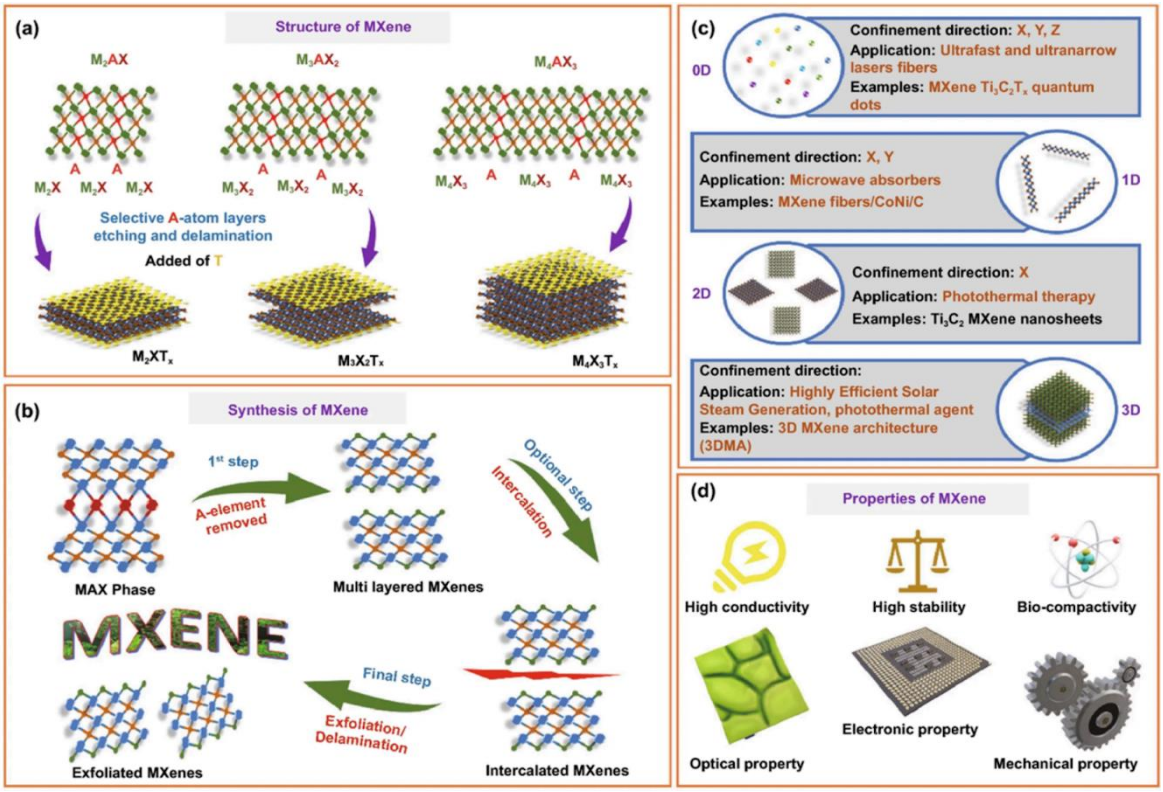


Figure 2. (a) Different structure of MXene (b)MXene synthesis (c)Classification of MXene (d) diverse properties of MXene, From reference [68].

While incorporating in environmental applications, the specific surface area (SSA) of MXenes is critical, necessitating stringent quality control. Recently, there has been significant progress in refining synthesis methods for high-quality nanomaterials. MXenes can be contrived using two primary approaches: top-down and bottom-up methods. Both single-layer and multilayer MXene nanostructures have been

successfully produced using these techniques [72]. The top-down method involves mechanical and chemical exfoliation, enabling direct exfoliation from bulk material [73]. Liquid phase exfoliation is a conventional and effective technique for creating MXenes at the nanoscale [74]. The synthesis process involves two main steps: first, converting the precursor MAX phase into 2D nanoscale MXene by selectively etching one "A" element from the MAX phase, known as delamination. Hydrofluoric acid (HF) is commonly used to etch bulk MAX to obtain stacked multilayer MXene. The second step involves the breakdown of organic molecular interactions through sonication to achieve single-layered MXene. For instance, Naguib et al. [75], Kotasthane et al. [76], and Mashtalir et al. [77] described the formation of MXene nanosheets in Ti_3AlC_2 through HF acid etching of Al layers, followed by liquid phase exfoliation in N-methyl pyrrolidone, resulting in delaminated Ti_3C_2 MXene 2D nanosheets [68]. The bottom-up synthesis approach involves assembling individual atoms to create 2D nanomaterials. Techniques for synthesizing MXenes include chemical vapor deposition (CVD)[79], sputtering MAX films onto sapphire supports[80], and ammonisation of MXenes at elevated temperatures[81]. Several experimental factors, such as temperature, particle size of MAX, etching duration, and HF concentration, significantly influence the purity and yield of MXenes [82].

3. Mass transfer of MXene-based materials and separation mechanism

Mass transport in MXene materials involves the movement of molecules, ions, and electrons within and between their layers and applied in a critical mechanism in supercapacitors [83], batteries [84, 85], catalysis [86], and membrane technology [87]. The diffusion of ions or molecules between MXene layers significantly affects device performance. Excellent electron transport is essential for achieving high electrical conductivity in electronic applications. In membrane technology, MXene membranes facilitate controlled mass transport for selective separation processes, with surface chemistry and functional groups playing a crucial role in this property. Researchers are investigating surface modifications to enhance these characteristics.

Recently, Xiang et al. [88], elaborated a vacuum filtering method to create MXene lamellar membranes on a porous nylon substrate using MXene nanosheets of varying lateral dimensions (552.3 nm, 397.5 nm, and 281.8 nm). Despite unchanged functional groups and d-spacing, the smallest variant, MXene($_S$)-M, exhibited a slightly higher contact angle and increased surface roughness. Mathematical calculations showed that

MXene(S)-M had the shortest mass transport pathway, resulting in the lowest rejection and highest water permeability [Fig. 3]. MXene(M)-M, with a medium lateral size (397.5nm), exhibited excellent water rejection and high permeability. This study provided foundational insights into the impact of MXene nanosheet lateral size on structural and transport characteristics, suggesting that future research should focus on optimizing interlayer spacing and lateral size to improve water flux and selectivity.

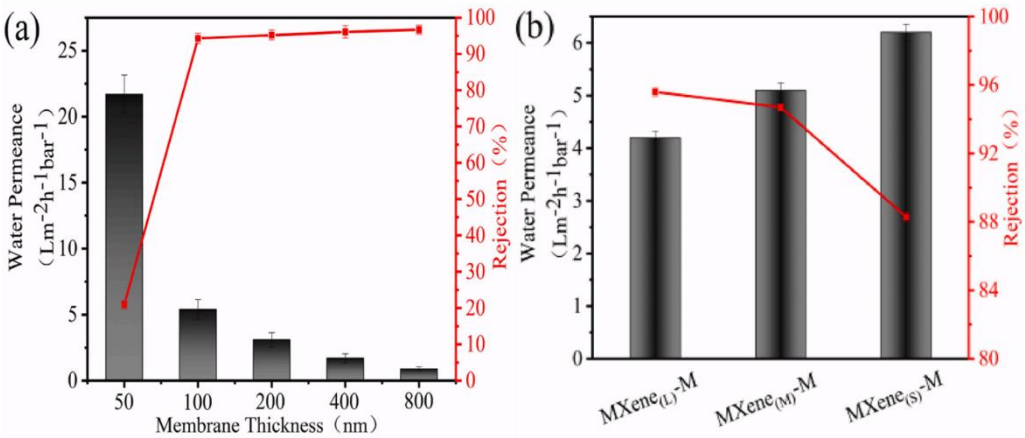


Figure 3. (a) MXene membrane of varying thickness showing rate of water permeation and rejection, (b) MXene membrane of varying lateral size showing rate of water permeation and rejection. From reference [88].

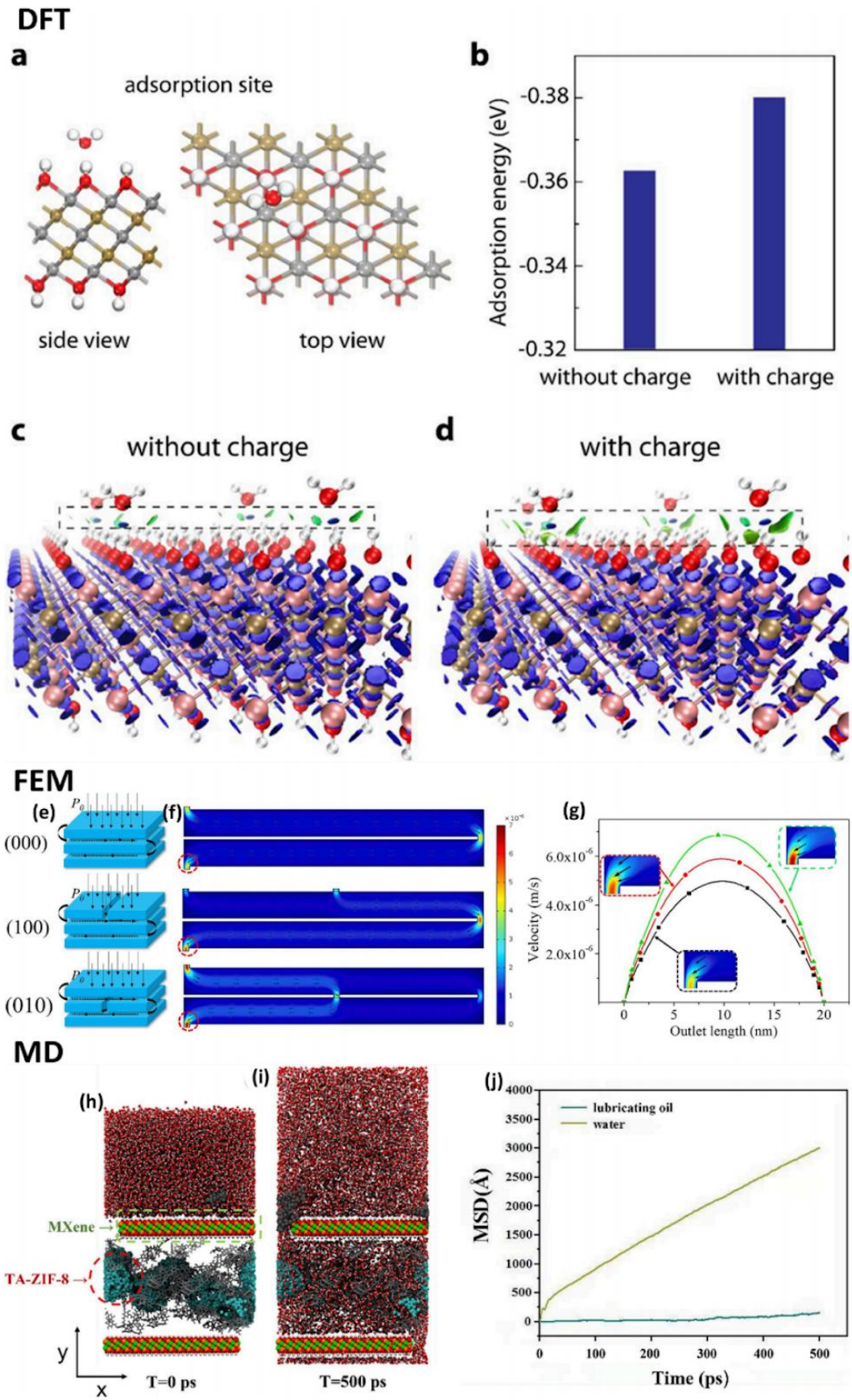
Kang et al. [89], recently reviewed theoretical and experimental advances in 2D laminar membranes for selective water and ion travel, discussing the effects of intrinsic membrane structure along with the extrinsic influences on membrane performance. This study offers promising directions for future membrane designs.

Wu et al. [90], studied ethanol dehydration using MXene membranes through a pervaporation process, finding that performance varied with feed ethanol concentration and operating temperature. At room temperature, the MXene membrane achieved a separation factor of 135.2 and a total flow of 263.4 g m^{-2} h^{-1} with a 95% ethanol to 5% water mixture. However, it did not surpass commercially available zeolite membranes due to longer mass transfer paths, increased interlayer spacing from swelling, and defects in the layered structure.

In wastewater treatment, various theoretical models help researchers understand MXene's adsorption and separation capabilities. The Langmuir and Freundlich adsorption models elucidate monolayer adsorption capacity and heterogeneous surface energetics. Pore diffusion models, combined with intraparticle diffusion, provide insights into rate-limiting steps in adsorption processes. Fick's Law of Diffusion models' diffusion processes within MXene membranes to assist in the design of ideal water treatment systems. Advanced approaches like Density Functional Theory (DFT) and Molecular Dynamics (MD) simulations offer atomic-level insights and predict separation efficiency. Finite Element Method (FEM) correlates permeation channels with water flux, enhancing understanding of MXene behaviour.

Zhang et al. [91], investigated the increased water percolation in MXene under negative voltage, attributing it to enhanced water/MXene interactions. MXene is comparatively less hydrophilic than graphene oxide due to fluoride on its nanosheets. Enhancing this interaction allows water to enter interlayer spaces more easily. Using Ab-initio DFT calculations, the study showed that water molecules prefer specific adsorption sites due to strong oxygen-hydrogen interactions, which are further enhanced by negative charges, simulating the effect of applying negative voltage. To carry out the study, separate sites were chosen out of which site 1 was preferred [Fig. 4(a)] as per calculations and was therefore chosen as a theoretical model site. The findings also involved the addition of negative charges followed by the application of negative charge to nanosheets, a rise in the adsorption energy of water on MXene. This revealed trends that are qualitative in adsorption behavior [Fig. 4(b)]. Development of hydrogen bonds during adsorption [Fig. 4(c)] is interpreted from the observation of strong interactions between oxygen atoms and nearby hydrogen atoms in water. Besides the adsorption energy data, interaction with added charges enhanced the interactions [Fig. 4(d)].

Lin et al. [92], developed a composite membrane of N-$Bi_2O_2CO_3$@MXene for oil/water separation, achieving a high-water flux of 815.3 $L \cdot m^{-2} \cdot h^{-1}$ and over 99.99% rejection ratios for various oil/water emulsions. DFT and FEM calculations showed that defects in the MXene layers increased water flux by providing additional pathways for water molecules [Fig. 4(e-g)].



(caption on next page)

Figure 4. (a) Computational simulations depict preferred sites for water adsorption on MXene nanosheets, presented from both side and top views. (b) Recorded data showcases adsorption energies with and without negative charge on the MXene surface. (c, d) Analysis of noncovalent interactions assesses the bonding between MXene and water molecules, considering the presence or absence of charge. From reference [91]. (e) Finite Element Method (FEM) measurements employ a 3D model comprising three MXene layers, with and without defects, denoted by '0' for no defects and '1' for one defect. (f) Illustration depicts velocity profiles of water flow within MXene slits with various defect configurations (0 0 0, 1 0 0, 0 1 0). (g) Water flow velocity is compared across different outlet lengths for varying defect formations, with inset images showing detailed velocity profiles near the outlet. From reference [92]. (h, i) Snapshots of the system at the initial (t = 0 ps) and final stage (t = 500 ps), along with corresponding trends in Mean Squared Displacement (MSD) for both lubricating oil and water molecules over simulation time. From reference [93].

Zeng et al. [93], created a composite membrane with tannic acid-ZIF-8@MXene/CA, showing excellent water flux and high oil/water emulsion separation performance, along with chemical stability in various filtration cycles. MD simulations [Fig. 4(h-j)] revealed that lubricating oil molecules had a slower diffusion rate than water and were effectively blocked by the membrane, while water passed through freely.

Theoretical calculations in the study of MXene for oil-water separation offer predictive insights, enabling researchers to optimize material properties for enhanced contaminant removal and separation performance. These calculations facilitate cost-effective and time-efficient tailoring of MXene materials, providing a deep understanding of underlying mechanisms and guiding experimental efforts to develop MXene-based solutions for various industries.

4. MXene-based materials for water pollutant removal

4.1. MXene-assisted heavy metal removal

After getting ingested, heavy metal ions in water are hard for the body to digest or eliminate, leading to dangerous accumulations that threaten health [94]. Due to their many OH and O functional groups, large specific surface area, and versatile surface

chemistry, MXenes have a removal capacity comparable to or exceeding other materials.

Heavy metals, typically with densities over 5 g/cm³ and atomic weights between 63.5 and 200.6[97], significantly pollute the environment through industrial wastewater [16,98]. Unlike organic pollutants, heavy metals do not degrade and conclude into accumulating in living organisms. Toxic heavy metals like arsenic, mercury, copper, nickel, cadmium, chromium, lead, and zinc pose severe treatment challenges for industrial wastewater. MXenes effectively remove heavy metals such as cadmium, mercury, chromium, copper, lead, and barium from the water via sorption-based methods due to their reactive surface groups.

Shahzad et al. [99], developed 2-D titanium carbide MXene ($Ti_3C_2T_x$) aerogel spheres using NH_4F for removing mercuric ions, achieving an adsorption capacity of 932.84 mg/g Hg^{2+}. Another study by Shahzad et al. [100], incorporated molybdenum disulfide (MoS_2) into Ti_3C_2Tx nanosheets, improving mercury ion removal efficiency to 1435.20 mg/g. Here, a hydrothermal treatment combined with ultrasonication was used to incorporate nanolayered molybdenum disulfide (MoS_2) into $Ti_3C_2T_x$ MXene nanosheets, enhancing their functionality [Figs. 5(a-c)]. This integration of oxygenated terminal and disulfide groups enabled effective adsorption and removal of mercury ions [Figs. 5(d, e)].

Isfahani et al. [101], introduced a straightforward one-step method for carboxylating $Ti_3C_2T_x$ using a linear chelating agent, resulting in robust, mobile carboxylic acid groups [Fig. 5(f)]. The TEM morphology of $Ti_3C_2T_x$ and COOH–$Ti_3C_2T_x$ sheets showed that the implementation process did not alter the flake's morphology [Fig. 5(g)]. Carboxylation of MXene reduced its zeta potential by 16–18 mV across a pH range of 2.0–8.5 and enhanced stability in the presence of molecular oxygen. Both $Ti_3C_2T_x$ and COOH-$Ti_3C_2T_x$ maintained nearly all their adsorption activity over a wide pH range (2 to 6). COOH-$Ti_3C_2T_x$, in addition, exhibited an equilibrium adsorption capacity of 499.7 mg/g at 50 ppm Hg^{2+} at pH 6 and could omit 95% of Hg^{2+} in under 1 minute [Fig. 5(h)]. The high density of functionalities in COOH-$Ti_3C_2T_x$ enables mercury ion removal through electrostatic interactions with Ti-O and Ti-COOH groups [100] [Fig. 5(i)]. The oxygen-functionalized Ti_3C_2 (Ti_3C2O_x) with a multilayer structure exhibited

a maximum adsorption capacity of approximately 4806 mg/g. At concentrations ranging from 10,400 to 33 g/L, $Ti_3C_2O_x$ demonstrated rapid adsorption kinetics and achieved a removal efficiency of about 95.6%[102].

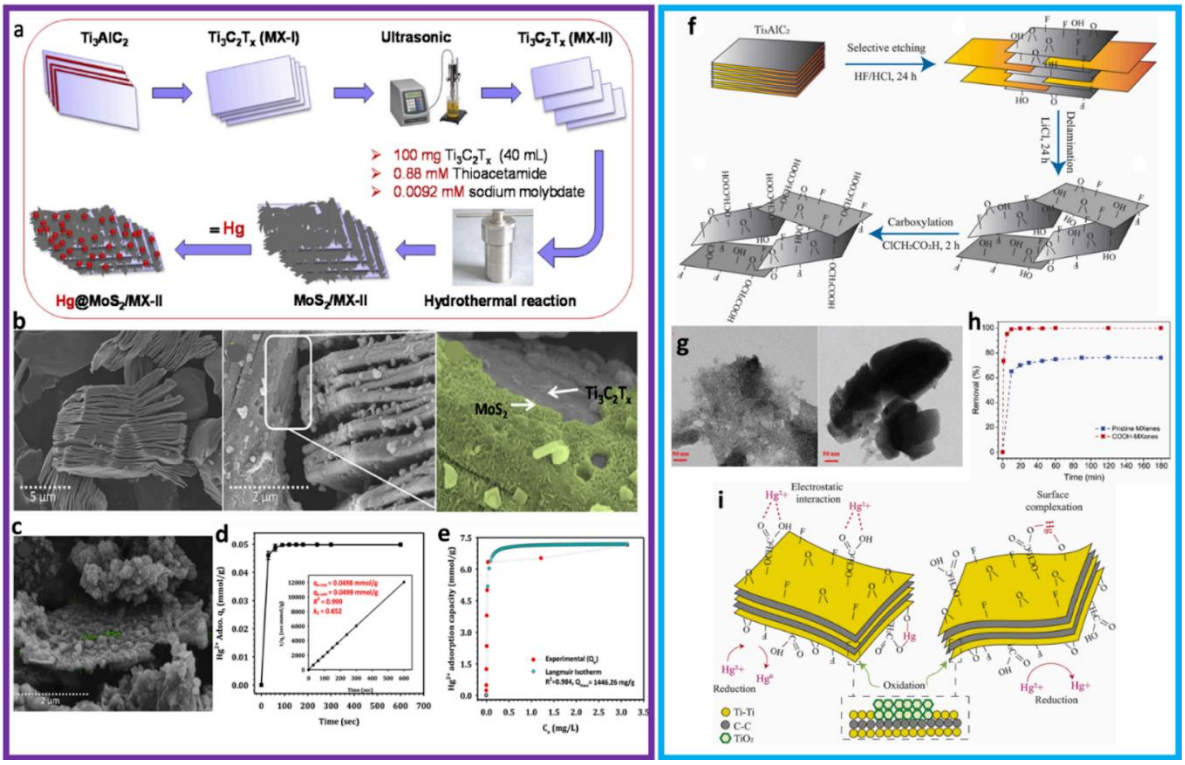


Figure 5. (a) Procedure for synthesizing a composite of MoS2 and 2D-MXene (Ti3C2Tx). (b) Scanning Electron Microscopy (SEM) images showing $Ti_3C_2T_x$ (left: scale bar = 5 µm), MoS_2/MX-I composite (middle: scale bar = 2 µm; right: enlarged view). (c) SEM image of the MoS_2/MX-II nanocomposite; scale bar = 2 µm. (d) Evaluation of adsorption kinetics for the MoS_2/MX-II composite for Hg^{2+} removal. (e) Analysis of Hg^{2+} adsorption onto MoS_2/MX-II using the Langmuir adsorption fitting model. Reprinted with permission from Reference [100]. (f) Detailed procedure for synthesizing COOH− $Ti_3C_2T_x$. (g) Transmission Electron Microscopy (TEM) images showing $Ti_3C_2T_x$ (left) and COOH–$Ti_3C_2T_x$ sheets (right). (h) Percentage of mercury removal values for pristine MXene and COOH-MXene. (i) Mechanism of mercury ion adsorption over COOH–$Ti_3C_2T_x$. From reference [101].

Lead (Pb), useful in various applications such as cement, oil refining, and lead-acid batteries, exists in water primarily as Pb^{2+}, $Pb_2(OH)^+$, and $Pb(OH)^+$[103]. Carbon-based structures like graphene oxide (GO) have been widely used for Pb(II) removal due to their short equilibrium time, large adsorption capacity, and high removal

efficiency[104]. However, carbonaceous nanomaterials and transition dichalcogenide-based membranes have not been widely adopted for industrial-scale wastewater treatment due to high production costs and complex synthesis processes [105-107]. Recently, MXene, known for its low cost, high efficiency, lightweight, and eco-friendly nature, has been successfully used for Pb(II) removal through ion exchange and electrostatic interactions[108]. Regardless of having a significantly lower specific surface area (SSA) of 10 m^2/g compared to activated carbon (~470 m^2/g), MXene's removal efficiency is higher due to its larger negative surface charge [109]. FTIR and XPS analysis, along with experimental data, indicated that ion exchange, electrostatic attraction, and inner-sphere complex formation are the primary mechanisms of removal. In the presence of Ca(II), Pb(II), and Mg(II) at high concentrations, 2D-alk MXene ($Ti_3C_2(OH/ONa)_xF_{2-x}$) still preferred Pb(II) removal with a performance of ~140.1 mg/g, achieving adsorption equilibrium in 120 seconds[110]. Dong et al. [111], developed a method where Ti_3AlC_2 was etched with hydrofluoric acid to create MXene, and the interlayer voids were filled with alginate powder, creating an optimal environment for lead adsorption. The MXene/alginate composite reached equilibrium in 15 minutes, with an enhanced adsorption performance of around 382.7 mg/g. To further improve Pb adsorption, Wang et al. [112,113], modified Ti_2CT_X nanosheets with three biosurfactants: chitosan, lignosulfonate, and enzymatic hydrolysis lignin, achieving a maximum adsorption performance of 232.9 mg/g^{-1} with enzymatic hydrolysis lignin. This non-ionic surfactant significantly increased the spacing between Ti_2CT_x nanosheets. Silane coupling agents, which combine hydrophobic and hydrophilic groups, are also commonly used to modify nanomaterials. Modifying $Ti_2C_2T_x$ with a silane coupling agent, KH570, improved Pb(II) separation effectiveness from 48.28 mg/g to 147.29 mg/g[114]. Zhang et al.[115], studied Pb(II) removal by alk-MXene-NH_2, highlighting the synergistic interaction between OH, ONa, and NH2 groups for efficient Pb(II) elimination. Additionally, some Pb(II) ions were removed through van der Waals and electrostatic interactions due to the significantly increased surface area of the amino-functionalized $Ti_3C_2T_x$ MXene (alk-MXene-NH_2).

It is important to remove other heavy metals such as chromium(VI) water protection, but lacks efficiency and speed discharge method, especially in emergency situations requiring

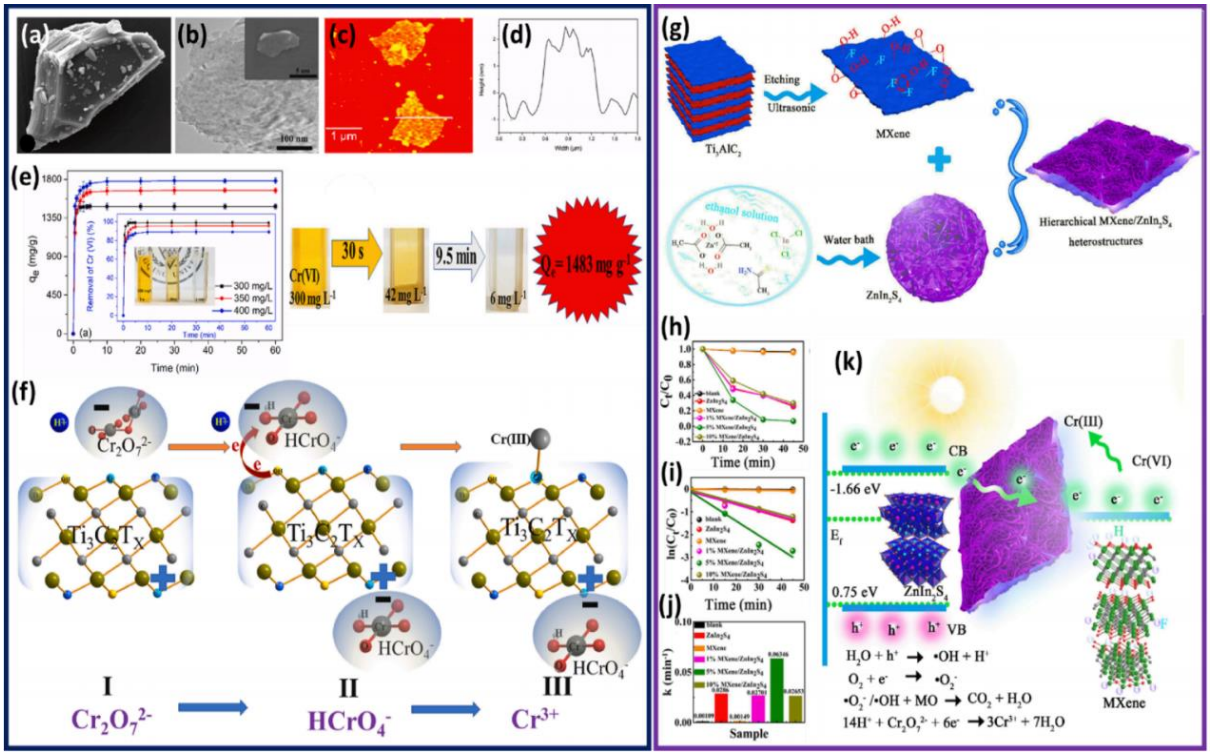


Figure 6. (a) SEM images display the morphology of synthesized Ti_3AlC_2. (b) TEM images exhibit the morphology of monolayer $Ti_3C_2T_x$ at 100 nm, with an inset showing an SEM image of the same sample at 5 µm, along with corresponding AFM images and height scale. (e) Graph depicting adsorption capacity over time for the prepared sample at various concentrations, with an inset showing the time-dependent efficiency of Cr (VI) removal. A real photo confirms efficient Cr (VI) removal in approximately 10 minutes. (f) Schematic representation illustrating the mechanism of Cr (VI) adsorption on the monolayer $Ti_3C_2T_x$ surface. From Reference [116]. (g) Schematic diagram presenting the synthetic method for the hierarchical heterostructure of MXene/$ZnIn_2S_4$. (h) Evaluation of photocatalytic performance, (i) determination of 1st order kinetics, and (j) calculation of rate constants for Cr (VI) degradation of individual materials and heterostructures prepared at different percentages of MXene. (k) Illustration demonstrating the visible light illuminated photocatalytic mechanism for the prepared MXene/$ZnIn_2S_4$ heterostructure. From reference [117].

fast action. Wang et al. [116], noted an (aqueous) solution of monolayer MXene "$Ti_3C_2T_x$" for effective Cr(VI) deposition from water [Fig. 6(a-d)]. The proposed solution is 2-dimensional $Ti_3C_2T^x$ nanosheets (NSs) that showed rapid adsorption kinetics (concentration decreases from 300 mg L^{-1} to 3 mg L^{-1} in 10 min) and specific activity of 1483 mg g^{-1} [Fig. 6(e)]. The author made a suggestion based on

psychological experience and density functional theory (DFT) data important role of removal reduction and electrostatic adsorption as it is very effective in removing Cr(VI) from water. In the context of this, it was identified that the OH-terminus on Ti_3C_2 are responsible at base in the reduction of Cr(VI), Cr(III) was included $Ti_3C_2T_x$ surface forms a complex with the O-terminus, i.e. is shown in [Fig. 6(f)]. Understanding the reduction and elimination process and the adsorption process are important for experiments with $Ti_3C_2T_x$ and the oxidation of heavy metal ions. Guo et al. [117], designed separate MXene ratios based on heterostructures (1, 5, and 10%) for the reduction of Cr(VI), as shown in Fig. 6(g). 5% MXene/$ZnIn_2S_4$ heterostructure showed low PL intensity with large photocurrent radius and small arc radius. This means that this heterostructure supports light absorption and provides good charging disassociation and low motivation to act[Fig. 6 (h-j)]. Also, Fig. 6(k) shows a better understanding of photo-generated electron pathways and the summative photocatalytic mechanism of the heterostructure.

4.2. MXene assisted dye removal

Dyeing, printing, and papermaking industries extensively use dyes, which significantly harm aquatic life and contribute to water contamination. The pollution of groundwater by medical waste, phenolic chemicals from manufacturers, and agricultural pesticides leads to the rise of new diseases. Additionally, banned and toxic food additives, such as azo dyes, can pollute clean water, posing health risks like disruption of beneficial bacteria in the intestines and on the skin, as well as causing carcinogenic effects and allergic reactions[118-120]. Thus, it is crucial to eliminate these hazardous materials to keep water bodies clean and maintain a healthy environment. Various techniques, including dye adsorption and photocatalytic degradation, are employed to remove these pollutants[121]. Among these methods, photocatalytic degradation, which utilizes photons to break down dyes, is particularly effective for environmental cleanup. MXenes play a key role in this process by improving the dispersibility of photocatalysts and serving as substrates for high-performance co-catalysts, which significantly reduce charge-carrier recombination, thereby enhancing the efficiency of dye degradation[52, 122-125].

Iqbal et al. [126], devised a nanohybrid based on MXene, specifically $BiFeO_3/Ti_3C_2$, to enhance the photocatalytic breakdown of organic dyes and colourless pollutants. The

increased surface area of this nanohybrid facilitates the interaction of electron-hole pairs, generated under visible light, with oxygen and hydroxyl radicals, resulting in the formation of superoxide free radicals. This mechanism effectively degrades Congo Red and acetophenone, a colorless contaminant, through photocatalysis. While chitosan (CS) offers potential in addressing dye contamination due to its hydroxyl and amino groups, its recyclability poses challenges. Recent work by Xu et al.[121], demonstrated that magnetic separation and surface functionalization with nano-Fe_3O_4 enhance dye removal efficiency and selectivity. They found that magnetic nanospheres composed of MXene@Fe_3O_4@CS effectively removed Congo Red (CR), with an impressive adsorption capacity of 620.22 mg·g−1, through electrostatic attraction and hydrogen bonding facilitated by –NH2 and –OH groups. Mashtalir et al.[127], observed that MXenes degrade Methylene Blue (MB) and Acid Blue 80 (AB 80) when exposed to UV light. Initially, MXenes absorbed 18% of MB and 0% of AB 80 in the dark, but exposure to UV light for 5 hours significantly increased these levels to 81% for MB and 62% for AB 80. In this context, TiO_2 generated through the partial oxidation of Ti3C2Tx-MXene's surface was primarily responsible for the photoactivity, with Ti3C2 acting as an adsorbent substrate in the lower layer, facilitating rapid charge transfer. Several studies have explored the photocatalytic potential of TiO_2-Ti_3C_2 composites [128–130]. Tran et al.[131], investigated $Ti_3C_2T_x$ MXene prepared through a selective etching method and found excellent adsorption characteristics for methylene blue (MB) in wastewater[Fig. 7(a)]. F-terminated $Ti_3C_2T_x$ MXene efficiently adsorbed nearly 92% of MB within 5 minutes in a 20 μM MB solution. However, its adsorption capacity diminished for other dyes such as methyl orange (MO) and Rhodamine B (RhB). In a subsequent study [132], Tran introduced a safflower-shaped heterostructure composed of TiO_2/Ti_3C_2 nanorods. The preparation process, involving hydrothermal oxidation, alkalization, ion exchange, and heating, significantly influenced the morphology, structure, and characteristics of the heterostructure[Fig. 7(b)]. This TiO_2/Ti_3C_2 heterostructure exhibited nearly 95% efficiency in removing RhB from aqueous solution after 60 minutes of light exposure, compared to only 19% for MXene (Ti3C2Tx). Notably, the heterostructure decomposed 88% of RhB within the first 15 minutes, attributed to rapid carrier production in TiO_2, Ti_3C_2's role in suppressing carrier recombination, and improved light absorption facilitated by the porous safflower framework. Recently, Xue et al. [133], presented MXene/biomass-based heterostructures for removing anionic azo dyes, the largest group of synthetic dyes with

an azo functional group (-N=N-) or chromophore in their molecular structure [Fig. 7(c-l)]. They examined three anionic azo dyes: allure red (AR), Congo red (CR), and sunset yellow (SY). Among these, the CTAB/MXene/BAC (CMAC) composite demonstrated the highest adsorption performance for CR, reaching about 1400 mg g^{-1}. Various models, including the Langmuir model, Pseudo-first order model (PFM), Pseudo-second order model (PSM), and intraparticle diffusion model (IDM), were employed to analyze the kinetics of AR, SY, and CR dye adsorption using the CMAC adsorbent. The study proposed a synergistic mechanism involving hydrogen bonding, physical adsorption, and electrostatic interactions in dye adsorption.

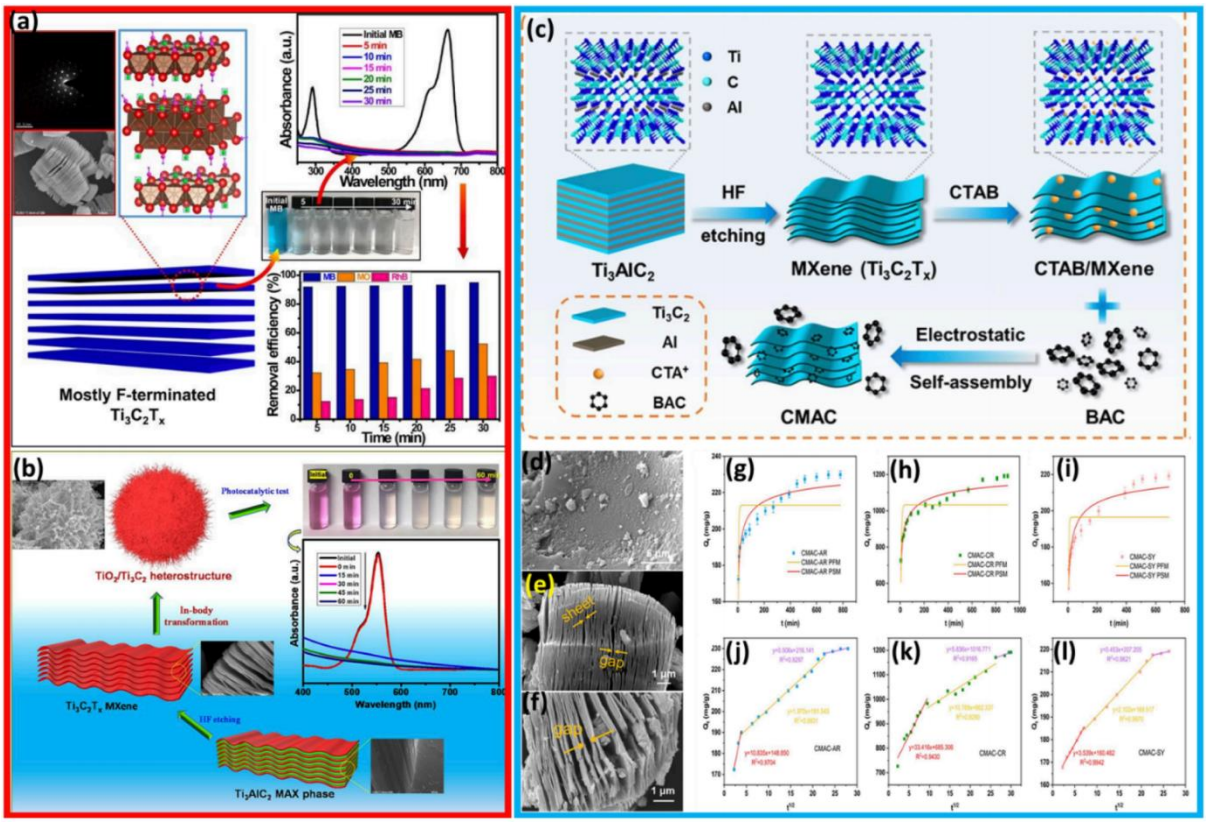


Figure 7. (a) Schematic depiction illustrating the utilization of $Ti_3C_2T_x$ MXene for the removal of methylene blue (MB) from wastewater. From Reference [131]. (b) Schematic view presenting TiO_2/Ti_3C_2 heterostructures employed for the removal of Rhodamine B (RhB) from aqueous solutions. Reprinted with permission from Reference [132]. (c) Procedure for synthesizing self-assembled CTAB/MXene/BAC (CMAC) heterostructure. (d) SEM image displaying the morphology of BAC; scale bar = 5 μm. (e) SEM image displaying the morphology of MXene; scale bar = 1 μm. (f) SEM image displaying the morphology of CMAC; scale bar = 1 μm. (g-i) Kinetic study

presenting experimental data for various dyes (AR, CR, SY) fitted using Pseudo-first order and pseudo-second order models. (j-l) Kinetic study displaying experimental data for various dyes (AR, CR, SY) fitted using the intraparticle diffusion model. From reference [133].

Water contamination, exacerbated by the discharge of insoluble oils and dyes from industrial wastewater, poses a growing threat to ecosystems worldwide [134–136]. In response, membrane separation technology has emerged as a leading solution due to its energy efficiency, high efficacy, and minimal environmental footprint [137–139]. Lin et al. [92], introduced a groundbreaking self-cleaning MXene composite membrane (N-$Bi_2O_2CO_3$@MXene) designed to efficiently remove dyes like Congo red, RhB, and Trypan blue, along with oil/water emulsions, under visible light. This membrane's success stems from the incorporation of nitrogen doping and the formation of 2D/2D heterojunctions, which significantly enhance its photocatalytic activity.

While MXene sheet membranes have shown promise in solvent nanofiltration, their effectiveness in pollutant removal has been limited. Feng et al. [140], addressed this challenge by developing composite membranes comprising rGO, polydopamine (PDA), and MXene [Fig. 8]. By optimizing MXene concentration, they achieved remarkable separation performance (>96%) for various dyes like MB, MO, MR, CO, and EB, as well as exceptional oil/water separation (>97%). Similarly, Zhang et al. [141], explored Janus mesoporous wood-derived membranes, which excel in aromatic dye removal, oil/water separation, and seawater desalination successively. These membranes leverage asymmetric wetting properties, PPy, and Ag/AgCl NPs to achieve impressive pollutant degradation (>86% for MB, >91% for RhB) and solar conversion (>95%). In another innovation, Lincy et al. [142], developed photothermal membranes based on polyelectrolyte complexes (PECs), capable of multifunctional water treatment. These membranes, derived from chondroitin sulfate and acrylamide-co-diallyl dimethylammonium chloride, exhibited excellent emulsion separation efficacy (99.4%) and solar steam generation for purifying polluted water. Overall, these advancements underscore the potential of composite membranes in addressing water pollution challenges, offering multifunctional solutions that hold promise for sustainable water management and environmental remediation.

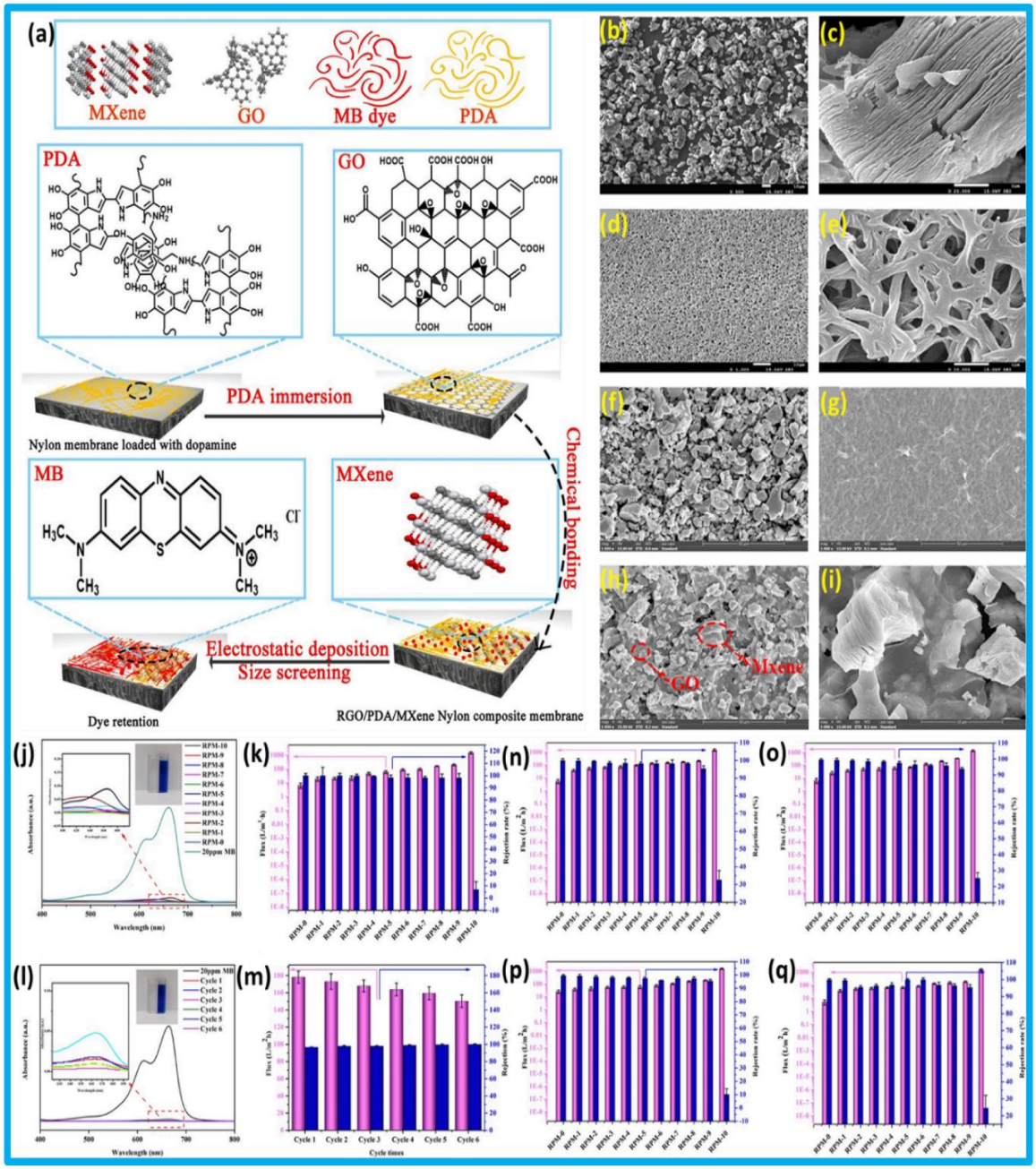


Figure 8. (a) Illustrative scheme depicting the membrane utilized for the dye removal process. (b) SEM image displaying the morphology of MXene, with a scale bar of 10 µm, and (c) an enlarged view of MXene with a scale bar of 1 µm. (d) SEM image showing the morphology of a pure nylon membrane, with a scale bar of 10 µm, and (e) an enlarged view of the pure nylon membrane with a scale bar of 1 µm. (f) SEM image displaying the morphology of a pure MXene membrane (sample: RPM-10). (g) SEM image showing the morphology of a pure GO membrane (sample: RPM-0). (h) SEM image displaying the morphology of a composite membrane (sample: RPM-8), and (i) an enlarged view of the RPM-8 membrane. (j) UV-Vis absorption data for MB dye before and after interaction with the composite membrane. (k) Values indicating the

flux and interception of MB dye through the composite membrane. (l) UV-Vis absorption data for MB dye for six cycles using sample RPM-8. (m) Values indicating the flux and interception of MB dye through sample RPM-8 for six cycles. Column chart representation showing the flux and rejection rate of (n) Methyl Red, (o) Methyl orange, (p) Congo red, and (q) Evans blue. From reference [140].

4.3. MXene and their hybrid composites for the mitigation of Pharmaceuticals

Pharmaceutical contamination can be divided into point source pollution, originating from specific, identifiable sources, and diffuse pollution, which spreads over large areas. Although diffuse pollution generally has a lesser environmental impact due to natural soil decomposition, it still poses significant environmental concerns [143]. Major sources of pharmaceutical pollution include landfill sites, wastewater from aquaculture, animal waste, household waste, medical facility waste, and industrial byproducts, all contributing contaminants to groundwater, surface water, and soil [143, 145].

Pharmaceutical-laden wastewater negatively affects various organisms. Drugs like antibiotics, anti-inflammatory agents, hormones, and analgesics are commonly found in aquatic environments. These substances often have high solubility but poor degradability, requiring attention [146, 147]. Even at low concentrations, there's a risk of synergistic effects among drugs with similar actions, potentially causing toxicity, genotoxicity, hormone imbalances, and immune system disruptions. The widespread use of antibiotics in human and veterinary medicine contributes to antibiotic-resistant pathogens, presenting a serious health issue [148]. Analgesics such as ibuprofen and diclofenac, along with estrogen-like compounds, are toxic to many organisms. The accumulation of these pharmaceuticals in water highlights the critical need for their removal to protect both human and aquatic life.

The quest for effective methods to extract active medicinal components has always been a key focus in research and development, leading to various approaches for mitigating associated risks. The process of eliminating harmful chemicals, natural contaminants, and suspended particles from water is known as water treatment technology and purification. Polluted water undergoes treatment for different purposes,

including drinking, industrial, chemical, medicinal, and pharmaceutical uses. Various methods have been reported for removing emerging contaminants (ECs) from water, including biological treatment technologies, chemical processes, and physical approaches. Biological treatment involves biodegradation by microorganisms, including microalgae, and can be aerobic or anaerobic. Examples include activated sludge and membrane bioreactors (MBRs), with MBRs showing promise for municipal and industrial wastewater treatment. Chemical methods encompass coagulation, flocculation, and oxidation processes like advanced oxidation. Advanced oxidation processes, such as ozonation and photo-Fenton, are effective against persistent contaminants. Physical methods include membrane filtration, like nanofiltration (NF) and reverse osmosis (RO), and adsorption techniques. Adsorption can be physisorption or chemisorption, influenced by factors like temperature and pH. Nanostructured materials like carbon nanotubes, graphene, and metal-organic frameworks are promising adsorbents for EC removal. Overall, these methods offer efficient ways to combat water pollution by contaminants [53].

Among the different methods, adsorption is the most effective water purification technique due to its simplicity, affordability, and the vast variety of available adsorbent materials [149, 150]. Adsorption is chosen because it reduces the resultant of secondary hazardous by-products by absorbing pollutants instead of reacting with them [151]. Effectual water treatment requires adsorbents with specific characteristics such as large surface area (SSA), pore size distribution, chemical stability, and large-scale production. Nanomaterials like graphene, iron oxide, carbon nanotubes, and chitosan have significantly improved the removal of various pollutants from wastewater. Recently, MXenes, with their outstanding 2D layered structure, large SSA, hydrophilicity, and enriched functionalities such as –OH and -O, have demonstrated exceptional adsorption properties. They can effectively remove both organic contaminants like urea and dyes and inorganic pollutants like heavy metals. MXenes' high negative zeta potentials make them suitable for adsorbing cations and polar organic molecules [152]. Understanding the interaction between pollutants and MXene-based adsorbents is crucial for assessing their effectiveness.

Kim et al. [153], assessed the potential of $Ti_3C_2T_X$ MXene for adsorbing selected pharmaceutical compounds. They selected six compounds for the study: amitriptyline

(AMT), verapamil, carbamazepine, 17α-ethinyl estradiol, ibuprofen, and diclofenac, and tested them at three pH levels (3.5, 7, and 10.5). AMT exhibited the highest adsorption capacity (58.7 mg/g) at pH 7, due to the electrostatic attraction to the negatively charged MXene. To enhance AMT adsorption, MXene was sonicated at various frequencies (0, 28, and 580 kHz), with the best adsorption observed at 28 kHz (214 mg/g). This improvement was attributed to the more uniform distribution of MXene and increased oxygenated functionalities formed by cavitation bubbles during sonication. To simulate real aquatic environments, the impact of various ions on adsorption was evaluated, showing that background inorganics hindered adsorption, while natural organic matter enhanced it. However, the cationic surfactant (CPC: cetylpyridinium chloride) negatively impacted adsorption due to competition with pharmaceutical compounds. When comparing sonicated MXene to activated carbon powder, the sonicated MXene demonstrated superior potential for pharmaceutical removal, thanks to its exceptional capacity, selectivity, and reusability.

In another study, Kumar et al. [154], introduced a novel photocatalyst system by combining MXene (Ti_3C_2) with g-C_3N_4 nanosheets, resulting in plasmonic photocatalysts with significant reusability (~3 cycles) for removing pharmaceutical pollutants, particularly cefixime, under visible light illumination. Optimization revealed that photocatalysts with 3 wt% MXenes effectively removed cefixime (~64.69%) within 105 minutes of visible light exposure [Fig. 9]. Mechanistic studies showed that incorporating Au nanomaterials and MXenes as nanocomposites improved charge carrier separation and increased active sites due to the interfacial interaction with g-C_3N_4 nanosheets. Additionally, the plasmonic effects of Au nanomaterials enhanced light absorption, boosting the photocatalytic activity of the nanocomposites. The semiconducting g-C_3N_4 nanosheets effectively captured energy from visible light, while MXene nanosheets acted as efficient
electron sinks, providing increased SSA for pollutant adsorption. MXenes also served as co-catalysts, further aiding charge carrier separation through their excellent metallic conductivity and abundant functional groups.

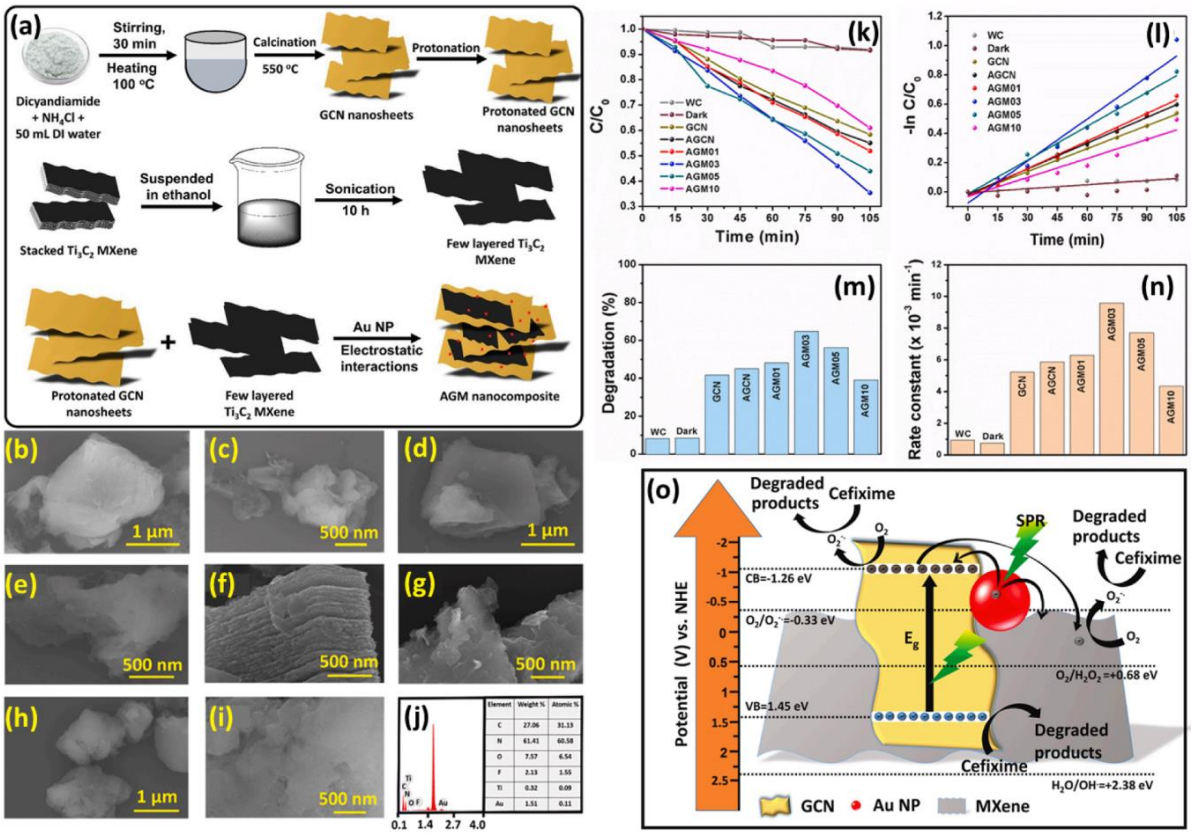


Figure 9. (a) Diagram illustrating the synthetic procedure for Au nanoparticle-decorated GCN/MXene (AGM) nanosheets. (b, c) SEM images depicting graphitic carbon nitride (GCN). (d, e) SEM images showing Au nanoparticles (NPs) decorated on GCN. (f, g) SEM images displaying Ti_3C_2 MXene. (h, i) SEM images revealing $AGM0_3$, which denotes Au NP GCN/MXene with 3 wt% of MXene. (j) Energy Dispersive X-ray (EDX) spectrum of AGM03 photocatalyst. (k, l) Results displaying the kinetic curve of cefixime decomposition. (m) Column bar chart illustrating the degradation rate (%) of all catalysts under visible light. (n) Column bar chart showing the rate constants of all catalysts under visible light. (o) Visual representation outlining the mechanism of photocatalytic degradation of cefixime using AGM nanocomposites under visible light irradiation. From reference [154].

5. Adsorption mechanisms (dye, heavy metal, and pharmaceuticals)

A thorough understanding of adsorption mechanisms for toxic elements requires comprehensive studies involving various spectroscopic analyses, adsorption isotherms, kinetics, and computational calculations using Density Functional Theory (DFT). The presence of surface functional groups and abundant reaction sites in novel

nanomaterials contributes to the efficient removal of organic dyes, heavy metals, and pharmaceuticals. Commonly observed mechanisms for removing toxic elements include chelation, diffusion, chemical coordination, electrostatic interaction, chemisorption, ion exchange, reductive adsorption, physisorption, van der Waals interactions, and surface complexation.

Dye pollution in wastewater, primarily discharged by textile industries, poses a significant environmental threat due to its wide range of types and substantial annual emissions, estimated at approximately 100 tons [155]. To address this issue, Thirumal et al. [156], introduced a unique industrial-scale production method for MXenes using a kitchen blender technique. In this context, the $Ti_3C_2T_x$ material demonstrated an impressive 98% efficiency and nearly complete degradation of dye molecules, highlighting the significant potential of MXene for removing toxic pollutants from wastewater. Titanium dioxide (TiO_2) is commonly used as a catalyst for photocatalytic pollutant degradation. Researchers [157] have developed TiO_2/MXene composites using a solvothermal method and modifying them with substances like C_2H_6O and C_3H_8O. In these composites, $Ti_3C_2T_x$ serves as a co-catalyst for capturing photogenerated electrons and enhancing electron transport efficiency. Uniform TiO_2 growth on $Ti_3C_2T_x$ MXene's surface further enhances these effects. The ending $TiO_2/Ti_3C_2T_x$ compound effectively stops the recombination of electron-hole pairs produced under light illumination, thereby enhancing the degradation of organic compounds. Among various materials, $TiO_2/Ti_3C_2T_x$-C_3H_8O exhibited the highest efficiency in degrading methyl orange (MO) by approximately 90.5%, surpassing single TiO_2 performance by 1.5 times. Hieu et al. [128], observed a significant enhancement in the degrading efficacy of Ti_3C_2-TiO_2 composite for methyl orange (MO), reaching 99% preceding 40 minutes of light exposure. Additionally, the $TiO_2@Ti_3C_2$ showed sustained photocatalytic activity for 5 cycles. The reaction mechanism for MO degradation using $TiO_2@Ti_3C_2$ involved the activation of photo-induced electrons within the conduction band (CB) of TiO_2, followed by swift transfer to the CB of Ti_3C_2 MXene due to its notable electrical conductivity [Fig. 10(a)]. This process created a Schottky barrier across the Ti_3C_2-TiO_2 interface, acting as an electron sink and enhancing photocatalytic efficiency. The photogenerated electrons then engaged with O2 to produce superoxide radicals (O2−), while the photogenerated holes reacted with adsorbed hydroxyl ions (OH–) to generate hydroxyl radicals (OH),

ultimately degrading MO molecules into oxidation products. This is done using the following reaction [Eqs. (1)-(5)]:

$TiO_2 + hv \rightarrow TiO_2(e^- + h^+)$ (1)

$TiO_2(e^- + h^+) + Ti_3C_2 \rightarrow TiO_2(h^+) + Ti_3C_2(e^-)$ (2)

$h^+ + OH^- \rightarrow OH^{\cdot}$ (3)

$e^- + O_2 \rightarrow O^{-2}$ (4)

$OH^{\cdot}$ /O^{-2} radicals + RhB dye → degraded products (5)

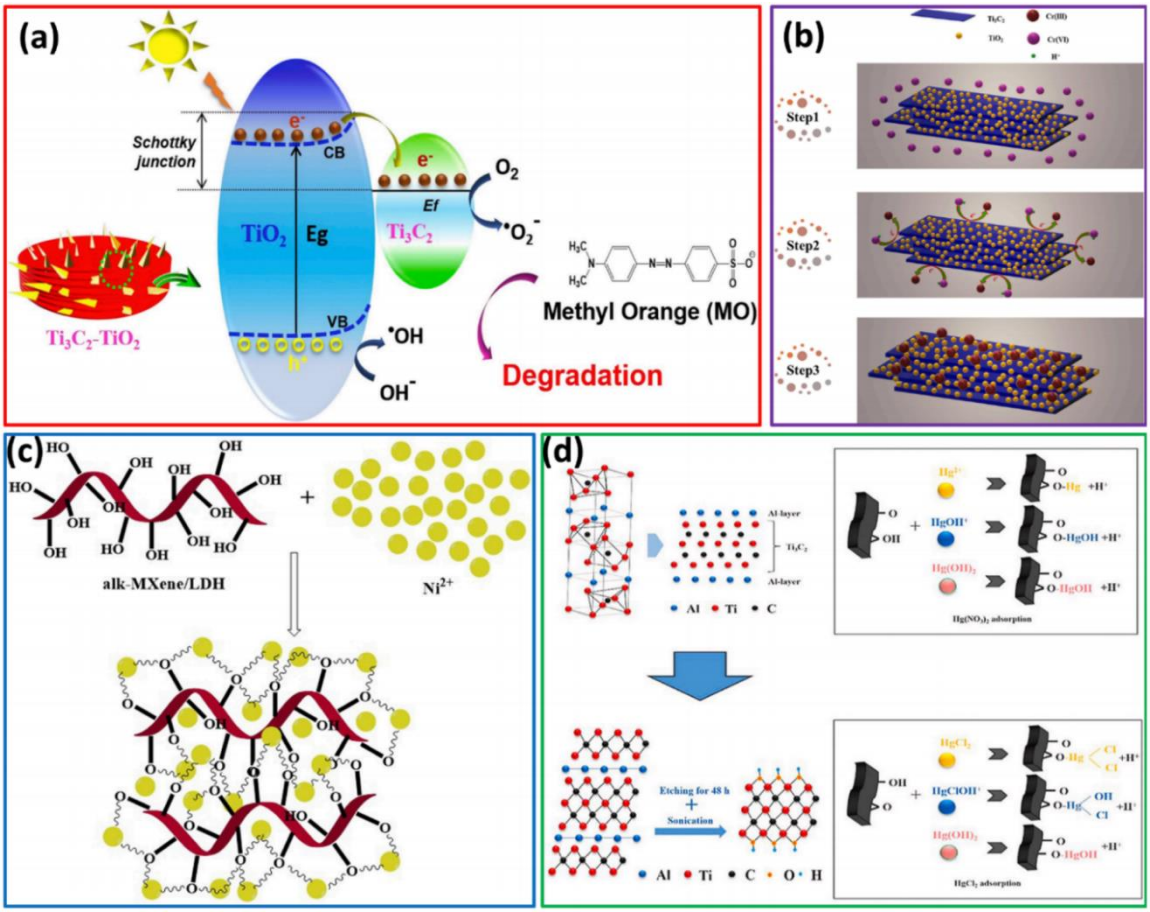


Figure 10. (a) Illustrative diagram presenting the proposed mechanism for photocatalysis of Methyl Orange (MO) on a Ti_3C_2-TiO_2 heterostructure. From reference [128].(b) Step-by-step demonstration depicting the removal of Chromium (VI) using a Ti_3C_2/TiO_2 composite. From reference [158]. (c) The adsorption mechanism of alkali-metal-intercalated MXene/LDH onto nickel under weak acidic conditions involves hydrolysis or exchange with sodium ions. Under weak alkaline conditions, it involves hydrolysis or exchange with sodium ions. Under strong alkaline conditions, the mechanism is characterized by direct precipitation. From reference

[159].(d) Illustration demonstrating the adsorption of mercury chloride and mercury nitrate over the MXene surface. From reference [160].

Moving forward, the adsorption process for heavy metals is elucidated in [Fig. 10(b)], illustrating a three-step uptake process for Cr(VI) onto Ti_3C_2/TiO_2 composites[158]. In acidic conditions, the abundance of H^+ ions and positive surface charge attracts negatively charged $Cr_2O_7^{2-}$, whereas this attraction diminishes in basic conditions due to elevated pH levels. Upon contact with the adsorbent surface, $Cr_2O_7^{2-}$ undergoes reduction, forming Ti-O-Cr(III) and Ti-C-Cr(III) as Cr(III) moieties covalently bond with the Ti-O bond[Fig. 10(c)] depicts the proposed mechanism for Ni(II) removal by alk-MXene/LDH under weak acidic conditions, involving the formation of a coordination complex/precipitate on the base-MXene/LDH surface[159]. In another investigation, zeta potential measurements indicate electrostatic adsorption of Hg(II) due to the negative charge on the material surface. FESEM micrographs further validate the adsorption of mercuric ions. The interaction mechanisms of mercury chloride and mercury nitrate over MXene are delineated in [Fig. 10(d)].

To delve into the adsorption mechanism for pharmaceuticals, Miri-Jahromi et al.[161], delved into the removal of three semisynthetic antibiotic compounds (amoxicillin, ampicillin, and cloxacillin) using three types of MXene-based removal agents (Mn_2C, Ti_2C, and V_2C) through molecular dynamics simulations. Among the studied MXenes, Ti_2C exhibited the highest efficiency in adsorbing antibiotic compounds. As depicted in [Fig. 11(a)], cloxacillin, amoxicillin, and ampicillin showed adsorption rates of 100%, 88%, and 44%, respectively. Moreover, functionalizing MXene with hydroxyl and amine groups increased the antibiotic adsorption capacity. The study also emphasized the reusability of Ti_2C as
an adsorbent.

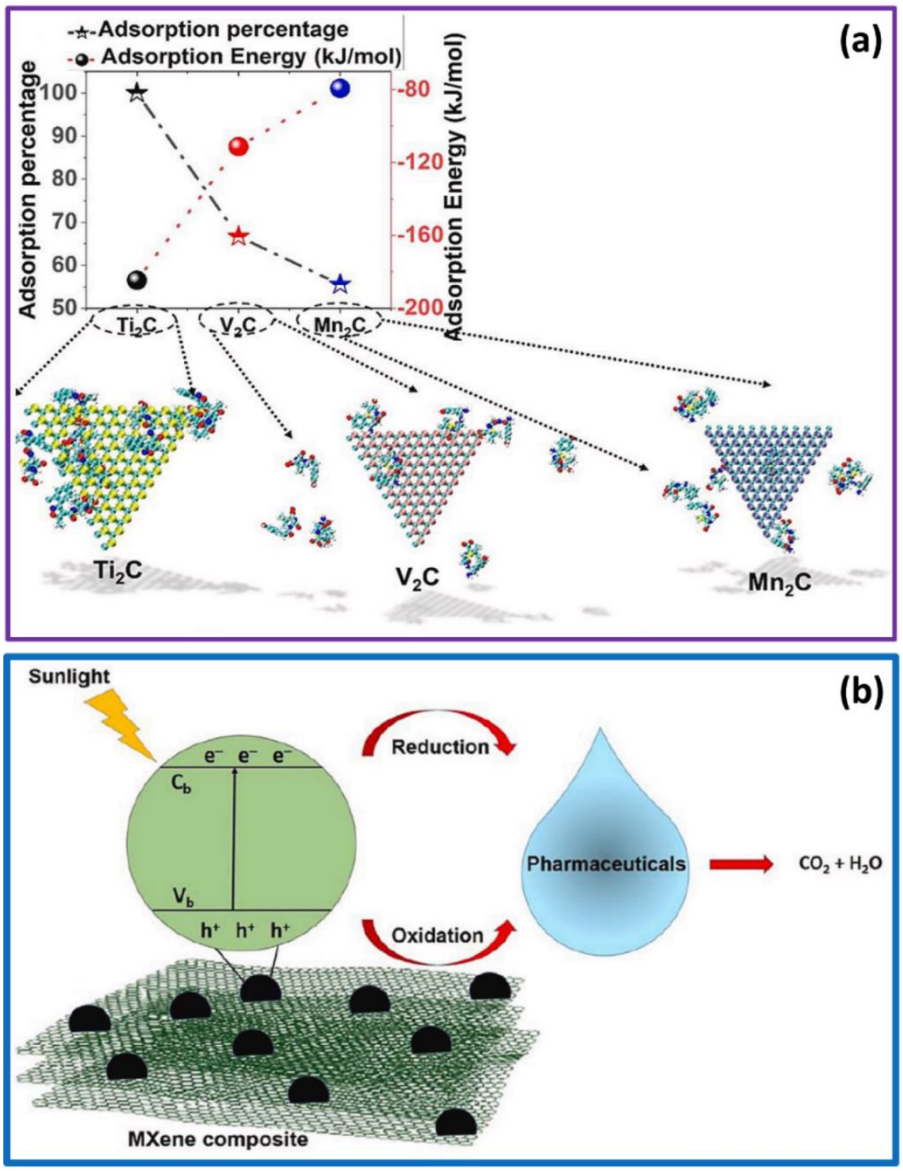


Figure 11. (a) Information regarding adsorption energy and adsorption percentage for cloxacillin interacting with MXenes. Reprinted with permission from reference [161]. (b) A standard photocatalytic degradation mechanism of pharmaceuticals using MXene composite materials. From reference [53].

Various experiments have unequivocally demonstrated $Ti_3C_2T_x$'s profound ability to effectively eliminate pharmaceutical waste by generating unstable radicals, as depicted in [Fig. 11(b)][53]. MXenes have shown remarkable potential as co-catalysts in degrading various pharmaceuticals in aqueous environments. The widespread presence of diverse pharmaceuticals, including antibiotics, anti-inflammatory drugs, hormones, and analgesics, in water bodies has been extensively reported [162].

These pharmaceutical compounds exhibit high solubility but demonstrate resistance to degradation, often being detected at extremely low concentrations, even at levels as minute as parts per billion or trillion[163]. Despite their dire concentrations, the potential for synergistic effects among pharmaceuticals sharing similar modes of action remains a concern, potentially resulting in adverse outcomes such as acute and chronic toxicity, genotoxicity, carcinogenicity, and intrusion with hormonal and immune systems.

Over the past few decades, antibiotics have gained increasing attention as a prominent class of contaminants and widely utilized pharmaceuticals. Various antibiotics, including tetracyclines, ciprofloxacin, sulfamethazine, lincomycin, and fluoroquinolones, are extensively employed in sectors such as livestock farming, medicine, and poultry production to combat bacterial infections[164]. The overuse and improper disposal of antibiotics into the environment, coupled with the rise of antibiotic resistance, pose significant public health challenges. Particularly, the excessive use of sulfonamides has led to severe environmental consequences[165]. Due to their high water solubility, persistence, chemical stability, and complex structure, sulfonamides and their mobile metabolic residues pose threats to both the environment and lives[166]. Consequently, environmental science endeavors to develop efficient photo-assisted removal techniques. A study by Cao et al.[167], brought in a novel heterojunction catalyst made for visible light-induced photodegradation of the antibiotic sulfamethazine. The composite's prolonged carrier lifetime and effective photoelectron transfer are attributed to the robust catalytic activity of the CFO/Ti_3C_2 composite. The research demonstrated substantial synergistic degradation, resulting in approximately 60% removal of sulfamethazine using the fabricated photocatalyst. Additionally, the study observed the adsorption of sulfamethazine molecules by the active material during the photocatalytic process. The degradation process of sulfamethazine on CFO/Ti_3C_2 involved S–N bond cleavage, aniline oxidation, and deamination, primarily driven by the bombardment of –OH radicals.

6. Factors affecting MXene efficiency for wastewater treatment

The efficacy of MXenes in removing pollutants from water is influenced by various factors. These factors include the nature of the pollutant and the attributes of the adsorbent, such as its surface area, the hydrophilic character of its functional groups, and its charge. Additionally, crucial considerations during the adsorption process

include the pH, temperature, and pollutant concentration within the water. Notably, the surface charge over MXene arises from electrostatically charged functional groups. MXene's surface undergoes subsequent processes of etching and intercalation, generating diverse functional groups like -O, -F, and –OH, which result in surface electrostatic charging. Consequently, MXenes interact electrostatically with water impurities having opposite charges, such as heavy metal ions, dyes, and pharmaceutical compounds. This electrostatic interaction includes the primary mechanism for MXene adsorption [168, 169].

pH is a pivotal parameter impacting MXene-based adsorbents' ability to extract pollutants. The concentration of hydrogen ions within water controls both MXene's surface charge and the adsorption rate of attached functional groups. The interplay of charge between adsorbent and adsorbate significantly influences the adsorption process. In low-pH conditions (e.g., below pH 2), a high concentration of H^+ ions competes with positively charged adsorbate substances (e.g., MB) in water, reacting with negatively charged ions on the MXene surface groups (–OH, -O, and -F). Consequently, the MXene surface becomes charged, leading to the cessation of electrostatic attraction due to the loss of its negative charge. Conversely, at higher pH levels, with a reduced H^+ concentration, MXene retains its negative charge. Overall, the pH of the water plays a significant role in MXene-based adsorption, as it governs the surface charge and, subsequently, the electrostatic interactions driving the adsorption process. Zhang et al. [170], explored the impact of pH on MB adsorption by MXene. Unlike prior examinations, the adsorption capacity achieved at pH 3 and 11 was around 10 mg/g. A decline in adsorption capacity was observed as the pH transitioned from 3 to 7, followed by an increase from pH 7 to 11. Consequently, pH 7 exhibited the lowest adsorption capacity, ~2 mg/g. The substantial adsorption capacity at pH 3 likely resulted from H bonding instead of electrostatic interaction, as evidenced by the high adsorption capacities achieved below the pHpzc of 5.1 based on zeta potential measurements. A significant rise in adsorption capacity beyond pH 7 suggests that the negatively charged MXene attracted positively charged adsorbates. But the adsorption efficiency at elevated pH was relatively low compared to what was observed for low pH, attributed to MB hydrolysis. Fig. 12 illustrates the behaviour of pH on MXene@Fe_3O_4-mediated MB adsorption, spanning the pH range of 3 to 11 and the interaction mechanism.

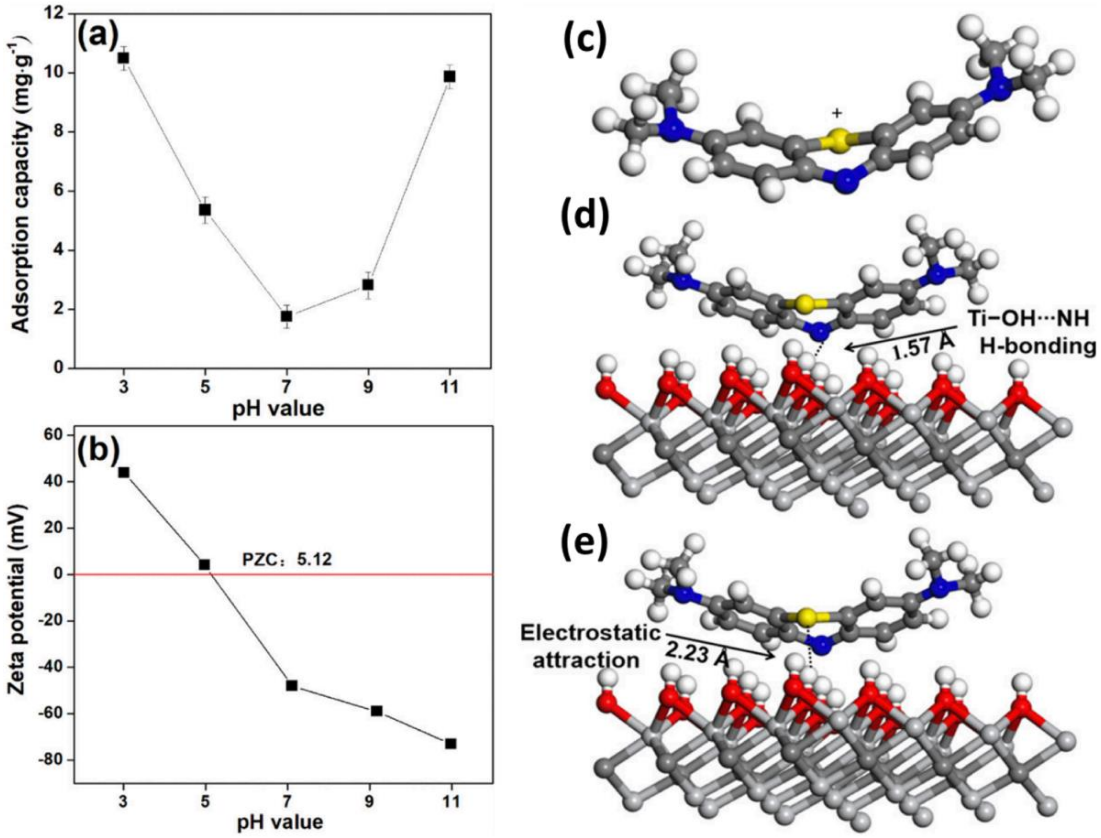


Figure 12. (a) Data illustrating the adsorption of Methylene Blue (MB) on MXene@Fe3O4 composite with varying pH values.(b) Measurement of zeta potential for MXene@Fe3O4 composite at different pH values.Theoretical representations of:(c) The molecular structure of MB dye.(d) Hydrogen bonding between MXene and MB. (e) Electrostatic interaction between MXene and MB, with elements denoted by colors: S (yellow), N (blue), O (red), H (white), C (gray), and Ti (light gray). From reference [170].

Similarly, extensive investigation has been conducted on the influence of temperature on MXene's behavior in adsorbing substances in water. Dev et al. [171], explain that temperature affects the adsorption process by impacting ion mobility, activation energy, and the feasibility of adsorption. As temperature increases, ions gain kinetic energy, enhancing their mobility and consequently accelerating the rate of adsorption. Parameters like standard enthalpy, entropy, and free energy, derived from the Gibbs free energy equation, help assess whether the adsorption process is endothermic or exothermic, spontaneous, or non-spontaneous [172–174]. A study focusing on the temperature effect on Pb adsorption using 2D MXene found results diverging from

typical patterns. The experiment, conducted at temperatures of 293 K, 303 K, and 313 K, aimed to understand how temperature influences MXene's Pb adsorption [175]. Surprisingly, the enthalpy and entropy change values exhibited a negative trend, contrary to other findings. Specifically, for MXene-25, -35, and -45, enthalpy values were -22.36 kJ mol^{-1}, -22.24 kJ mol^{-1}, and -23.10 kJ mol^{-1}, respectively, while entropy change values were -66.34 J mol^{-1}, -62.91 J mol^{-1}, and -63.04 J mol^{-1}, respectively. Consequently, the computed free energy change values were negative as well. Notably, as the temperature rose from 295 K to 313 K, the free energy change values for all three synthesized MXenes increased by approximately 1.3 kJ mol^{-1} on average. In summary, based on these findings, all thermodynamic quantities showed negativity, indicating an exothermic, reversible, and spontaneous adsorption reaction.

Furthermore, the literature emphasizes MXenes' distinctive features, such as their unique two-dimensional structure, significant porosity, intricate branching patterns, and various functional groups. These inherent characteristics greatly add to their exceptional adsorption capabilities, primarily due to their large surface area and numerous accessible functional groups capable of interacting with pollutants. For instance, the effective adsorption of dyes is facilitated by the strong interaction between randomly distributed F and OH functional groups on MXenes and dye molecules. Particularly, the adsorption process for dyes can be explained by the interplay of mechanisms like Ti−OH···N bonding (at pH = 3), electrostatic attraction (at pH = 11), and reductivity. These mechanisms collectively underlie MXenes' adsorption capacity and functionality.

7. Environmental influence and toxicity

Regarding etching techniques for MXene-based materials, most methods entail either directly using HF or generating HF in-situ through fluorine salts. However, HF is notorious for its high corrosiveness and toxicity, raising concerns about environmental contamination upon its release. Additionally, the synthesis process can emit potentially hazardous metal substances like Al and Ti, warranting serious attention. The aging of MXene compounds leads to surface oxidation and TiO2 formation, posing challenges for water purification applications. This oxidation, developing during or after exposure to contaminants, can produce adsorbed pollutants, leading to secondary water pollution. Therefore, it's necessary to thoroughly grasp the long-term aging effects to evaluate the environmental suitability and sustainability of MXene-based materials [176,177].

Transitioning from laboratory-scale research to practical applications requires a comprehensive assessment of MXene's biocompatibility and toxicity. The toxicity of MXene-based materials depends on factors such as size, dosage, and surface coating [178]. For instance, Arabi Shamsabadi et al. [179], synthesized Ti3C2Tx MXene of various sizes (lateral) and examined its antibacterial effectiveness against Bacillus subtilis and Escherichia coli. Their results indicated that smaller MXene materials exhibited stronger antimicrobial effects against both bacteria. Moreover, surface chemistry significantly influences potential toxicity. Etching along with delamination conditions, post-synthesis treatments, and surface functionalization influence MXene's toxicity [180]. Exploring fluorine-free methods for MXene preparation could mitigate toxicity and enhance biocompatibility. Surface modification by combining MXene with other materials is another strategy to reduce toxicity. Coating MXene with substances like chitosan, collagen, and silk fibroin has been demonstrated to decrease toxicity and enhance biocompatibility. For example, Ti3C2Tz/chitosan includes showed antibacterial properties against E. coli and S. aureus [171,172]. While some studies have investigated the toxicity of Ti3C2Tx MXenes, there are still various variants that require examination. To effectively utilize MXenes in large-scale wastewater treatment, thorough research is necessary, covering aging effects, associated toxicity, and the desorption process for adsorbed pollutants in diverse environments.

8. MXene-based adsorbent regeneration evaluation

Recovering pollutants such as dyes, heavy metals, and pharmaceuticals from MXene-based adsorbents and exploring their potential for reuse are crucial steps in cost management, environmental risk mitigation, and addressing the challenge of disposing of toxic sludge. Existing research offers insights into different eluents like HCl, HNO_3, NH_4OH, H_2SO_4, Na_2CO_3, NaOH, KOH, and DI-water for removing adsorbed pollutants from MXene-derived adsorbents [183]. For example, a study investigated the recyclability of the MoS_2/MX-II adsorbent, finding that initial desorption of Hg(II) using a 5 M HCl eluent was approximately 37.3% past a 3-hour contact time. Interestingly, desorption efficiency increased to 55% with prolonged contact time of up to 30 hours [70]. Notably, even with projected contact time and high eluent concentration, the MoS2/MX-II adsorbent maintained excellent performance, even at low Hg(II) concentrations (0.08 mM) over five cycles [100].

Ghani et al. [184], orchestrated sodium-intercalated Ti3C2Tx (SI-Ti3C2Tx) MXene nanosheets through a straightforward batch reaction process, which were then utilized in adsorption and electrochemical regeneration procedures. Results revealed an intercalation process leading to an expansion in the 'd' spacing of the MXene, significantly enhancing its adsorption capacity compared to pristine Ti3C2Tx MXene and similar nanostructures reported previously. This expansion supported the superior adsorption capability of SI-Ti3C2Tx. Hereafter, the intercalation process facilitated the substitution of single bond F terminations with single bond O and single bond OH groups. SI-Ti3C2Tx MXene exhibited remarkably rapid kinetic rates, aligning well with the Elovich kinetic model. The adsorption isotherm followed the Redlich-Peterson isotherm model, indicating a likely chemisorption mechanism driven by electrostatic attraction between the adsorbent and adsorbate, regulated by rate-controlling steps. With its high electrical conductivity, SI-Ti3C2Tx demonstrated rapid electrochemical regeneration rates, enabling the complete removal of the adsorbate (ciprofloxacin: CPX)[Fig. 13]. These findings highlight the significant promise of MXene-based adsorbents for efficient utilization, showcasing the remarkable potential for heavy metal removal and meeting criteria for recycling and metal ion recovery.

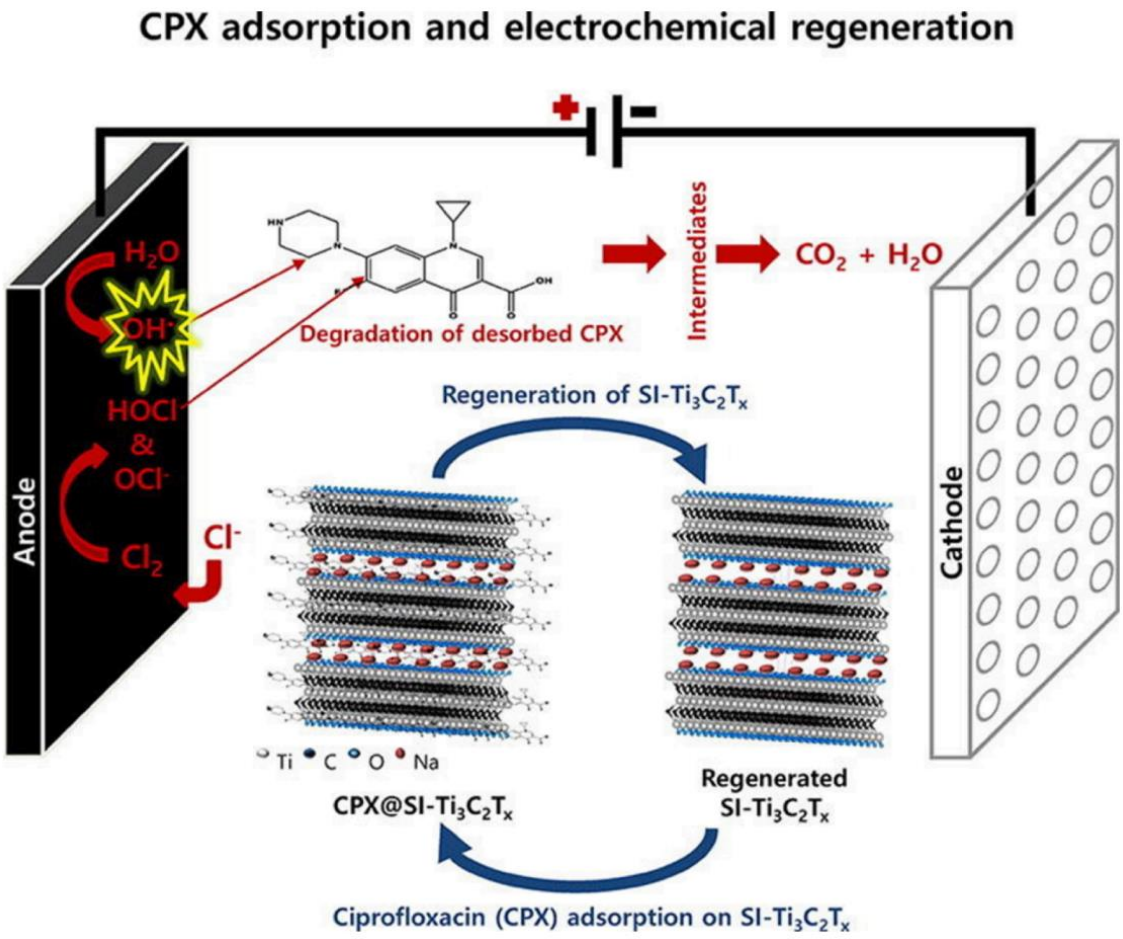


Figure 13. The mechanism of adsorption and regeneration of CPX using an SI-$Ti_3C_2T_x$ composite. From reference [184].

9. Challenges and future prospects

The unique attributes of MXene render it an appealing option for wastewater treatment. MXene's capacity for adsorbing heavy metals, dyes, and organic pollutants from water sources is significant due to its expansive surface area and diverse surface chemistry. Moreover, MXene's electrochemical properties make it a potential contender for the elimination of persistent organic pollutants alongside its utilization in advanced oxidation processes. Additionally, MXene-based membranes show great promise as separation and filtration technology, enabling the selective removal of pollutants from water. The tunable nature of MXene structures allows for customization to target specific pollutants, enhancing adaptability to different wastewater compositions. The practical applications of MXene demonstrate its efficacy and versatility in addressing the complex challenges of wastewater treatment. However, there are numerous

obstacles to overcome before MXene can be considered for membrane manufacture in wastewater treatment. Enhancing the efficiency and reproducibility of MXene synthesis is crucial for meeting the demands of large-scale membrane production. Finding cost-effective supplies and processing methods to make MXene-based membranes commercially viable is another significant challenge. Long-term stability in real-world wastewater treatment scenarios poses a challenge due to potential structural changes over time. Developing MXene structures that are highly selective for pollutants while allowing water molecules to pass through presents a considerable challenge. To fully leverage MXene in commercial membrane applications for wastewater treatment, collaboration across scientific, engineering, and regulatory sectors is essential. The central obstacles and avenues for future research are outlined below:

Firstly, enhanced synthesis techniques are needed to produce MXene structures with specific characteristics tailored for various applications. This improvement would facilitate the creation of MXene-based composites and membranes with desired attributes. Addressing environmental and health concerns associated with toxic chemicals like HF in MXene synthesis is crucial, and innovations in HF-free synthesis methods are needed. Furthermore, the expense and low yield of lab-scale synthesis techniques for MXene and its derived adsorbents necessitate the development of more effective methodologies for upscaling MXene nanocomposites at a reasonable cost. Evaluating the potential of MXene-based adsorbents on a commercial scale and under real-world conditions is essential to position these materials for diverse applications. Understanding the intricate mechanisms underlying the capture of pollutants from the aquatic environment requires exploration using various characterization tools and theoretical models. Regenerating MXene-derived adsorbents post-loading is crucial for assessing their efficiency, economic viability, and stability. Therefore, consideration should be given to using alternative eco-friendly eluents instead of traditional acidic, alkali, and basic agents to align with environmental considerations.

Ti_3C_2 is commonly utilized in water treatment, the broad spectrum of structures within the MXene family necessitates exploration of alternatives beyond Ti_3C_2. Moreover, MXene-derived composites show promise in various applications such as light-trapping, rapid charge transfer, electromagnetic shielding, energy storage, and photo-electrochemical catalysis, demanding thorough investigation. A significant challenge

lies in the stability and storage of MXenes, as they are prone to oxidation in aqueous environments. For instance, Ghassemi et al. [185], demonstrated deliberate oxidation of $Ti_3C_2T_x$ MXenes in ambient air, resulting in TiO_2 formation by adjusting heating rates, temperature ranges, and exposure durations. They observed that gradual temperature increases produced rutile TiO_2 particles, while rapid heating led to anatase TiO_2 particle synthesis, verified through TEM analysis. Maleski et al. [74], applied Hildebrand and Hansen's solubility theory to study $Ti_3C_2T_x$ dispersion in various organic solvents, noting that $Ti_3C_2T_x$ turned white in water but remained black in organic solvents, indicating different reaction dynamics. To address these issues, Habib et al. [186], investigated $Ti_3C_2T_x$ oxidation in different media, finding the slowest oxidation in liquid and the fastest in solid media, with $Ti_3C_2T_x$ oxidizing over two weeks in water. They suggested that colloidal stability and black color might not accurately signify oxidation, contrary to previous findings. To prevent oxidation or create a redispersible powder, $Ti_3C_2T_x$ can be freeze-dried or preserved in ice, albeit to a lesser extent in certain organic solvents. Polymer addition does not prevent oxidation, as $Ti_3C_2T_x$ composites with varying polymer amounts exhibit identical conductivity profiles. $Ti_3C_2T_x$ films oxidize faster under UV radiation. Recently, Zhao et al. [187] [Fig. 14], used sodium L-ascorbate (NaAsc) as an antioxidant to extend colloidal $Ti_3C_2T_x$ nanosheet stabilization in aqueous dispersion. The absence of this antioxidant results in rapid $Ti_3C_2T_x$ to TiO_2 transition, reducing conductivity and inducing aggregation in $Ti_3C_2T_x$ films, whereas “NaAsc” maintains $Ti_3C_2T_x$ nanosheet crystalline structure, shape, stability, chemical composition, and electrical conductivity in water for 21 days, preventing oxidation. These results suggest the possibility of engineering-grade MXene-based materials and shelf-stable MXenes.

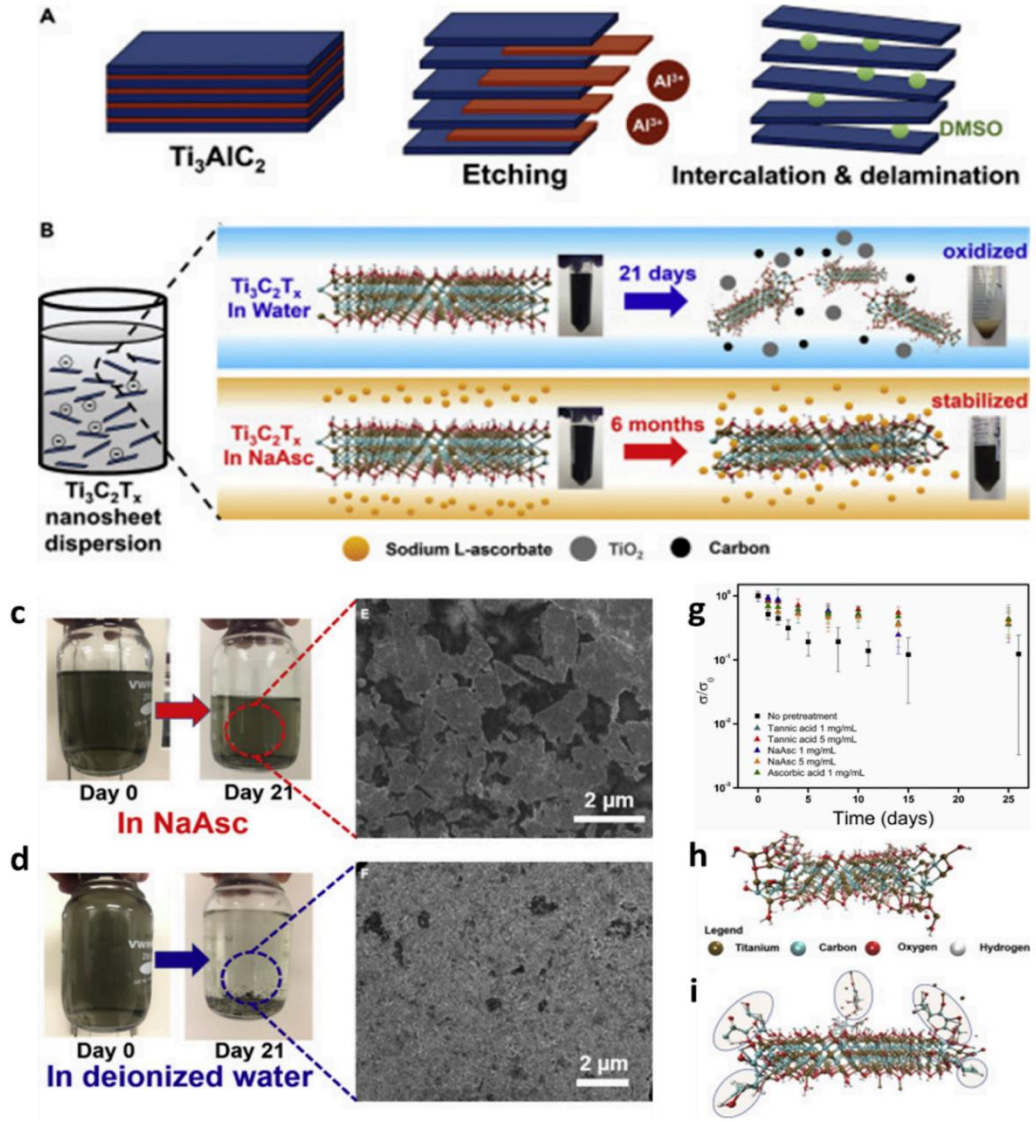


Figure 14. (a) Diagram illustrating the synthesis of MXene.(b) Scheme demonstrating shelf-stable $Ti_3C_2T_x$ dispersed in water and antioxidant Sodium L-Ascorbate.(c, d) Real samples dispersed in water and NaAsc at fresh and after 21 days.(e) Corresponding SEM image of Ti_3C_2Tx nanosheets stored for 21 days in 1 mg/mL NaAsc solution, displaying stable MXene nanosheet morphology.(f) SEM image of $Ti_3C_2T_x$ nanosheets stored for 21 days in DI water, showing dense and amorphous morphology of MXene nanosheets.(g) Graph depicting conductivity versus time, where improved conductivity for MXene treated with antioxidant is attributed to oxidation prevention.(h) Molecular dynamic simulation for prepared MXene in water.(i) Molecular dynamic simulation for prepared MXene in antioxidant. The attached groups of L-Ascorbate prevent further reaction among water and MXene nanosheets. From reference [187].

Furthermore, MXene-based membranes [93] show important promise in various applications due to their unique properties. These membranes, obtained from two-dimensional MXene materials, impart exceptional mechanical strength and flexibility crucial for membrane technology. Some MXenes, like titanium carbide (Ti_3C_2), offer high electrical conductivity, suitable for electronic devices integrated into membranes and sensors. MXene's tunable surface chemistry allows for tailored selectivity in separation processes. With a large surface area from their layered structure, MXene-based membranes provide numerous active sites fruitful for dye and antibiotic adsorption out of wastewater [188, 189]. Their chemical stability entrusts them with being suitable for aggressive environments, ensuring membrane integrity over time. MXene membranes can be reindered for selective permeability, fit for filtration applications. The ease of synthesis and sustainable nature of MXenes contribute to their appeal in green technologies. Live research suggests that advancements may enhance MXene membrane viability for water purification, desalination, gas separation, and energy storage devices. Despite challenges such as scalability and long-term stability, the versatile nature of MXenes positions them as promising candidates for diverse applications. Addressing these issues is crucial to fully realizing the potential of MXene across diverse applications. Additionally, a thorough assessment of the potential toxicity and environmental implications of MXene materials is essential to protect both human health and the ecosystem.

In conclusion, unlocking the full capabilities of MXene-based materials demands collaborative efforts to overcome challenges related to synthesis methods, scalability, real-world implementation, understanding mechanisms, regeneration, structural investigation, wide-ranging applications, stability, and environmental impact assessment.

10. Practical applications of MXene-based membranes

Research has also been conducted on the applicability of MXene-based membranes in natural water systems containing a diverse range of microbes and competing ions. In a study focused on removing microplastics (MPs) from untreated wastewater, the h-$Ti_3C_2T_x$ membrane was employed [Figs. 15(a, b)]. The researchers fabricated a series of h-$Ti_3C_2T_x$ membranes with varying thicknesses and assessed their efficacy in filtering MPs using polystyrene (PS) spheres with fluorescent properties of different

sizes. Negative pressure extraction was utilized to obtain the filtered solution through

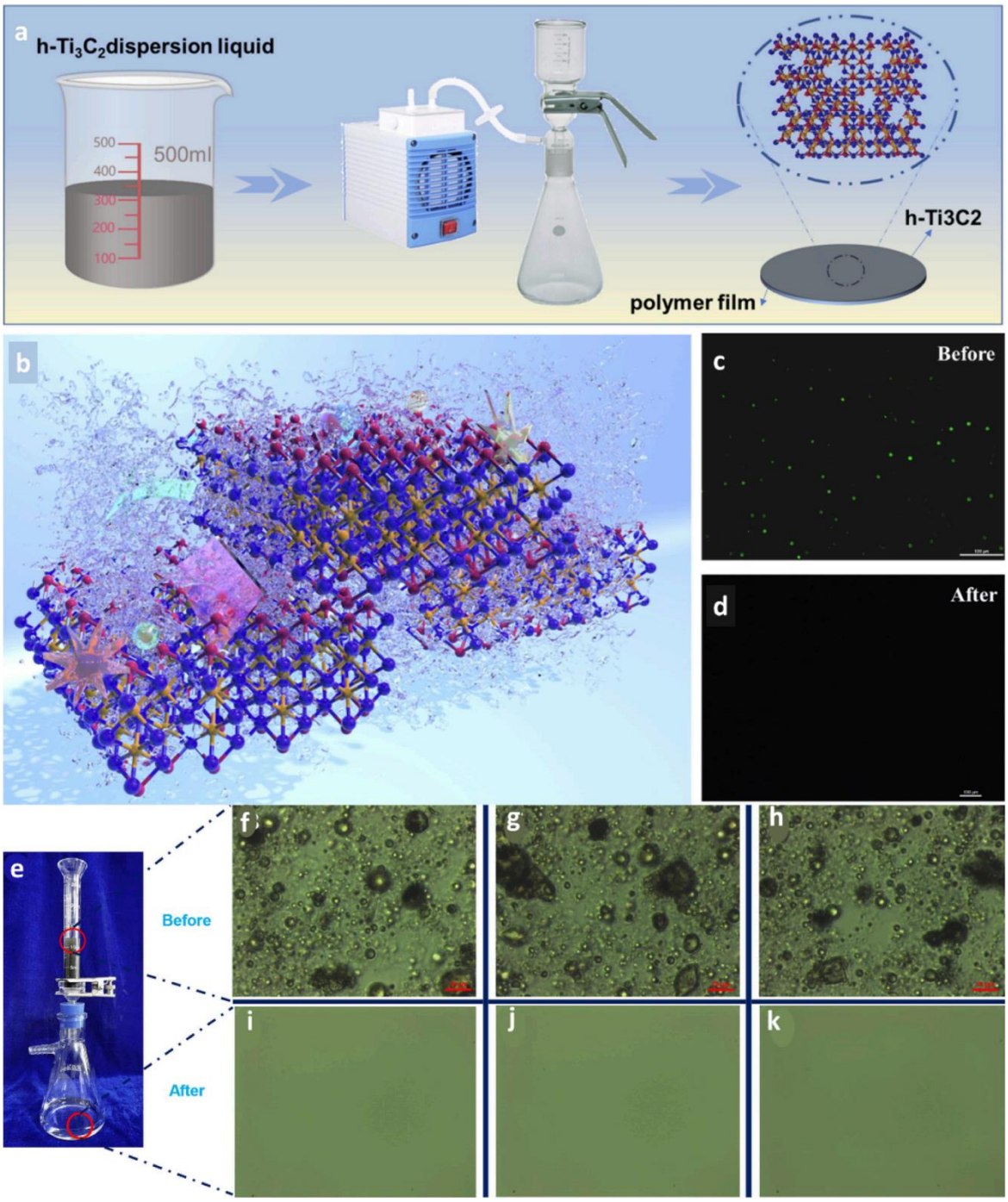


Figure 15. (a) Schematic diagram depicting the synthesis of an MXene h-$Ti_3C_2T_x$ membrane.(b) Scheme illustrating the filtration of microplastics (MPs).(c, d) Images captured from fluorescence microscopy before and after the filtration of wastewater.(e) Real photograph of the filtration setup utilized for wastewater treatment.(f-h) Initial photographs obtained using an optical microscope before the removal process.(i-k) Final photographs acquired using an optical microscope after the removal process, i.e., filtered wastewater (scale bar = 10 µm). From reference [190].

the h-$Ti_3C_2T_x$ membrane. The source solution containing 0.001 mol/l of fluorescent PS was filtered, and microscopic examination revealed significant removal of 100 nm fluorescent PS spheres by the h-$Ti_3C_2T_x$ membrane[Figs. 15(c, d)]. Subsequently, untreated wastewater was collected and filtered through the h-$Ti_3C_2T_x$ membrane to assess its impact on removing MPs and suspended particles in a real environmental context. Fig. 15(e) holds a representation of untreated water. Figs. 15(f-h) and Figs. 15(i-k) demonstrates microscopic images showing the particle size of MPs and suspended particles ranging from half a micrometer to thirty micrometers in the pre-filtered wastewater. However, the h-$Ti_3C_2T_x$ membrane effectively removed these contaminants, as the filtered wastewater showed no particle matter [Figs. 15(i-k)]. This demonstrates the considerable potential of h-$Ti_3C_2T_x$ membranes for removing MPs and emerging contaminants under real-world water conditions.

12. Conclusion

This survey underscores a thorough analysis of recent advancements in utilizing MXene-based adsorbents for purifying water from potentially harmful pollutants such as dyes, heavy metals, and pharmaceuticals. The ability of these materials to remove toxic pollutants from water holds significant promise. MXene-based adsorbents exhibit high adsorption capacities, the potential for regeneration, and a high level of selectivity in removing target pollutants from water. However, despite these promising findings, several challenges hinder their widespread adoption in practical water treatment systems.

Nonetheless, current research indicates that MXenes, two-dimensional (2D) materials, have the potential to revolutionize the energy storage, water treatment, and desalination industries in the near future. Since their discovery in 2011, MXenes have become valuable tools for various industries and environmental protection efforts. Recent studies have demonstrated effective methods for producing various MXene-based adsorbents. Furthermore, research suggests that pure MXenes may not be as effective as MXene-based composites in wastewater cleanup. However, there are still unresolved issues that need to be addressed before MXenes can be widely used.

Additionally, a burgeoning area of research is the development and application of MXene-based membranes for water purification and organic solvent filtration. MXene-based membranes surpass conventional membranes in terms of permeance and the removal of various inorganic and organic pollutants. However, research in wastewater treatment using MXene-based membranes remains limited.

In summary, MXenes, as a materials, hold great promise as adsorbents for removing dyes, metals, and antibiotic contaminants from water. The survey discusses important factors that can enhance these materials for environmental cleanup and provides new insights into MXene synthesis processes. It delves into crucial aspects such as operating conditions, compound characteristics, and the influence of synthesis pathways on MXene-based composites in detail.

Objective and Scope

Objective of the research topic.

The main goal of the research is to come up with a new method for making a material called MXene. MXene has shown promise for various applications due to its unique properties. One area of interest is its potential use in removing certain pollutants, specifically nitrophenol compounds, from the environment. By developing a novel synthetic strategy for producing MXene and studying its performance in pollutant removal, the research aims to contribute to the development of effective solutions for environmental cleanup.

Scope:

- Synthesis Methods: To develop novel synthetic strategy to synthesis $Ti_3C_2T_x$ MXene flakes.
- Characterization Techniques: The scope encompasses a comprehensive characterization of the synthesized nanomaterials using advanced analytical techniques to provide detailed insights into their structure and properties.
- Pollutant Removal: The scope involves investigating the efficacy of $Ti_3C_2T_x$ MXene nanomaterials as a catalyst in removing different types of pollutants commonly found in wastewater.
- Optimization Parameters: The scope includes optimizing various parameters influencing the adsorption process to maximize the removal efficiency of pollutants while minimizing the usage of nanomaterials and energy consumption.
- Reusability Studies: The scope includes study of the reusability of the catalyst by reusing it for more than one catalytic cycle and measuring the change in its catalytic effect. This also takes in measurement of the same sample after a period and the change in its catalytic effect.
- Stability Studies: The scope further carries out the study of the stability of the catalyst by reusing it for more than one catalytic cycle and measuring the change in its catalytic effect
- Practical Applications: The scope extends to exploring the practical application of $Ti_3C_2T_x$ MXene nanomaterials in real-world wastewater treatment scenarios, considering factors such as scalability, cost, and feasibility.

Characterization Tools

Different instrumentations have been employed to confirm the formation of the nanomaterials and also to investigate their interesting characteristics in details. This section describes the basic features and operating principles of some commonly employed instruments commonly used for nanomaterial studies.

1. X-Ray Diffraction (XRD):

The first step after synthesis of a nanomaterial is to confirm its phase purity. X-ray diffraction (XRD) analysis helps in proper identification of the phases of the as-synthesized nanomaterials. After the discovery of X-ray by Roentgen in 1895, gradual research led to the understanding of its diffraction patterns by crystal's atomic planes. This eventually revealed a whole new direction for precisely investigating the structure of matter of either amorphous or crystalline form.

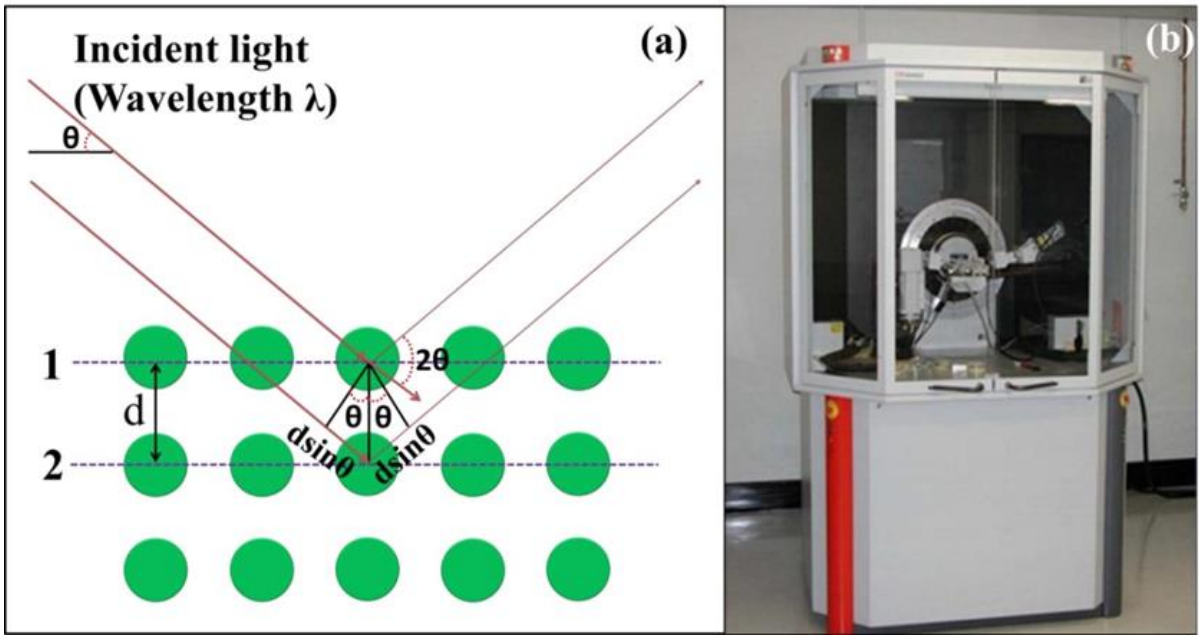


Figure 16. (a) Schematic depiction of Bragg's law, (b) digital image of the experimental set-up of an XRD instrument.

When an X-ray of monochromatic nature is incident on a crystal lattice, reflection of these X-

rays are caused by the atomic planes, where each atom functions as an epicentre of scattering. The schematic representation is shown in where two atomic planes are denoted as 1 and 2. Reflected X-rays from plane 1 and plane 2 will have a path difference in between them. Only those reflected beams will undergo constructive interference when their path difference is an integral multiple of the incident X-ray's wavelength. This phenomenon is described by the Bragg's law [191], which is given as below:

$2d\sin\theta = n\lambda$ ……

where, 'n' is an integer, denoted as the order of diffraction, 'λ' is the incident X-ray beam's wavelength, 'θ' is the glancing angle, also known as the Bragg's angle, and 'd' is the interplanar spacing representing the distance between two consecutive atomic planes.

To carry out the X-ray diffraction analysis of the synthesized nanomaterials in the present work, a Rigaku Ultima III X-ray diffractometer has been employed, the digital image of which is shown in Fig. 16. The diffraction pattern has been recorded in θ-2θ configuration, and Cu Kα X-ray having a wavelength λ of 1.5404 Å has been used as the source of irradiation of the samples under investigation. The diffractometer operates at a voltage of 40 kV and current of 30 mA. To collect the data, the samples have been scanned with a rate of 2^{o}/min. After collection of data, the XRD pattern has been background corrected for further analysis. Additionally, the observed peaks have been confirmed from the International Centre for Diffraction Data (ICDD) resource.

2. Scanning Electron Microscopy

Scanning Electron Microscopy (SEM) is a powerful imaging technique used to visualize the surface morphology and topography of materials at a nanometer to micrometer scale. When applied to nanoparticles, SEM offers valuable insights into their size, shape, distribution, and aggregation, providing crucial information for various scientific and technological applications. Here's a detailed overview of SEM applied to nanoparticles:

Principle of SEM:

SEM operates on the principle of scanning a focused beam of electrons over the surface of a sample. When the electrons interact with the atoms at the sample's surface, various signals are generated, including secondary electrons, backscattered electrons, and characteristic X-rays. These signals are detected and used to create high-resolution images of the sample's surface.

Sample Preparation:

Preparing nanoparticles for SEM analysis requires careful attention to ensure optimal results. Common techniques include:

1. Sample Deposition: Nanoparticles are typically deposited onto a substrate, such as a silicon wafer or a conductive carbon tape, using methods like drop-casting, spin-coating, or vacuum deposition.
2. Fixation: To prevent aggregation or movement of nanoparticles during analysis, they may be fixed onto the substrate using adhesives or chemical treatments.
3. Drying: Nanoparticle samples are often dried thoroughly to remove any residual solvent or moisture, which can interfere with imaging.

Imaging Modes:

SEM offers various imaging modes, each providing specific information about the sample:

1. Secondary Electron Imaging (SEI): This mode detects secondary electrons emitted from the sample's surface due to electron beam interactions. SEI provides high-resolution images revealing surface morphology and topography.
2. Backscattered Electron Imaging (BEI): BEI detects electrons that are backscattered from the sample's bulk. It provides contrast based on atomic number variations, making it useful for distinguishing different materials and phases within the sample.
3. Energy-Dispersive X-ray Spectroscopy (EDS): EDS enables elemental analysis by detecting characteristic X-rays emitted when the sample is bombarded with electrons. It provides qualitative and quantitative information about the chemical composition of nanoparticles.
4. Electron Backscatter Diffraction (EBSD): EBSD maps crystallographic orientations and grain boundaries within nanoparticles, aiding in the analysis of their crystalline structure and texture.

3. Field emission scanning electron microscope (FESEM):

FESEM analysis is performed to examine the morphologies of the as-prepared samples in the present investigation. It is an electron microscopy instrument operating in a high-vacuum system and employs an electron beam emitted from a field emission source. The interaction between an electron beam and the atoms of a matter results in two kinds of scattering phenomena: elastic and inelastic. For electrons which are scattered elastically, their direction can change with collision, but their velocity and kinetic energy remain constant. Conversely, for inelastic scattering, the incident beam of electrons has the ability to displace the electrons from the orbits surrounding the nuclei of the atom of the sample under investigation. These interacting electrons can generate signals depending upon the target sample's morphology as well as composition. Moreover, secondary electrons are generated due to the interaction occurring between the surface of the sample and the incident electron beam, and these electrons can be converted into voltage.

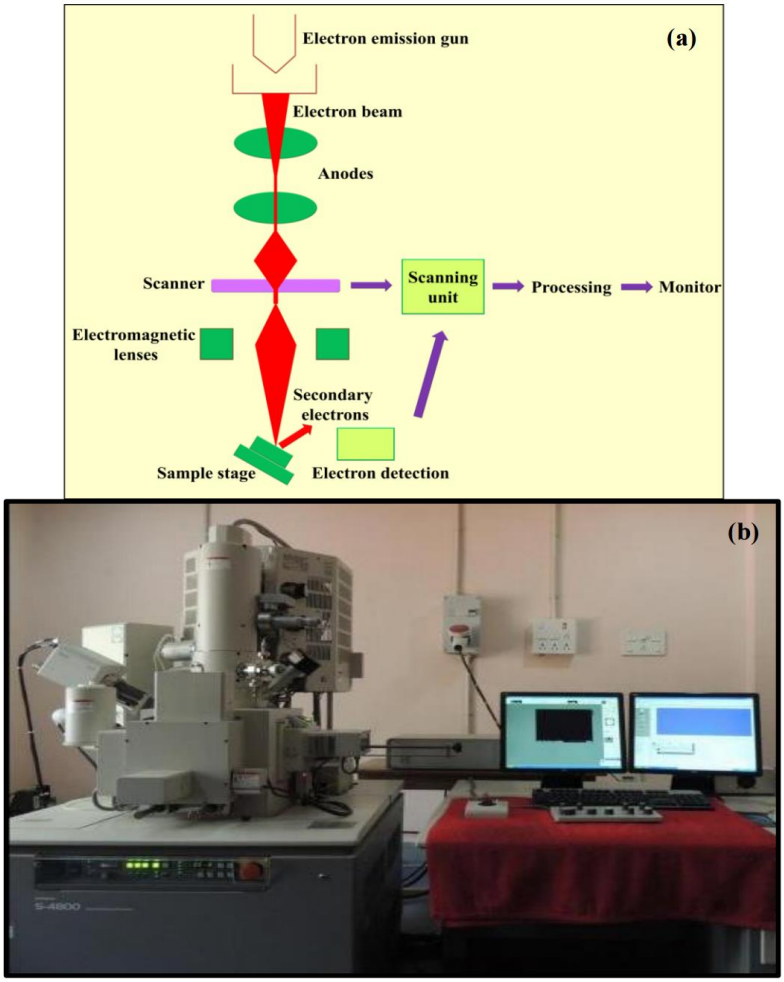


Figure 17. (a) Schematic depiction of working principle of FESEM, (b) digital image of the experimental set-up of an FESEM instrument.

The machine consists of a field emission gun to produce an electron beam, electromagnetic lenses and apertures for focusing the electron beam, a detector, and an ultra-high vacuum system. The electron gun has the capability to generate a stable beam of electron having characteristics of (i) high current, (ii) small spot size, (iii) adjustable energy, and (iv) small dispersion of energy. Tungsten hairpin or lanthanum hexaboride (LaB6) are employed as the field emission sources in modern-day FESEM instruments. A high intensity electric field formed on the very finely oriented tip of the source (which acts as the cathode) facilitates the electron emission. These electrons are attracted towards the anode, forming a powerful electron beam. The electron beam is finally focused strongly on the material under investigation by the combined help of the various types of electromagnetic lenses and apertures. These lenses are also used to control the size and position of the electron beam.

In the present works, an FESEM instrument (FESEM, S-4800, Hitachi) developed by Hitachi has been utilised in studying the morphologies of the samples. The machine operates at an accelerating voltage less than 15 kV. For samples with insulating properties, coating of its surface with Au or Ag nanoparticles is required to exclude the surface charge imbalance and to achieve better resolution. Powder samples are pasted on carbon tape prior to measurement. The digital image of an FESEM instrument is provided in Fig. 17(b). Generally, energy-dispersive X-ray spectroscopic analysis (EDS) is performed in association with FESEM measurement. EDS is an efficient analytical tool to analyse the elemental composition of the specimens under investigation. During EDS measurement, inside an electron microscope, bombardment of the target material is done by an electron beam. The incident electrons with high intensity undergo collision with the target sample's atom, thus knocking off some of the electrons from the inner shells of the atom in the process. The void left behind by the inner shell electrons after their emission is eventually filled up by the electrons from the outer shell have higher energy. The energy difference existing between the higher energy and the lower energy shells are released or emitted as X-rays from the atoms. X-ray energies are characteristic of the element's atomic structure from which they are emitted, thereby facilitating in measuring the chemical composition of the sample. In the present works, EDS analysis has been performed by an EDS part attached with the FESEM

Hitachi instrument. This attachment has been manufactured by Thermo Scientific having the model: Noran System - Thermo Scientific UltraDry EDS Detector.

4. Ultraviolet-Visible Spectroscopy (UV-Vis):

Optical properties of a material are measured by UV-Vis spectroscopy. This method generally, refers to absorption, transmittance, or reflectance spectroscopy in the UV, visible, and near IR range of the electromagnetic spectrum. The underlying concept of this technique is the absorption of photon energy by a material corresponding to UV or visible wavelength, resulting in the generation of distinct spectra in the UV-visible region. The photon energy absorbed by the sample material corresponds to its band gap energy. When a material absorbs a photon, excitation of an electron occurs to higher energy states or molecular orbitals (MO) denoted as the excited states

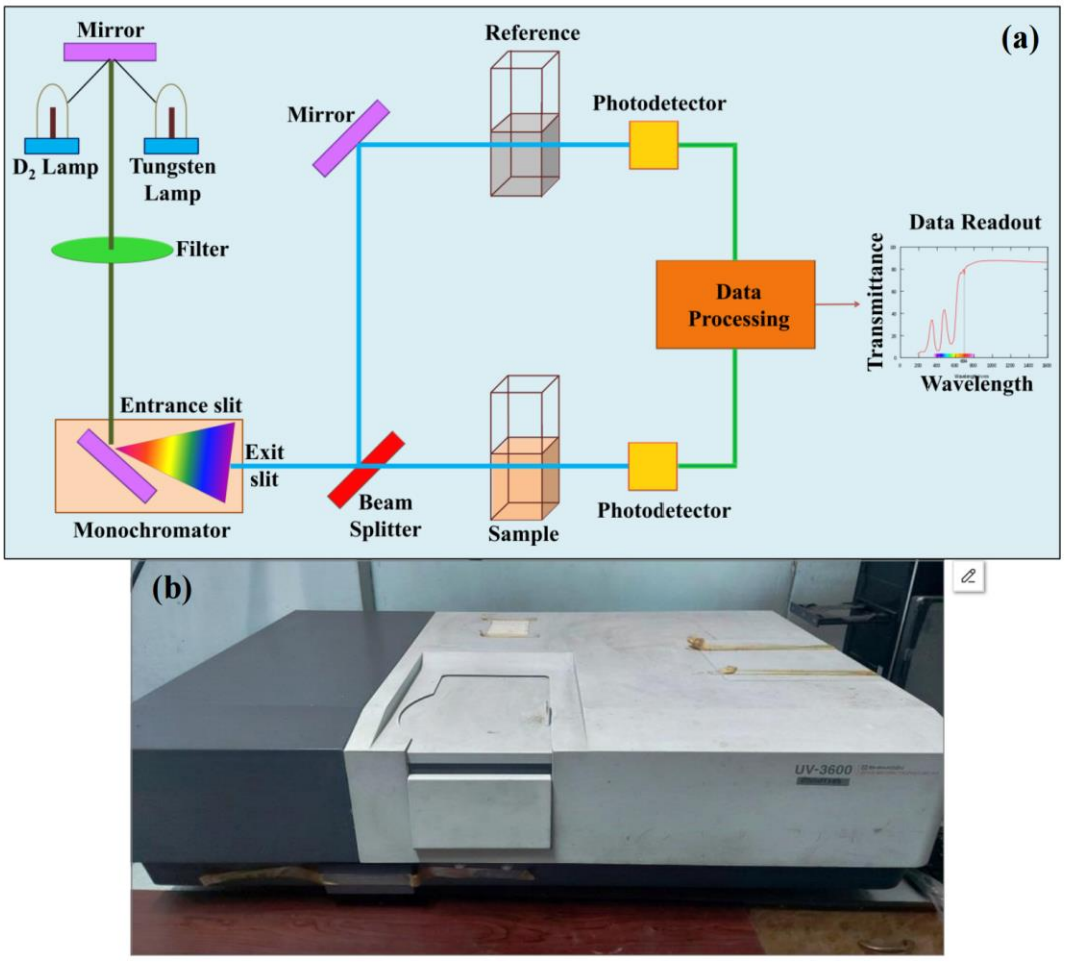


Figure 18. (a) Schematic depiction of working principle of UV-Vis, (b) digital image of the experimental set-up of an UV-Vis instrument.

The concept of absorption of light by a material is explained from two laws, Lambert's law and Beer's law. The UV-vis measurement of a material dispersed in a solvent is carried out in a cuvette made of quartz material. A photon is incident on this cuvette with an intensity of I0. Some of the photon energy is absorbed by the material and the rest gets transmitted through the material with a reduced intensity of I. The ratio of (I/I0) is known as the transmittance (T). Absorbance (A) of a material is defined as (- log10T), which represents the amount of photon energy absorbed by the molecules in a material. The Lambert's law states that this absorbance has a direct proportional relation to the cuvette's thickness (10 mm) that is the path length traversed by the light. Beer's law states that concentration of the material in the solution is directly proportional to the absorbance. Combination of these two laws gives the Beer-Lambert's law stated below

$$\boldsymbol{log_{10}\left(\frac{I_0}{I}\right) = A = \alpha cd}$$

where, 'α' is a constant termed as molar absorptivity, 'c' is concentration of the solution, and 'd' is the path length. A schematic depiction is given in Fig. 18(a). The constituent parts of an UV-vis spectrometer along with the digital image of the instrument are given in Fig. 18 (b). The instrument consists of: (i) a light source, (ii) a monochromator; which is again composed of an entrance slit, a dispersive element, and an exit slit, and (iii) a detector. UV-vis measurement of a material is primarily performed to calculate its band gap, which helps in providing information about the opto-electronic properties of the material. In case of liquid samples, homogenous solutions, solid samples which can be uniformly dispersed in a solvent, and thin-film samples, UV-vis measurement in absorbance or transmittance mode is performed to calculate their respective band gaps following Tauc's plot method. Conversely, for powder samples, measurement is done in reflectance mode (also known as diffuse reflectance spectroscopy or DRS), and in this case Kubelka-Munk method is employed for calculating the optical energy gaps of the samples. The Tauc's equation and Kubelka-Munk equation are given as equation

$$\boldsymbol{\alpha h\upsilon = A(h\upsilon - E_g)^n}$$

$$\boldsymbol{[F(R_\infty)h\upsilon] = A(h\upsilon - E_g)^n}$$

$$\boldsymbol{[F(R_\infty)] = \frac{k}{s} = \frac{(1-R_\infty)^2}{2R_\infty}}$$

where, ‘A’ is a constant, ‘υ’ is denoted as the light-wave’s frequency, ‘Eg’ is the band gap, ‘k’ is the absorption coefficient (similar to α), ‘s’ is the scattering coefficient, ‘R∞’ is the diffuse reflectance, and [F(R∞)] is the Kubelka-Munk function. ‘n’ represents the nature of electronic transition, whether the transition is direct or indirect in nature. Values of ‘n’ as 1/2, 3/2, 2, and 3 denote direct allowed, direct forbidden, indirect allowed, and indirect forbidden transitions respectively. Tauc’s plot is a typical plot between (αhυ)1/n in the ordinate and (hυ) in the abscissa. A tangent is drawn passing through the linear region of this plot which cuts the x-axis at a particular value, denoted as the band gap Eg value. The UV instrument used in the research works is Shimadzu 3600 UV-Vis-NIR spectrophotometer, which employs deuterium lamp as the source of light for the UV range, and halogen lamp as the light source for visible and near IR range. For measuring the reflectance of a powder sample, barium sulphate is employed as the reference since it exhibits 100 % reflectance in the UV-vis-NIR region. For absorbance measurement of a sample dispersed in a solvent, the solvent without the sample dispersed in it is considered as the reference.

5. High-resolution transmission electron microscope (HRTEM):

HRTEM is an important and useful tool for characterisation purpose of microstructure of the nanomaterials along with their detailed crystal structure at atomic level by implementing the concept of diffraction and imaging technologies. In contrast to FESEM analysis, whose resolution is only limited up to the nanometric scale; HRTEM can provide detailed information about the inter-lattice spacing (d) of the nanomaterial under investigation. The accelerating voltage of electrons in HRTEM is much higher (about 160-300 kV) as compared to FESEM (5-30 kV). Such high accelerating voltage enables the electrons to move almost with the speed of light, resulting in much higher resolution of images. Like FESEM, HRTEM also operates in a high-vacuum (~ 10-10 Pa) system. In a conventional HRTEM instrument, an electron beam having uniform current density is generated from an electron gun source which is either made of tungsten or LaB6. The instrument employs sets of electromagnetic lenses made of Cu, and they are: (i) two condenser lenses, (ii) one objective lens, and (iii) six image forming lenses. The electron beam passes through these series of lenses along with apertures to illuminate the sample. The collimated electron beam gets transmitted through the nanomaterial and the corresponding image is digitally recorded with help of a charge coupled device (CCD) camera. The working principle of HRTEM along with its digital image is displayed in Fig. 19(a,b). For investigating the nanostructures of the as-synthesized samples, minute quantity of the powder sample is first uniformly dispersed in a solvent (preferably ethanol) by ultrasonication. Then

the solution is carefully drop-casted on a carbon-coated copper grid. After the grid is properly dried, the sample is used for measurement using an HRTEM instrument manufactured by JEOL (model: JEOL JEM-2100).

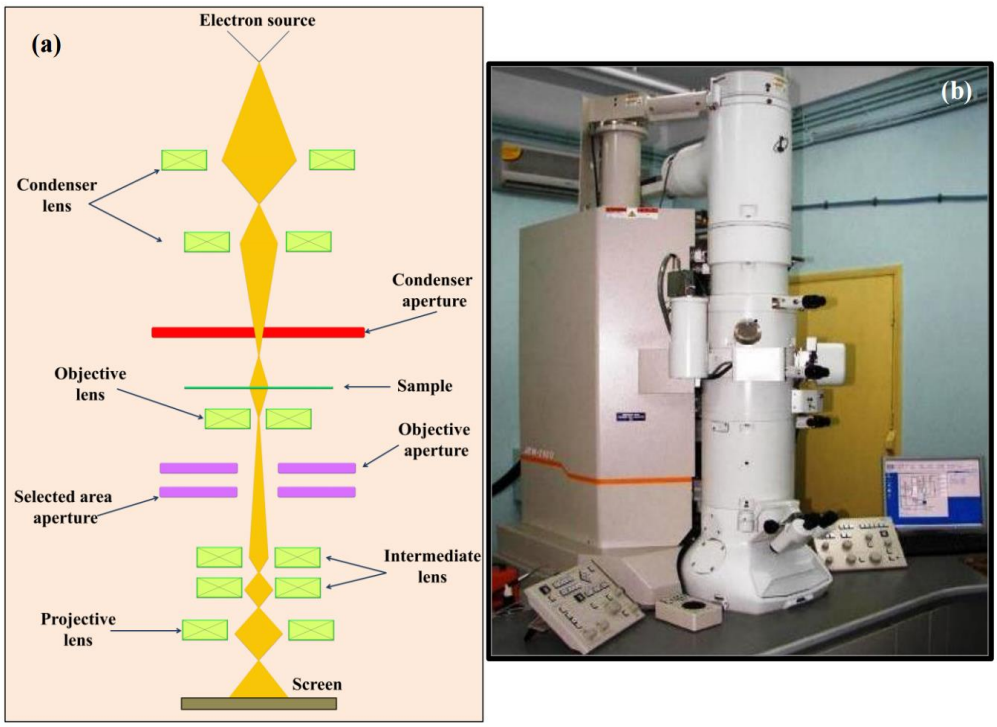


Figure 19. (a) Schematic depiction of working principle of HRTEM, (b) digital image of the experimental set-up of an HRTEM instrument.

Methodology

Materials

Ti_3AlC_2 (200 mesh, 98 wt.%) was purchased from Nanoshed Company.

KOH (AR). HCl , LiF, 4-nitrophenol, all these materials of highest purity were purchased from Merck. Deionized water was used throughout all experimental procedures.

All reagents were used without further purification. Synthesis of $Ti_3C_2T_x$ MXene flakes.

Synthesis of catalyst

Ti_3AlC_2 nanofibers (NFs) were initially produced through a hydrolysis process involving 2 grams of Ti_3AlC_2 added to a 20 mL solution of 6M KOH. The mixture was stirred for 96 hours at room temperature, followed by centrifugation and washing with deionized water until reaching a pH of approximately 7. Subsequently, the material was dried at 40 degrees Celsius for 24 hours to yield Ti_3AlC_2 NFs. $Ti_3C_2T_x$ MXene were then synthesized by selectively etching aluminium from the Ti_3AlC_2 NFs [193]. During this procedure, a solution comprising 25 mL of hydrochloric acid (11.8 M), 25 mL of water, and 0.7 g of lithium fluoride was introduced into a 400 mL Teflon autoclave. Following this, Ti_3AlC_2 precursor was included. The autoclave was tightly sealed and placed in an oven at 140°C for 24 hours. Subsequently, the resulting mixture underwent centrifugation and was rinsed with deionized water to stabilize the pH. The material was then dried under a nitrogen atmosphere at 30°C for 24 hours, yielding $Ti_3C_2T_x$ flakes.

Traditional $Ti_3C_2T_x$ flakes were synthesized by directly etching bulk Ti_3AlC_2 with HF. Typically, 0.5 grams of Ti_3AlC_2 were added to a 10 mL solution of 40 wt.% HF and stirred for 72 hours at 40 degrees Celsius. After centrifugation and washing with deionized water until pH neutrality, the material was dried at 30 degrees Celsius for 24 hours under a nitrogen atmosphere to obtain $Ti_3C_2T_x$ flakes [192].

$Ti_3AlC_2 + 3HF = Ti_3C_2 + AlF_3 + 3/2H_2$

Characterization of catalyst

The microstructure was examined using scanning electron microscopy, while transmission electron microscopy was employed to study the structure of $Ti_3C_2T_x$ MXene flakes. X-ray photoelectron spectroscopy was utilized to analyse the elemental composition and chemical bonds present in $Ti_3C_2T_x$ MXene.

The synthesis process for $Ti_3C_2T_x$ nano particles is outlined in Fig. 19a [192]. Initially, Ti_3AlC_2 MAX NFs were produced through the hydrolysis of Ti_3AlC_2 MAX phases in a 6 M KOH solution with vigorous stirring. In Fig. 19b SEM image of Ti_3AlC_2 revealed the surface morphology and structure of the material at a microscale level.

Further comparison of the XRD spectra between Ti_3AlC_2 flakes and the resulting $Ti_3C_2T_x$ MXene flakes is illustrated in Fig. 19c. All XRD peaks of MXene closely match those of $Ti_3C_2T_x$ MXene flakes and previously reported $Ti_3C_2T_x$ MXene synthesized using the conventional HF etching method from bulk Ti_3AlC_2 [193].

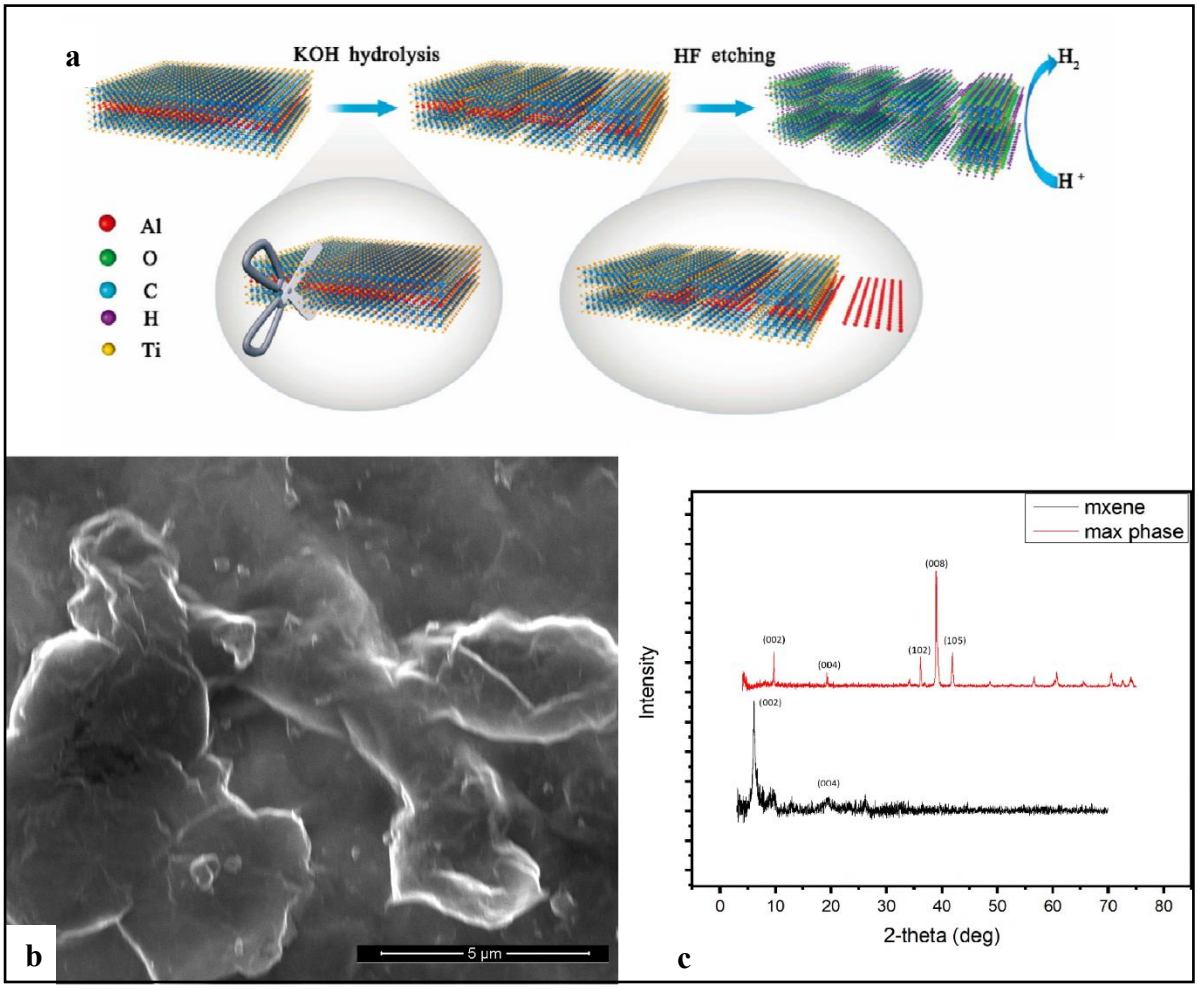


Figure 20. (a) The schematic diagram for synthesis of $Ti_3C_2T_x$ MXene nano particles. From reference [192]. (b) SEM image of $Ti_3C_2T_x$ MXene nano particles (c) XRD spectra of $Ti_3C_2T_x$ MXene nano particles.

6. Catalytic hydrogenation reactions:

Catalytic hydrogenation technique for reduction of pollutant compounds employs a cheap and convenient reducing agent (preferably sodium borohydride, $NaBH_4$) along with a suitable catalyst nanomaterial, and the process takes place in absence of any source of irradiation. The concept of this type of reduction reactions is solely based on the relay or transport of electrons from the $NaBH_4$ compound to the organic pollutant compounds via the catalyst material. The primary criterion for initiating this type of reaction is the proper adsorption of both $NaBH_4$ and pollutant compounds on the catalyst's surface. Moreover, the catalyst material should be capable of providing a smooth transmission channel for the passage of electrons from $NaBH_4$ to the pollutants. The sources of H+ and electron required for the pollutant reduction process are identified as H_2O and $NaBH_4$ respectively. These active charges following a series of chemical reactions can reduce the toxic pollutants to their less-toxic or non-toxic forms. There are plenty of on-going researches to unravel the plausible reactions that occur during catalytic hydrogenation method; however, there are very few reports which have been able to successfully prove them. Nonetheless, this extremely rapid, cost-effective, simple, and efficient method has been extensively employed to perform the reduction of various toxic compounds commonly existing in wastewater. In the present works, we have tried to provide some fundamental ideas regarding this technology following substantial theoretical calculations. The detailed discussions will be provided in the following chapters.

Results and Observation

The catalytic performance of $Ti_3C_2T_x$ MXene was assessed using the reduction of 4-Nitrophenol (4-NP) to 4-Aminophenol (4-AP) in the presence of excess $NaBH_4$ as a model reaction. Time-dependent UV-Vis absorption spectroscopy was employed to monitor the catalytic evolution process, allowing for the observation of changes in absorption spectra over time as the reaction progresses.

From Fig. 21, it is evident that the mild yellow-coloured 4-nitrophenol (4-NP) solution, when dissolved in water, exhibits an absorption peak at 316 nm in its pristine condition. Upon addition of $NaBH_4$, this peak undergoes a significant shift to a higher wavelength, around 400 nm, indicating the formation of 4-nitrophenolate ions. Additionally, the solution's color changes to bright yellow in the presence of $NaBH_4$.

As the reaction progresses, the peak at 400 nm gradually disappears, while a new peak emerges around 297 nm. This suggests the formation of 4-aminophenol (4-AP) through the reduction of 4-NP in the presence of $NaBH_4$. Finally, after the completion of the reaction procedure, the solution turns colourless. The time dependent UV-Vis absorption spectroscopy can be used to monitor the catalytic evolution processes.

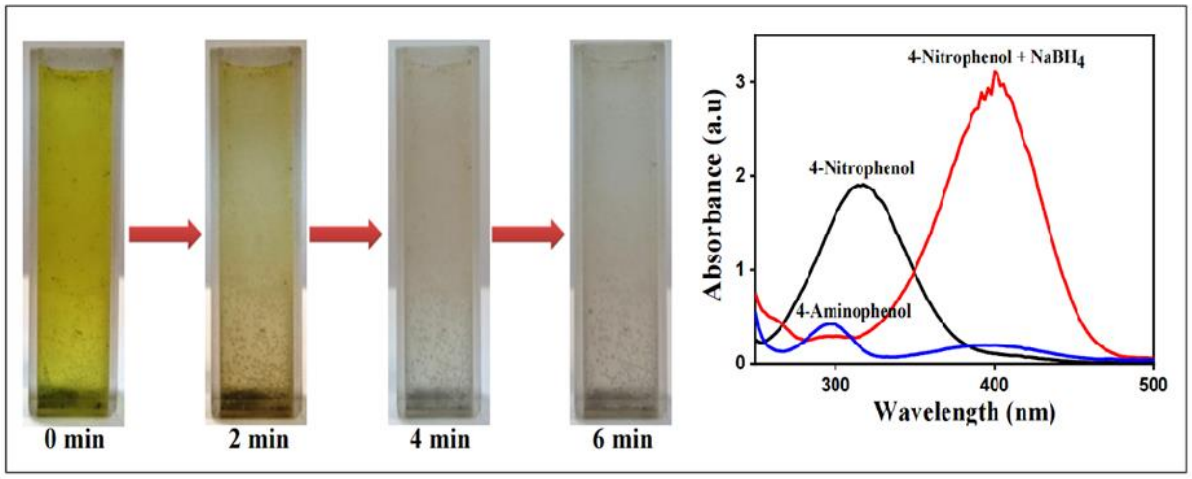


Figure 21. Absorption spectra of pure 4-NP solution without $NaBH_4$ addition, absorption after addition of $NaBH_4$ in 4-NP solution, and absorption spectra of 4-aminophenol; digital images showing the gradual transformation of 4-NP to 4-AP in presence of $Ti_3C_2T_x$ MXene catalyst and $NaBH_4$.

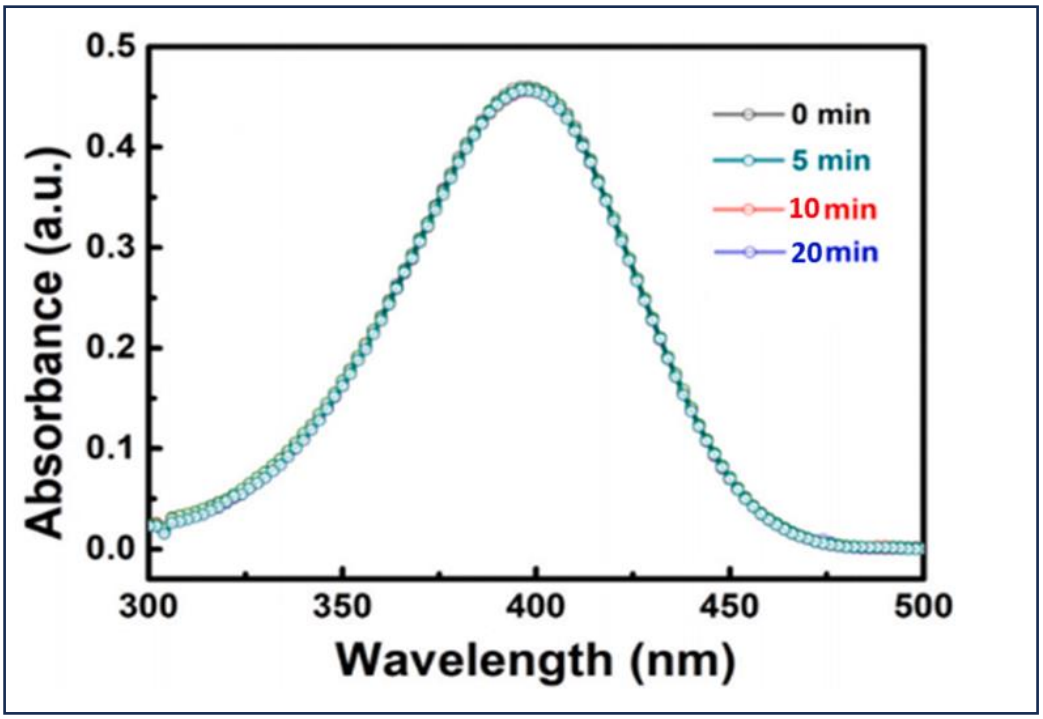


Figure 22. Absorbance spectra of 4-Nitro phenol and $NaBH_4$ in absence of catalyst over a time of 20 minutes.

It is observed that $NaBH_4$ at 1mM is entirely inactive without the catalyst in the reductive transformation of 4-NP; as there is no observable change in the peak absorbance at 400 nm as shown in the graph in Fig. 22.

Addition of $Ti_3C_2T_x$ MXene nano particles in the mixture of 4-Nitro phenol and $NaBH_4$ even at a small proportion initiates the reaction.

With increase in $Ti_3C_2T_x$ MXene nano particles concentration the change in rate of reaction. The absorbtion peak formed observed near 300 is formation of 4-Aminophenol.

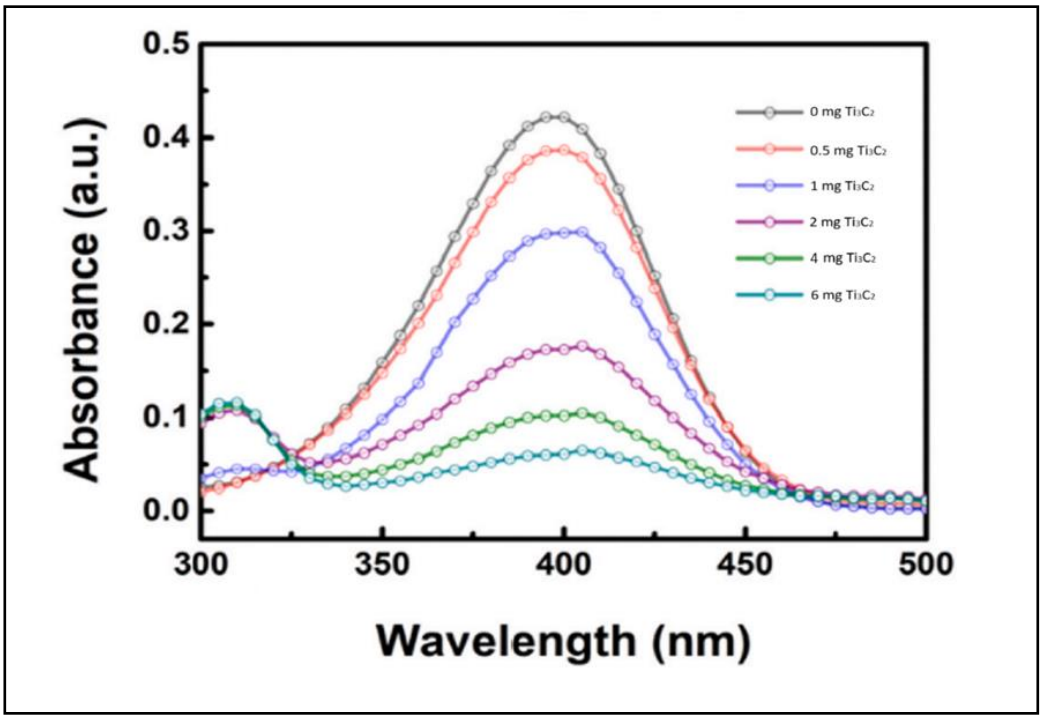


Figure 23. Absorbance spectra of mixture of 4-Nitro phenol and $NaBH_4$ in presence of different dose of catalyst after a time of 5 minutes.

The absorption spectra of 1 millimolar (mM) 4-Nitrophenol (4-NP) and 1 mM $NaBH_4$ in the presence of varying concentrations of the $Ti_3C_2T_x$ MXene catalyst are illustrated in Fig. 23. The graph represents the decrease in pollutants over a span of 5 minutes, with no catalyst as the reference point. As the concentration of the catalyst is raised from 0.5 milligrams to 6 milligrams while keeping other variables constant, there is a noticeable decrease in pollutants within the 5-minute duration. This decrease in pollutant concentration accelerates with higher amounts of catalyst in the solution, likely due to the increased availability of catalytic active sites.

The mechanism for the catalytic reduction of 4-NP typically involves electron transfer from the BH_4- donor to the 4-NP acceptor, thereby enhancing reduction efficiency significantly. The most efficient catalytic reduction seems to be at 2mg $Ti_3C_2T_x$ at the given concentation of pollutant .However, further increasing the catalyst dosage beyond this certain point does not accelerate the reaction further, as the concentration of $NaBH_4$ is fixed and contributes electrons to the solution. Therefore, the electron transfer behavior mediated by catalysts is critical to the observable catalytic performance.

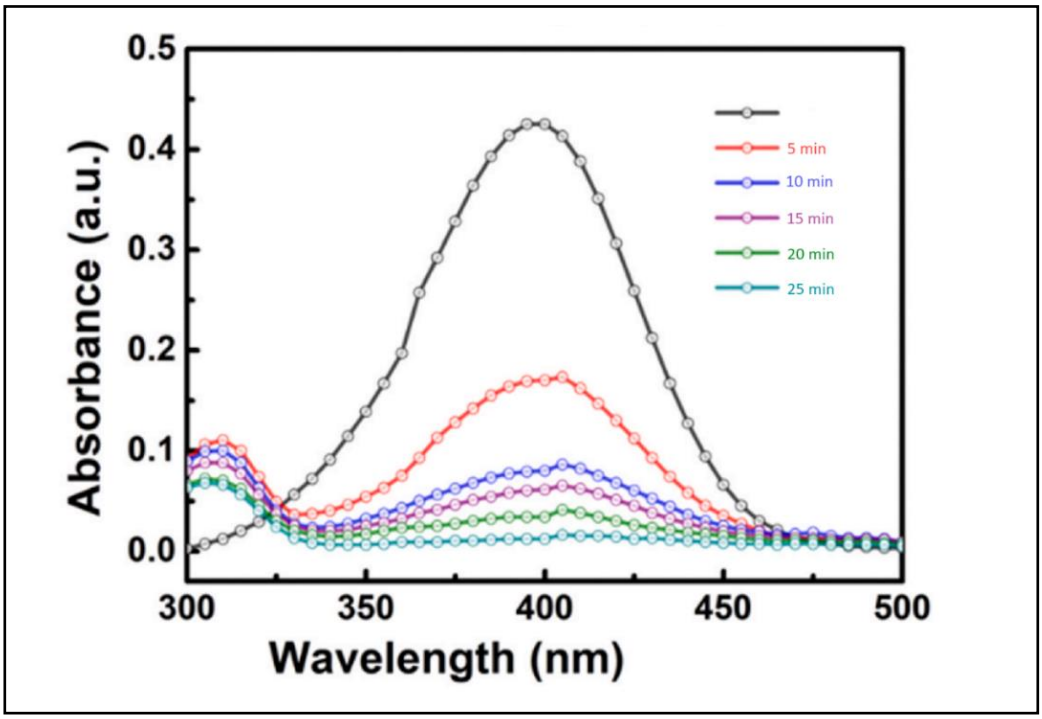


Figure 24. Absorbance spectra of mixture of 4-Nitro phenol and $NaBH_4$ in constant concentration $Ti_3C_2T_x$ MXene of 2 mg.

These results demonstrate that $Ti_3C_2T_x$ MXene nano particles exhibits activity in catalyzing the reduction reaction of 4-NP.

The graph in Fig. 24 illustrates the absorption spectra of 1 mM 4-Nitrophenol and 1 mM $NaBH_4$ in the presence of a constant concentration of $Ti_3C_2T_x$ (2 mg) over time. As time progresses, there is a gradual decrease in the peak intensity around 400 nm. Concurrently, a new peak emerges around 297 nm. This observed phenomenon indicates the formation of 4-aminophenol (4-AP) through the reduction of 4-Nitrophenol (4-NP) in the presence of $NaBH_4$.

Reusability test of the catalysts:

The stability of the catalyst was examined by reusing it for more than one catalytic cycle. Freshly prepared $Ti_3C_2T_x$ underwent a stability test, where the catalyst was subjected to a series of cycles. In each cycle, 6 mg of Ti_3C_2 was extracted from the dye-$NaBH_4$ solution after completing the catalytic process, followed by filtration, repeated washing with DI water, and drying at 50°C to obtain the product. However, as depicted in Fig. 25, the rate constant values showed a significant decrease with each subsequent cycle, indicating a gradual loss of

efficiency. By the third wash, the catalyst exhibited no catalytic activity, suggesting that $Ti_3C_2T_x$ lacked available active catalytic sites.

Stability test of the catalysts:

The same $Ti_3C_2T_x$ catalyst was stored in an air tight glass bottle for 45 days. Similar test was performed with the sample. The process involved retrieving the used catalyst, which consisted of 6 mg of $Ti_3C_2T_x$ catalyst, from the dye-$NaBH_4$ solution once a specific catalytic cycle was completed. The catalytic test was performed for an interval of 25 minutes. Even if the reaction was incomplete the sample was filtered, followed by multiple washes with deionized (DI) water. Subsequently, the catalyst was dried at 50°C to obtain the final product. As observed in Fig. 26 the reduction of 4-Nitrophenol was poor. The catalyst degraded over time and by second wash is barely reactive.

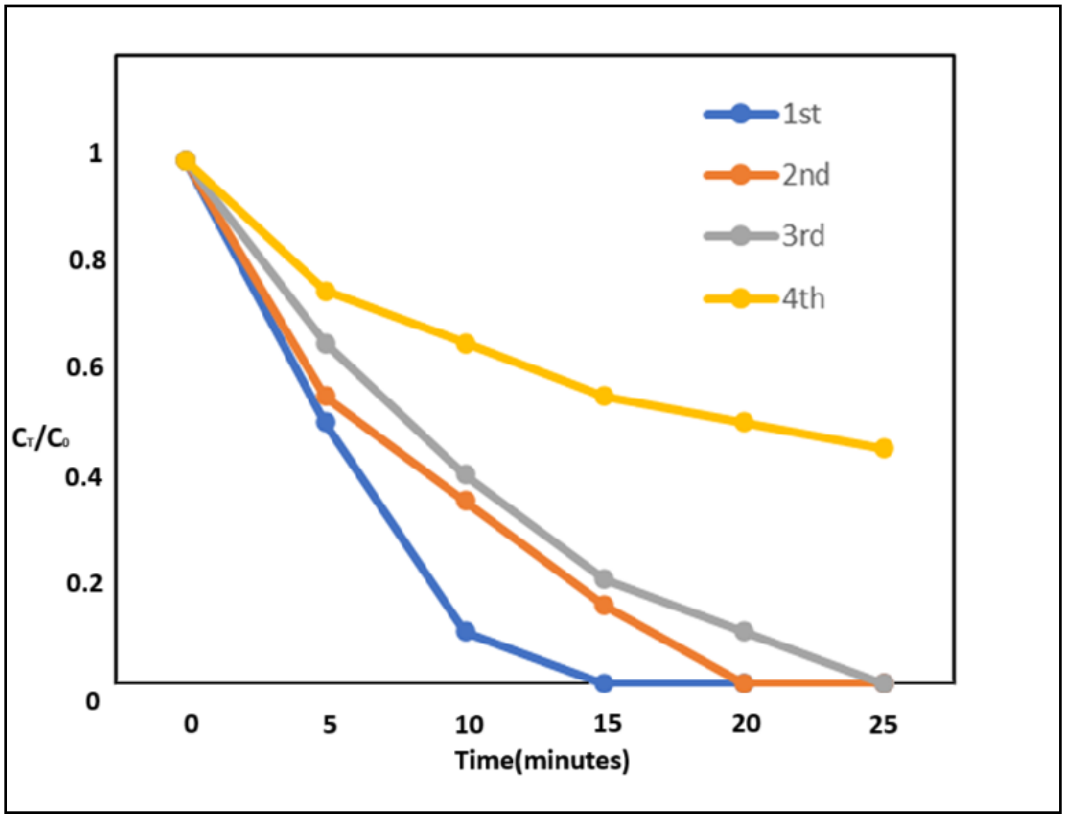


Figure 25. The catalytic activity of freshly prepared $Ti_3C_2T_x$ MXene was evaluated for its ability to degrade 4-Nitrophenol (4-NP) over four consecutive cycles. The efficiency of 4-NP degradation was assessed after each cycle to determine the stability and effectiveness of the $Ti_3C_2T_x$ catalyst over multiple cycles.

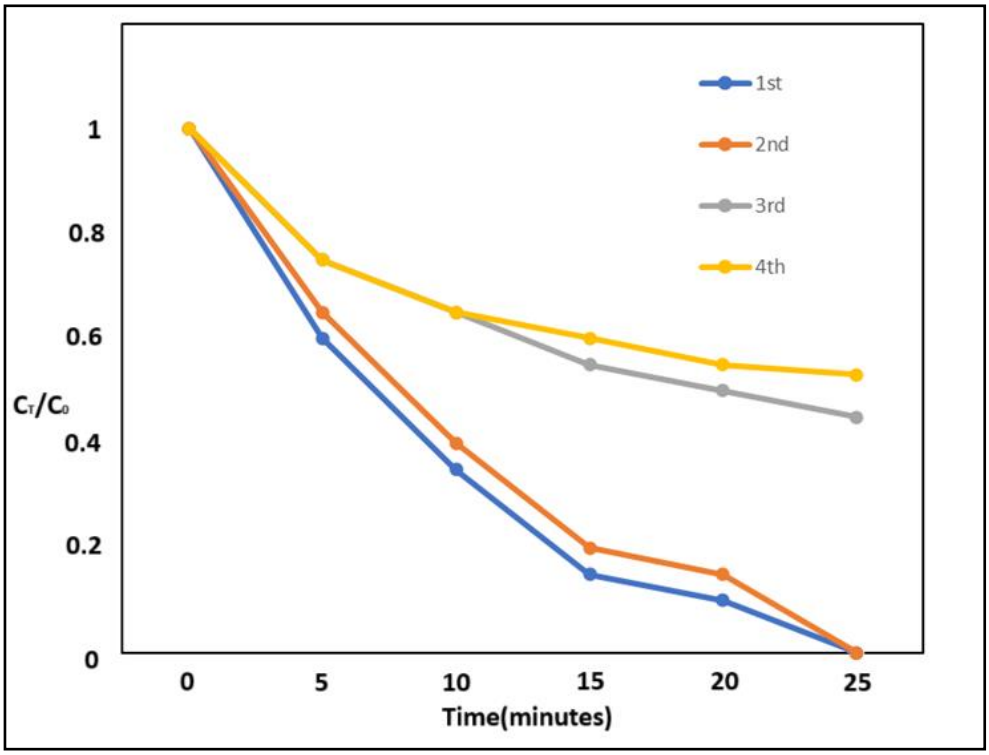


Figure 26. The catalytic activity of $Ti_3C_2T_x$ prepared 60 days prior was assessed for its ability to degrade 4-Nitrophenol (4-NP) over four cycles. The efficiency of 4-NP degradation was evaluated after each cycle to determine the stability and effectiveness of the $Ti_3C_2T_x$ MXene catalyst over time.

Future Scope

The future scope for $Ti_3C_2T_x$ MXene in the catalytic reduction of pollutants is promising, driven by its unique properties and potential applications in environmental remediation. Here's a detailed overview of the future prospects:

1. Enhanced Catalytic Performance:

$Ti_3C_2T_x$, as a member of the MXene family, possesses high surface area, tunable surface chemistry, and excellent electrical conductivity. These properties make it a promising candidate for catalytic applications, including the reduction of pollutants such as heavy metals, organic dyes, and other toxic compounds. Future research aims to optimize the catalytic performance of $Ti_3C_2T_x$ by modifying its surface chemistry, controlling its nanostructure, and exploring novel synthesis methods.

2. Selective Catalysis:

One of the key challenges in pollutant degradation is achieving high selectivity towards target compounds while minimizing side reactions. $Ti_3C_2T_x$ -based catalysts offer the potential for selective catalysis through precise control over surface functionalization and catalytic active sites. Future studies will focus on designing $Ti_3C_2T_x$ catalysts with tailored surface properties to enhance selectivity towards specific pollutants, thereby improving overall catalytic efficiency.

3. Heterogeneous Catalysis in Water Treatment:

$Ti_3C_2T_x$ -based catalysts show promise for application in heterogeneous catalysis for water treatment. By leveraging the abundant active sites and rapid electron transfer kinetics of $Ti_3C_2T_x$, researchers aim to develop efficient catalysts for the removal of pollutants from water sources. Future research directions include exploring the scalability, stability, and recyclability of $Ti_3C_2T_x$ catalysts for large-scale water treatment applications.

4. Photocatalytic and Electrocatalytic Applications:

In addition to traditional heterogeneous catalysis, $Ti_3C_2T_x$ exhibits potential in photocatalytic and electrocatalytic applications for pollutant degradation. By harnessing its excellent light

absorption properties and efficient charge transport capabilities, $Ti_3C_2T_x$ -based catalysts can drive photocatalytic and electrocatalytic reactions for pollutant remediation under solar irradiation and electrochemical conditions. Future efforts will focus on optimizing the photocatalytic and electrocatalytic performance of $Ti_3C_2T_x$ catalysts through structural engineering and surface modification strategies.

5. Synergistic Catalytic Systems:

Future research may explore the integration of $Ti_3C_2T_x$ with other catalytic materials to create synergistic catalytic systems with enhanced performance and multifunctionality. By combining the unique properties of $Ti_3C_2T_x$ with those of other nanomaterials, such as metal nanoparticles, metal oxides, or carbon-based materials, researchers can develop hybrid catalysts with tailored properties for specific pollutant degradation reactions. Synergistic catalytic systems hold promise for overcoming existing limitations and achieving breakthroughs in pollutant remediation technology.

In summary, the future scope for $Ti_3C_2T_x$ in the catalytic reduction of pollutants is wide-ranging, encompassing enhanced catalytic performance, selective catalysis, water treatment applications, photocatalytic and electrocatalytic processes, and synergistic catalytic systems. Continued research efforts aimed at exploring and harnessing the unique properties of $Ti_3C_2T_x$ will drive advancements in environmental catalysis and pave the way for sustainable solutions to pollution challenges.

References

[1] P. Jangid, P. and M.P. Inbaraj, Mater. Today: Proc., 2021, 43, 2877-2881.

[2] https://www.nano.gov

[3] T.A. Saleh, Environ. Technol. Innov., 2020, 20, 101067.

[4] K. Sakaushi and M. Antonietti, Acc. Chem. Res., 2015, 48, 1591-1600.

[5] Y. Wang, X. Wang and M. Antonietti, Angew. Chem. Int. Ed., 2012, 51, 68-89.

[6] Q. Yang, W. Wang, Y. Zhao, J. Zhu, Y. Zhu and L. Wang, RSC Adv., 2015, 5, 54978-54984.

[7] Q. Lu, K. Eid, W. Li, A.M. Abdullah, G. Xu and R.S. Varma, Green Chem., 2021, 23, 5394-5428.

[8] J. Ehrmaier, T.N. Karsili, A.L. Sobolewski and W. Domcke, J. Phys. Chem. A, 2017, 121, 4754-4764.

[9] S.C. Yan, Z.S. Li and Z.G. Zou, Langmuir, 2009, 25, 10397-10401.

[10] Y. Wang, J. Yao, H. Li, D. Su and M. Antonietti, J. Am. Chem. Soc., 2011, 133, 2362-2365

[11] J.T. Jasper, Y. Yang, M.R. Hoffmann, Toxic Byproduct Formation during Electrochemical Treatment of Latrine Wastewater, Environ. Sci. Technol. 51 (12) (2017) 7111–7119.

[12] G. Saxena, D. Purchase, S.I. Mulla, G.D. Saratale, R.N. Bharagava, Phytoremediation of heavy metal-contaminated sites: eco-environmental concerns, field studies, sustainability issues, and future prospects, Rev. Environ. Contam. Toxicol. 249 (2020) 71–131.

[13] A. Rehman, S.-J. Park, Environmental remediation by microporous carbon: An efficient contender for CO2 and methylene blue adsorption, J. CO2 Util. 34 (2019) 656–667.

[14] G. Nazir, A. Rehman, S. Hussain, A.M. Afzal, G. Dastgeer, M.A. Rehman, Z. Akhter, T.I. Al-Muhimeed, A.A. AlObaid, Heteroatoms-doped hierarchical porous carbons:

Multifunctional materials for effective methylene blue removal and cryogenic hydrogen storage, Colloids Surf. A Physicochem. Eng. Asp. 630 (2021) 127554.

[15] I.A. Saleh, N. Zouari, M.A. Al-Ghouti, Removal of pesticides from water and wastewater: Chemical, physical and biological treatment approaches, Environ. Technol. Innov. 19 (2020) 101026.

[16] Z. Rahman, V.P. Singh, The relative impact of toxic heavy metals (THMs)(arsenic (As), cadmium (Cd), chromium (Cr)(VI), mercury (Hg), and lead (Pb)) on the total environment: an overview, Environ. Monit. Assess. 191 (2019) 1–21.

[17] O.M. Rodriguez-Narvaez, J.M. Peralta-Hernandez, A. Goonetilleke, E.R. Bandala, Treatment technologies for emerging contaminants in water: A review, Chem. Eng. J. 323 (2017) 361–380.

[18] A.A. Mohana, S. Farhad, N. Haque, B.K. Pramanik, Understanding the fate of nano-plastics in wastewater treatment plants and their removal using membrane processes, Chemosphere 284 (2021) 131430.

[19] J.O. Eniola, R. Kumar, M. Barakat, J. Rashid, A review on conventional and advanced hybrid technologies for pharmaceutical wastewater treatment, J. Clean. Prod. 356 (2022) 131826.

[20] U. Stottmeister, A. Wießner, P. Kuschk, U. Kappelmeyer, M. K¨astner, O. Bederski,R. Müller, H. Moormann, Effects of plants and microorganisms in constructed wetlands for wastewater treatment, Biotechnol. Adv. 22 (1–2) (2003) 93–117.

[21] P. Yaashikaa, P.S. Kumar, S.J. Varjani, A. Saravanan, Advances in production and application of biochar from lignocellulosic feedstocks for remediation of environmental pollutants, Bioresour. Technol. 292 (2019) 122030.

[22] M.A. Albrecht, C.W. Evans, C.L. Raston, Green chemistry and the health implications of nanoparticles, Green Chem. 8 (5) (2006) 417–432.

[23] A. Saravanan, P.S. Kumar, S. Jeevanantham, S. Karishma, B. Tajsabreen, P. Yaashikaa, B. Reshma, Effective water/wastewater treatment methodologies for toxic pollutants removal: Processes and applications towards sustainable development, Chemosphere 280 (2021) 130595.

[24] H. Ali, E. Khan, I. Ilahi, Environmental chemistry and ecotoxicology of hazardous heavy metals: environmental persistence, toxicity, and bioaccumulation, J. Chem. 2019 (2019).

[25] K.H.H. Aziz, F.S. Mustafa, K.M. Omer, S. Hama, R.F. Hamarawf, K.O. Rahman, Heavy metal pollution in the aquatic environment: efficient and low-cost removal approaches to eliminate their toxicity: a review, RSC Adv. 13 (26) (2023) 17595–17610.

[26] C.V. Rekhate, J. Srivastava, Recent advances in ozone-based advanced oxidation processes for treatment of wastewater-A review, Chem. Eng. J. Adv. 3 (2020) 100031.

[27] J. Du, B. Zhang, J. Li, B. Lai, Decontamination of heavy metal complexes by advanced oxidation processes: A review, Chin. Chem. Lett. 31 (10) (2020) 2575–2582.

[28] J.L. Wang, L.J. Xu, Advanced oxidation processes for wastewater treatment: formation of hydroxyl radical and application, Crit. Rev. Environ. Sci. Technol. 42 (3) (2012) 251–325.

[29] S. Foteinis, A.G. Borthwick, Z. Frontistis, D. Mantzavinos, E. Chatzisymeon, Environmental sustainability of light-driven processes for wastewater treatment applications, J. Clean. Prod. 182 (2018) 8–15.

[30] S.N. Ahmed, W. Haider, Heterogeneous photocatalysis and its potential applications in water and wastewater treatment: a review, Nanotechnology 29 (34) (2018) 342001.

[31] P.A. Soares, R. Souza, J. Soler, T.F. Silva, S.M.G.U. Souza, R.A. Boaventura, V. J. Vilar, Remediation of a synthetic textile wastewater from polyester-cotton dyeing combining biological and photochemical oxidation processes, Sep. Purif. Technol. 172 (2017) 450–462.

[32] A. Kuliˇsťakov ´ a, ´ Removal of pharmaceutical micropollutants from real wastewater matrices by means of photochemical advanced oxidation processes–A review, J. Water Process Eng. 53 (2023) 103727.

[33] A. Rehman, G. Nazir, K.Y. Rhee, S.-J. Park, Valorization of orange peel waste to tunable heteroatom-doped hydrochar-derived microporous carbons for selective CO2 adsorption and separation, Sci. Total Environ. 849 (2022) 157805.

[34] G. Nazir, A. Rehman, S. Hussain, Q. Mahmood, M. Fteiti, K. Heo, M. Ikram, M.A. U. Din, Towards a sustainable conversion of biomass/biowaste to porous carbons for CO2 adsorption: Recent advances, current challenges, and future directions, Green Chem. (2023).

[35] A. Rehman, G. Nazir, K. Heo, S. Hussain, M. Ikram, Q. Mahmood, T. Alshahrani, H.S. Abd-Rabboh, Single step strategy to prepare highly microporous carbons derived from melamine and terephthalaldehyde for high-performance materialbased hydrogen storage, J. Storage Mater. 66 (2023) 107468.

[36] D. Berslin, A. Reshmi, B. Sivaprakash, N. Rajamohan, P.S. Kumar, Remediation of emerging metal pollutants using environment friendly biochar-Review on applications and mechanism, Chemosphere 290 (2022) 133384.

[37] R. Saxena, M. Saxena, A. Lochab, Recent progress in nanomaterials for adsorptive removal of organic contaminants from wastewater, ChemistrySelect 5 (1) (2020) 335–353.

[38] R. Gusain, N. Kumar, S.S. Ray, Recent advances in carbon nanomaterial-based adsorbents for water purification, Coord. Chem. Rev. 405 (2020) 213111.

[39] M. Zeng, M. Chen, D. Huang, S. Lei, X. Zhang, L. Wang, Z. Cheng, Engineered two dimensional nanomaterials: An emerging paradigm for water purification and monitoring, Mater. Horiz. 8 (3) (2021) 758–802.

[40] H.M. Saleh, A.I. Hassan, Synthesis and Characterization of Nanomaterials for Application in Cost-Effective Electrochemical Devices, Sustainability 15 (14) (2023) 10891.

[41] A. Dey, S. Varagnolo, N.P. Power, N. Vangapally, Y. Elias, L. Damptey, B.N. Jaato, S. Gopalan, Z. Golrokhi, P. Sonar, Doped MXenes—a new paradigm in 2D systems: synthesis, properties and applications, Prog. Mater Sci. 101166 (2023).

[42] F.A. Janjhi, I. Ihsanullah, M. Bilal, R. Castro-Munoz, ˜ G. Boczkaj, F. Gallucci, MXene-based materials for removal of antibiotics and heavy metals from wastewater–A review, Water Resour. Ind. (2023) 100202.

[43] N. Gull, A. Islam, A. Mannan, T. Riaz, A. Khalid, S.M. Khan, R.U. Khan, Challenges and Future Perspectives of Mxenes, Handbook of Functionalized Nanostructured MXenes: Synthetic Strategies and Applications from Energy to Environment Sustainability, Springer, 2023, pp. 377-387.

[44] M. Bilal, A.K. Singh, H.M. Iqbal, G. Boczkaj, Enzyme-conjugated MXene nanocomposites for biosensing and biocatalysis acuities, Chem. Eng. J. (2023) 145020.

[45] L. Cao, H. Wang, K. Peng, Y. Zhou, L. Gao, H. Liu, Z. Tian, H. Yin, Strong adsorption and high stability of the thin-layered MXene adsorbent: Simple synthesis and application to reduce the toxicity of wastewater towards mung beans, Surf. Interfaces 41 (2023) 103172.

[46] L. Huang, L. Ding, J. Caro, H. Wang, MXene-based Membranes for Drinking Water Production, Angew. Chem. Int. Ed. (2023) e202311138.

[47] N. Kitchamsetti, A.L. de Barros, Recent Advances in MXenes Based Composites as Photocatalysts: Synthesis, Properties, and Photocatalytic Removal of Organic Contaminants from Wastewater, ChemCatChem e202300690.

[48] J. Peng, X. Chen, W.-J. Ong, X. Zhao, N. Li, Surface and heterointerface engineering of 2D MXenes and their nanocomposites: insights into electro-and photocatalysis, Chem 5 (1) (2019) 18–50.

[49] H. Ali, A. Ali, J.A. Buledi, A.A. Memon, A.R. Solangi, J. Yang, K.H. Thebo, MXene based nanocomposites: emerging candidates for the removal of antibiotics, dyes, and heavy metal ions, Mater. Chem. Front. 7 (22) (2023) 5519–5544.

[50] Z. Ahmed, F. Rehman, U. Ali, A. Ali, M. Iqbal, K.H. Thebo, Recent advances in MXene-based separation membranes, ChemBioEng Rev. 8 (2) (2021) 110–120.

[51] I. Mahar, F.K. Mahar, N. Mahar, A.A. Memon, A.A.A. Pirzado, Z. Khatri, K. H. Thebo, A. Ali, Fabrication and characterization of MXene/carbon composite-based nanofibers (MXene/CNFs) membrane: An efficient adsorbent material for removal of Pb+ 2 and As+ 3 ions from water, Chem. Eng. Res. Des. 191 (2023) 462–471.

[52] Y.A. Al-Hamadani, B.-M. Jun, M. Yoon, N. Taheri-Qazvini, S.A. Snyder, M. Jang, J. Heo, Y. Yoon, Applications of MXene-based membranes in water purification: A review, Chemosphere 254 (2020) 126821.

[53] M. Tawalbeh, S. Mohammed, A. Al-Othman, M. Yusuf, M. Mofijur, H. Kamyab, MXenes and MXene-based materials for removal of pharmaceutical compounds from wastewater: Critical review, Environ. Res. (2023) 115919.

[54] K. Gopalram, A. Kapoor, P.S. Kumar, A. Sunil, G. Rangasamy, MXenes and MXene-Based Materials for Removal and Detection of Water Contaminants: A Review, Ind. Eng. Chem. Res. 62 (17) (2023) 6559–6583.

[55] S.S. Ray, T.S.K. Sharma, R. Singh, A. Ratley, W.M. Choi, Y.-H. Ahn, D. Sangeetha, Y.-N. Kwon, Towards the next generation improved throughput MXene-based membrane for environmental applications: A holistic review, J. Environ. Chem. Eng. (2023) 110243.

[56] C. Wang, J. Ye, L. Liang, X. Cui, L. Kong, N. Li, Z. Cheng, W. Peng, B. Yan, G. Chen, Application of MXene-based materials in Fenton-like systems for organic wastewater treatment: A review, Sci. Total Environ. 862 (2023) 160539.

[57] I. Mahar, F.H. Memon, J.-W. Lee, K.H. Kim, R. Ahmed, F. Soomro, F. Rehman, A. A. Memon, K.H. Thebo, K.H. Choi, Two-dimensional transition metal carbides and nitrides (MXenes) for water purification and antibacterial applications, Membranes 11 (11) (2021) 869.

[58] K. Gopalram, A. Kapoor, P.S. Kumar, A. Sunil, G. Rangasamy, MXenes and MXene-Based Materials for Removal and Detection of Water Contaminants: A Review, Ind. Eng. Chem. Res. (2023).

[59] M. Benchakar, L. Loupias, C. Garnero, T. Bilyk, C. Morais, C. Canaff, N. Guignard, S. Morisset, H. Pazniak, S. Hurand, One MAX phase, different MXenes: A guideline to understand the crucial role of etching conditions on Ti_3C_2 Tx surface chemistry, Appl. Surf. Sci. 530 (2020) 147209.

[60] A. VahidMohammadi, J. Rosen, Y. Gogotsi, The world of two-dimensional carbides and nitrides (MXenes), Science 372 (6547) (2021) eabf1581.
[61] Y. Gogotsi, B. Anasori, The Rise of MXenes, ACS Nano 13 (8) (2019) 8491–8494.

[62] M. Naguib, V.N. Mochalin, M.W. Barsoum, Y. Gogotsi, 25th anniversary article: MXenes: a new family of two-dimensional materials, Adv. Mater. 26 (7) (2014) 992–1005.

[63] S. Yu, H. Tang, D. Zhang, S. Wang, M. Qiu, G. Song, D. Fu, B. Hu, X. Wang, MXenes as emerging nanomaterials in water purification and environmental remediation, Sci. Total Environ. 811 (2022) 152280.

[64] X. Li, Z. Huang, C.E. Shuck, G. Liang, Y. Gogotsi, C. Zhi, MXene chemistry, electrochemistry and energy storage applications, Nat. Rev. Chem. 6 (6) (2022) 389–404.

[65] X. Zhao, L.-Y. Wang, C.-Y. Tang, X.-J. Zha, Y. Liu, B.-H. Su, K. Ke, R.-Y. Bao, M.- B. Yang, W. Yang, Smart Ti_3C_2 T x MXene fabric with fast humidity response and joule heating for healthcare and medical therapy applications, ACS Nano 14 (7) (2020) 8793–8805.

[66] A. Parihar, A. Singhal, N. Kumar, R. Khan, M.A. Khan, A.K. Srivastava, Nextgeneration intelligent MXene-based electrochemical aptasensors for point-of-care cancer diagnostics, Nano-Micro Letters 14 (1) (2022) 100.

[67] S. Iravani, R.S. Varma, Bioinspired and biomimetic MXene-based structures with fascinating properties: Recent advances, Mater. Adv. (2022).

[68] K. Khan, A.K. Tareen, M. Iqbal, Z. Ye, Z. Xie, A. Mahmood, N. Mahmood, H. Zhang, Recent Progress in Emerging Novel MXenes Based Materials and their Fascinating Sensing Applications, Small (2023) 2206147.

[69] M. Naguib, M.W. Barsoum, Y. Gogotsi, Ten years of progress in the synthesis and development of MXenes, Adv. Mater. 33 (39) (2021) 2103393.

[70] A. Perera, K. Madhushani, B.T. Punchihewa, A. Kumar, R.K. Gupta, MXene-based nanomaterials for multifunctional applications, Materials 16 (3) (2023) 1138.

[71] V. Shukla, The tunable electric and magnetic properties of 2D MXenes and their potential applications, Mater. Adv. 1 (9) (2020) 3104–3121.

[72] H. Lin, Y. Chen, J. Shi, Insights into 2D MXenes for versatile biomedical applications: current advances and challenges ahead, Adv. Sci. 5 (10) (2018) 1800518.

[73] T.H. Le, Y. Oh, H. Kim, H. Yoon, Exfoliation of 2D materials for energy and environmental applications, Chem.–A Eur. J. 26 (29) (2020) 6360–6401.

[74] K. Maleski, V.N. Mochalin, Y. Gogotsi, Dispersions of two-dimensional titanium carbide MXene in organic solvents, Chem. Mater. 29 (4) (2017) 1632–1640.

[75] M. Naguib, M. Kurtoglu, V. Presser, J. Lu, J. Niu, M. Heon, L. Hultman, Y. Gogotsi, M.W. Barsoum, Two-dimensional nanocrystals produced by exfoliation of Ti3AlC2, Adv. Mater. 23 (37) (2011) 4248–4253.

[76] V. Kotasthane, Z. Tan, J. Yun, E.B. Pentzer, J.L. Lutkenhaus, M.J. Green, M. Radovic, Selective Etching of Ti3AlC2 MAX Phases Using Quaternary Ammonium Fluorides Directly Yields Ti_3C_2 T z MXene Nanosheets: Implications for Energy Storage, ACS Appl. Nano Mater. (2023).

[77] O. Mashtalir, M. Naguib, B. Dyatkin, Y. Gogotsi, M.W. Barsoum, Kinetics of aluminum extraction from Ti3AlC2 in hydrofluoric acid, Mater. Chem. Phys. 139 (1) (2013) 147–152.

[78] R. Xiao, C. Zhao, Z. Zou, Z. Chen, L. Tian, H. Xu, H. Tang, Q. Liu, Z. Lin, X. Yang, In situ fabrication of 1D CdS nanorod/2D Ti_3C_2 MXene nanosheet Schottky heterojunction toward enhanced photocatalytic hydrogen evolution, Appl Catal B 268 (2020) 118382.

[79] A. Khosla, H.T.A. Sonu, K.S. Awan, R. Gaurav, Z. Walvekar, A. Zhao, M. Kaushik, V.C. Khalid, Emergence of MXene and MXene–Polymer Hybrid Membranes as Future-Environmental Remediation Strategies, Adv. Sci. 9 (36) (2022) 2203527.

[80] J. Halim, M.R. Lukatskaya, K.M. Cook, J. Lu, C.R. Smith, L.-Å. N¨aslund, S.J. May,

L. Hultman, Y. Gogotsi, P. Eklund, Transparent conductive two-dimensional titanium carbide epitaxial thin films, Chem. Mater. 26 (7) (2014) 2374–2381.

[81] P. Urbankowski, B. Anasori, K. Hantanasirisakul, L. Yang, L. Zhang, B. Haines, S. J. May, S.J. Billinge, Y. Gogotsi, 2D molybdenum and vanadium nitrides synthesized by ammoniation of 2D transition metal carbides (MXenes), Nanoscale 9 (45) (2017) 17722–17730.

[82] L. Zhang, W. Song, H. Liu, H. Ding, Y. Yan, R. Chen, Influencing Factors on Synthesis and Properties of MXene: A Review, Processes 10 (9) (2022) 1744.

[83] M. Algaradah, A mercapto based nanoscavenger as promising tool for the dispersion preconcentration of trace elements in contaminated waters, Egypt, J. Chem. 65 (3) (2022) 29–38.

[84] Y. Dong, H. Shi, Z.S. Wu, Recent advances and promise of MXene-based nanostructures for high-performance metal ion batteries, Adv. Funct. Mater. 30 (47) (2020) 2000706.

[85] Q. Zhao, Q. Zhu, Y. Liu, B. Xu, Status and prospects of MXene-based lithium–sulfur batteries, Adv. Funct. Mater. 31 (21) (2021) 2100457.

[86] A. Rehman, G. Nazir, K.Y. Rhee, S.-J. Park, Electrocatalytic and photocatalytic sustainable conversion of carbon dioxide to value-added chemicals: State-of-theart progress, challenges, and future directions, J. Environ. Chem. Eng. (2022)

108219.

[87] H.E. Karahan, K. Goh, C. Zhang, E. Yang, C. Yıldırım, C.Y. Chuah, M.G. Ahunbay, J. Lee, S¸ .B. Tantekin-Ersolmaz, Y. Chen, MXene materials for designing advanced separation membranes, Adv. Mater. 32 (29) (2020) 1906697.

[88] J. Xiang, X. Wang, M. Ding, X. Tang, S. Zhang, X. Zhang, Z. Xie, The role of lateral size of MXene nanosheets in membrane filtration of dyeing wastewater: Membrane characteristic and performance, Chemosphere 294 (2022) 133728.

[89] Y. Kang, Y. Xia, H. Wang, X. Zhang, 2D laminar membranes for selective water and ion transport, Adv. Funct. Mater. 29 (29) (2019) 1902014.

[90] Y. Wu, L. Ding, Z. Lu, J. Deng, Y. Wei, Two-dimensional MXene membrane for ethanol dehydration, J. Membr. Sci. 590 (2019) 117300.

[91] L. Zhang, X. Kan, T. Huang, J. Lao, K. Luo, J. Gao, X. Liu, K. Sui, L. Jiang, Electric field modulated water permeation through laminar Ti_3C_2Tx MXene membrane, Water Res. 219 (2022) 118598.

[92] Q. Lin, G. Zeng, G. Yan, J. Luo, X. Cheng, Z. Zhao, H. Li, Self-cleaning photocatalytic MXene composite membrane for synergistically enhanced water treatment: Oil/water separation and dyes removal, Chem. Eng. J. 427 (2022) 31668.

[93] G. Zeng, Y. Liu, Q. Lin, S. Pu, S. Zheng, M.B.M.Y. Ang, Y.-H. Chiao, Constructing composite membranes from functionalized metal organic frameworks integrated MXene intended for ultrafast oil/water emulsion separation, Sep. Purif. Technol. 293 (2022) 121052.

[94] M. Jaishankar, T. Tseten, N. Anbalagan, B.B. Mathew, K.N. Beeregowda, Toxicity, mechanism and health effects of some heavy metals, Interdiscip. Toxicol. 7 (2) (2014) 60.

[95] W.S. Chai, J.Y. Cheun, P.S. Kumar, M. Mubashir, Z. Majeed, F. Banat, S.-H. Ho, P. L. Show, A review on conventional and novel materials towards heavy metal adsorption in wastewater treatment application, J. Clean. Prod. 296 (2021) 126589.

[96] A. Shahzad, K. Rasool, W. Miran, M. Nawaz, J. Jang, K.A. Mahmoud, D.S. Lee, Two-dimensional Ti_3C_2T x MXene nanosheets for efficient copper removal from water, ACS Sustain. Chem. Eng. 5 (12) (2017) 11481–11488.

[97] A. Yadav, P. Chowdhary, G. Kaithwas, R.N. Bharagava, Toxic metals in the environment: Threats on ecosystem and bioremediation approaches, Handbook of metal-microbe interactions and bioremediation, CRC Press, 2017, pp. 128-141.

[98] A. Abbas, A.M. Al-Amer, T. Laoui, M.J. Al-Marri, M.S. Nasser, M. Khraisheh, M. A. Atieh, Heavy metal removal from aqueous solution by advanced carbon nanotubes: critical review of adsorption applications, Sep. Purif. Technol. 157 (2016) 141–161.

S.H. Woo, D.S. Lee, Ti_3C_2Tx MXene core-shell spheres for ultrahigh removal of mercuric ions, Chem. Eng. J. 368 (2019) 400–408.

[100] A. Shahzad, J. Jang, S.-R. Lim, D.S. Lee, Unique selectivity and rapid uptake of molybdenum-disulfide-functionalized MXene nanocomposite for mercury adsorption, Environ. Res. 182 (2020) 109005.

[101] A.P. Isfahani, A.A. Shamsabadi, F. Alimohammadi, M. Soroush, Efficient mercury removal from aqueous solutions using carboxylated Ti_3C_2Tx MXene, J. Hazard. Mater. 434 (2022) 128780.

[92] K. Fu, X. Liu, D. Yu, J. Luo, Z. Wang, J.C. Crittenden, Highly efficient and selective Hg (II) removal from water using multilayered Ti_3C_2O x MXene via adsorption coupled with catalytic reduction mechanism, Environ. Sci. Tech. 54 (24) (2020) 16212–16220.

[103] Q. Liu, Y. Liu, Distribution of Pb (II) species in aqueous solutions, J. Colloid Interface Sci. 268 (1) (2003) 266–269.

[104] M. Ghorbani, O. Seyedin, M. Aghamohammadhassan, Adsorptive removal of lead (II) ion from water and wastewater media using carbon-based nanomaterials as unique sorbents: A review, J. Environ. Manage. 254 (2020) 109814.

[105] F.H. Memon, F. Rehman, J. Lee, F. Soomro, M. Iqbal, S.M. Khan, A. Ali, K. H. Thebo, K.H. Choi, Transition metal dichalcogenide-based membranes for water desalination, gas separation, and energy storage, Sep. Purif. Rev. 52 (1) (2023) 43–57.

[106] F. Rehman, F. Hussain Memon, S. Ullah, M.A. Jafar Mazumder, A. Al-Ahmed, F. Khan, K. Hussain Thebo, Recent Development in Laminar Transition Metal Dichalcogenides-Based Membranes Towards Water Desalination: A Review, Chem. Rec. 22 (9) (2022) e202200107.

[107] M.K. Shahzad, F.H. Memon, F. Soomro, M. Iqbal, A. Ibrar, A.A. Memon, J.H. Lim, K.H. Choi, K.H. Thebo, MoS2-based Lamellar Membranes for Mass Transport Applications: Challenges and Opportunities, J. Environ. Chem. Eng. (2023) 109329.

[108] Q. Shafiq, S.M. Husnain, F. Shahzad, M.T. Mehran, S.A.R. Kazmi, S. Mujtaba-l-Hassan, J. Ahmad, Z. Iqbal, Rational design of MXene coated polyurethane foam for the removal of Pb2+, Mater. Lett. 304 (2021) 130600.

[109] B.-M. Jun, N. Her, C.M. Park, Y. Yoon, Effective removal of Pb (ii) from synthetic wastewater using Ti 3 C 2 T x MXene, Environ. Sci. Water Res. Technol. 6 (1) (2020) 173–180.

[110] B. Pan, Q. Zhang, W. Zhang, B. Pan, W. Du, L. Lv, Q. Zhang, Z. Xu, Q. Zhang, Highly effective removal of heavy metals by polymer-based zirconium phosphate: a case study of lead ion, J. Colloid Interface Sci. 310 (1) (2007) 99–105.

[111] Y. Dong, D. Sang, C. He, X. Sheng, L. Lei, Mxene/alginate composites for lead and copper ion removal from aqueous solutions, RSC Adv. 9 (50) (2019) 29015–29022.

[112] S. Wang, Y. Liu, Q.-F. Lü, H. Zhuang, Facile preparation of iosurfactant-functionalized Ti2CTX MXene nanosheets with an enhanced adsorption performance for Pb (II) ions, J. Mol. Liq. 297 (2020) 111810.

[113] Y. Wang, K. Ding, R. Xu, D. Yu, W. Wang, P. Gao, B. Liu, Fabrication of BiVO4/ BiPO4/GO composite photocatalytic material for the visible light-driven degradation, J. Clean. Prod. 247 (2020) 119108.

[114] Y. Du, B. Yu, L. Wei, Y. Wang, X. Zhang, S. Ye, Efficient removal of Pb (II) by Ti_3C_2T x powder modified with a silane coupling agent, J. Mater. Sci. 54 (20) (2019) 13283–13297.

[115] G. Zhang, T. Wang, Z. Xu, M. Liu, C. Shen, Q. Meng, Synthesis of mino-functionalized Ti 3 C 2 T x MXene by alkalization-grafting modification for efficient lead adsorption, Chem. Commun. 56 (76) (2020) 11283–11286.

[116] H. Wang, F. Wu, Z. Wang, Y. Wang, S. Zhang, H. Luo, Z. Zheng, L. Fang, Ultra-fast and ultra-efficient removal of Cr (VI) by the aqueous solutions of monolayer MXene (Ti_3C_2Tx), Chemosphere 308 (2022) 136573.

[117] S. Guo, H. Luo, Y. Bao, Y. Li, H. Guan, Y. Zhu, Construction of hierarchical Ti_3C_2Tx MXene/ZnIn2S4 heterostructures for efficiently photocatalytic reduction of Cr (VI) under visible light, Appl. Surf. Sci. 575 (2022) 151753.

[118] K.-T. Chung, Azo dyes and human health: A review, J. Environ. Sci. Health C 34 (4) (2016) 233–261.

[119] S. Rajendran, T. Priya, K.S. Khoo, T.K. Hoang, H.-S. Ng, H.S.H. Munawaroh, C. Karaman, Y. Orooji, P.L. Show, A critical review on various remediation approaches for heavy metal contaminants removal from contaminated soils, Chemosphere 287 (2022) 132369.

[120] S.I. Siddiqui, E.S. Allehyani, S.A. Al-Harbi, Z. Hasan, M.A. Abomuti, H.K. Rajor, S. Oh, Investigation of Congo Red Toxicity towards Different Living Organisms: A Review, Processes 11 (3) (2023) 807.

[121] J. Xu, G. Zeng, Q. Lin, Y. Gu, X. Wang, Z. Feng, A. Sengupta, Application of 3D magnetic nanocomposites: MXene-supported Fe3O4@ CS nanospheres for highly efficient adsorption and separation of dyes, Sci. Total Environ. 822 (2022) 153544.

[122] J. Ran, G. Gao, F.-T. Li, T.-Y. Ma, A. Du, S.-Z. Qiao, Ti_3C_2 MXene co-catalyst on metal sulfide photo-absorbers for enhanced visible-light photocatalytic hydrogen production, Nat. Commun. 8 (1) (2017) 13907.

[123] X. Zhang, X. Jia, R. Xu, X. Lu, H. Liu, Y. Niu, Ellipsoidal α-Fe_2O_3@ SnO2/ Ti_3C_2 MXene core-shell nanoparticles for photodegradation of organic dyes, J. Alloy. Compd. 923 (2022) 166315.

[124] C. Prasad, X. Yang, Q. Liu, H. Tang, A. Rammohan, S. Zulfiqar, G.V. Zyryanov, S. Shah, Recent advances in MXenes supported semiconductors based photocatalysts: Properties, synthesis and photocatalytic applications, J. Ind. Eng. Chem. 85 (2020) 1–33.

[125] R. Morsi, M. Bilal, H.M. Iqbal, S.S. Ashraf, Laccases and peroxidases: the smart, greener and futuristic biocatalytic tools to mitigate recalcitrant emerging pollutants, Sci. Total Environ. 714 (2020) 136572.

[126] M.A. Iqbal, A. Tariq, A. Zaheer, S. Gul, S.I. Ali, M.Z. Iqbal, D. Akinwande, S. Rizwan, Ti_3C_2-MXene/bismuth ferrite nanohybrids for efficient degradation of organic dyes and colorless pollutants, ACS Omega 4 (24) (2019) 20530–20539.

[127] O. Mashtalir, K.M. Cook, V.N. Mochalin, M. Crowe, M.W. Barsoum, Y. Gogotsi, Dye adsorption and decomposition on two-dimensional titanium carbide in aqueous media, J. Mater. Chem. A 2 (35) (2014) 14334–14338.

[128] V.Q. Hieu, T.K. Phung, T.-Q. Nguyen, A. Khan, V.D. Doan, V.A. Tran, Photocatalytic degradation of methyl orange dye by Ti_3C_2–TiO_2 heterojunction under solar light, Chemosphere 276 (2021) 130154.

[129] C. Peng, H. Wang, H. Yu, F. Peng, (111) TiO_2-x/ Ti_3C_2: Synergy of active facets, interfacial charge transfer and Ti3+ doping for enhance photocatalytic activity, Mater. Res. Bull. 89 (2017) 16–25.

[130] V.T. Quyen, D.M. Thanh, Q. Van Le, N.M. Viet, N.T. Nham, P.Q. Thang, Advanced synthesis of MXene-derived nanoflower-shaped TiO_2@ Ti_3C_2heterojunction to enhance photocatalytic degradation of Rhodamine B, Environ. Technol. Innov. 21 (2021) 101286.

[131] N.M. Tran, Q.T.H. Ta, A. Sreedhar, J.-S. Noh, Ti_3C_2Tx MXene playing as a strong methylene blue adsorbent in wastewater, Appl. Surf. Sci. 537 (2021) 148006.

[132] N.M. Tran, Q.T.H. Ta, J.-S. Noh, Unusual synthesis of safflower-shaped TiO_2/ Ti_3C_2 heterostructures initiated from two-dimensional Ti_3C_2 MXene, Appl. Surf. Sci. 538 (2021) 148023.

[133] H. Xue, X. Gao, M.K. Seliem, M. Mobarak, R. Dong, X. Wang, K. Fu, Q. Li, Z. Li, Efficient adsorption of anionic azo dyes on porous heterostructured MXene/ biomass activated carbon composites: Experiments, characterization, and theoretical analysis via advanced statistical physics models, Chem. Eng. J. 451 (2023) 138735.

[134] J. Zhang, Q. Xue, X. Pan, Y. Jin, W. Lu, D. Ding, Q. Guo, Graphene oxide/ polyacrylonitrile fiber hierarchical-structured membrane for ultra-fast microfiltration of oil-water emulsion, Chem. Eng. J. 307 (2017) 643–649.

[135] L. Li, Z. Liu, Q. Zhang, C. Meng, T. Zhang, J. Zhai, Underwater superoleophobic porous membrane based on hierarchical TiO 2 nanotubes: multifunctional integration of oil–water separation, flow-through photocatalysis and selfcleaning, J. Mater. Chem. A 3 (3) (2015) 1279–1286.

[136] R. Du, X. Gao, Q. Feng, Q. Zhao, P. Li, S. Deng, L. Shi, J. Zhang, Microscopic dimensions engineering: Stepwise manipulation of the surface wettability on 3D substrates for oil/water separation, Adv. Mater. 28 (5) (2016) 936–942.

[137] W.J. Koros, C. Zhang, Materials for next-generation molecularly selective synthetic membranes, Nat. Mater. 16 (3) (2017) 289–297.

[138] Q. Yang, Y. Su, C. Chi, C. Cherian, K. Huang, V. Kravets, F. Wang, J. Zhang, A. Pratt, A. Grigorenko, Ultrathin graphene-based membrane with precise molecular sieving and ultrafast solvent permeation, Nat. Mater. 16 (12) (2017) 1198–1202.

[139] J. Deng, Z. Lu, L. Ding, Z.-K. Li, Y. Wei, J. Caro, H. Wang, Fast electrophoretic preparation of large-area two-dimensional titanium carbide membranes for ion sieving, Chem. Eng. J. 408 (2021) 127806.

[140] X. Feng, Z. Yu, R. Long, Y. Sun, M. Wang, X. Li, G. Zeng, Polydopamine intimate contacted two-dimensional/two-dimensional ultrathin nylon basement membrane supported RGO/PDA/MXene composite material for oil-water separation and dye removal, Sep. Purif. Technol. 247 (2020) 116945.

[141] M. Zhang, L. Shi, X. Du, Z. Li, Y. Shi, C. An, J. Li, C. Wang, J. Shi, Janus mesoporous wood-based membrane for simultaneous oil/water separation, aromatic dyes removal, and seawater desalination, Ind. Crop. Prod. 188 (2022) 115643.

[142] V. Lincy, A. Prasannan, R. Jayachitra, H.-C. Tsai, P.-D. Hong, Integrated multifunctional photothermal membrane for oil/water emulsion separation, dye effluent removal, and solar water purification, J. Clean. Prod. 368 (2022) 133094.

[143] A. Javaid, S. Latif, M. Imran, N. Hussain, M. Bilal, H.M. Iqbal, MXene-based hybrid composites as photocatalyst for the mitigation of pharmaceuticals, Chemosphere 291 (2022) 133062.

[144] T. Eggen, M. Moeder, A. Arukwe, Municipal landfill leachates: a significant source for new and emerging pollutants, Sci. Total Environ. 408 (21) (2010) 5147–5157.

[145] T. Heberer, Tracking persistent pharmaceutical residues from municipal sewage to drinking water, J. Hydrol. 266 (3–4) (2002) 175–189.

[146] M.R. Letsoalo, T. Sithole, S. Mufamadi, Z. Mazhandu, M. Sillanpaa, A. Kaushik, T. Mashifana, Efficient detection and treatment of pharmaceutical contaminants to produce clean water for better health and environmental, J. Clean. Prod. (2022) 135798.

[147] H. Ghazal, E. Koumaki, J. Hoslett, S. Malamis, E. Katsou, D. Barcelo, H. Jouhara, Insights into current physical, chemical and hybrid technologies used for the treatment of wastewater contaminated with pharmaceuticals, J. Clean. Prod. 361 (2022) 132079.

[148] C.G. Daughton, T.A. Ternes, Pharmaceuticals and personal care products in the environment: agents of subtle change? Environ. Health Perspect. 107 (suppl 6) (1999) 907–938.

[149] P. Kumari, M. Alam, W.A. Siddiqi, Usage of nanoparticles as adsorbents for waste water treatment: an emerging trend, Sustain. Mater. Technol. 22 (2019) e00128.

[150] R. Sivaranjanee, P.S. Kumar, A review on cleaner approach for effective separation of toxic pollutants from wastewater using carbon Sphere's as adsorbent: Preparation, activation and applications, J. Clean. Prod. 291 (2021) 125911.

[151] C. Medjili, N. Lakhdari, D. Lakhdari, A. Berchi, N. Osmani, I. Laourari, Y. Vasseghian, M. Berkani, Synthesis of novel PANI/PVA-NiCu composite material for efficient removal of organic dyes, Chemosphere 313 (2023) 137427.

[152] M.R. Lukatskaya, O. Mashtalir, C.E. Ren, Y. Dall'Agnese, P. Rozier, P.L. Taberna, M. Naguib, P. Simon, M.W. Barsoum, Y. Gogotsi, Cation intercalation and high volumetric capacitance of two-dimensional titanium carbide, Science 341(6153) (2013) 1502-1505.

[153] S. Kim, F. Gholamirad, M. Yu, C.M. Park, A. Jang, M. Jang, N. Taheri-Qazvini, Y. Yoon, Enhanced adsorption performance for selected pharmaceutical compounds by sonicated $Ti_3C_2T_X$ MXene, Chem. Eng. J. 406 (2021) 126789.

[154] A. Kumar, P. Majithia, P. Choudhary, I. Mabbett, M.F. Kuehnel, S. Pitchaimuthu, V. Krishnan, MXene coupled graphitic carbon nitride nanosheets based plasmonic photocatalysts for removal of pharmaceutical pollutant, Chemosphere 308 (2022) 136297.

[155] I. Ihsanullah, MXenes (two-dimensional metal carbides) as emerging nanomaterials for water purification: Progress, challenges and prospects, Chem. Eng. J. 388 (2020) 124340.

[156] V. Thirumal, R. Yuvakkumar, P.S. Kumar, S. Keerthana, G. Ravi, D. Velauthapillai, B. Saravanakumar, Efficient photocatalytic degradation of hazardous pollutants by homemade kitchen blender novel technique via 2D-material of few-layer MXene nanosheets, Chemosphere 281 (2021) 130984.

[157] J. Chen, H. Zheng, Y. Zhao, M. Que, W. Wang, X. Lei, Morphology and photocatalytic activity of TiO2/MXene composites by in-situ solvothermal method, Ceram. Int. 46 (12) (2020) 20088–20096.

[158] H. Wang, H. Cui, X. Song, R. Xu, N. Wei, J. Tian, H. Niu, Facile synthesis of heterojunction of MXenes/TiO2 nanoparticles towards enhanced hexavalent chromium removal, J. Colloid Interface Sci. 561 (2020) 46–57.

[159] X. Feng, Z. Yu, R. Long, X. Li, L. Shao, H. Zeng, G. Zeng, Y. Zuo, Self-assembling 2D/2D (MXene/LDH) materials achieve ultra-high adsorption of heavy metals Ni2+ through terminal group modification, Sep. Purif. Technol. 253 (2020) 117525.

[160] X. Hu, C. Chen, D. Zhang, Y. Xue, Kinetics, isotherm and chemical speciation analysis of Hg (II) adsorption over oxygen-containing MXene adsorbent, Chemosphere 278 (2021) 130206.

[161] A. Miri-Jahromi, M. Didandeh, S. Shekarsokhan, Capability of MXene 2D material as an amoxicillin, ampicillin, and cloxacillin adsorbent in wastewater, J. Mol. Liq. 351 (2022) 118545.

[162] K. Samal, S. Mahapatra, M.H. Ali, Pharmaceutical wastewater as Emerging Contaminants (EC): Treatment technologies, impact on environment and human health, Energy Nexus 6 (2022) 100076.

[163] E.J. Bishop, S. Mitra, On-line membrane preconcentration for continuous monitoring of trace pharmaceuticals, J. Pharm. Biomed. Anal. 37 (1) (2005) 81–86.

[164] O.M. Ghimpețeanu, E.N. Pogurschi, D.C. Popa, N. Dragomir, T. Dragotoiu, ˘ O. D. Mihai, C.D. Petcu, Antibiotic use in livestock and residues in food—A public health threat: A review, Foods 11 (10) (2022) 1430.

[165] W. Baran, E. Adamek, A. Włodarczyk, J. Lazur, W. Opoka, B. Muszynska, ´ The remediation of sulfonamides from the environment by Pleurotus eryngii mycelium. Efficiency, Products and Mechanisms of Mycodegradation, Chemosphere 262 (2021) 128026.

[166] J. Han, L. Kiss, H. Mei, A.M. Remete, M. Ponikvar-Svet, D.M. Sedgwick, R. Roman, S. Fustero, H. Moriwaki, V.A. Soloshonok, Chemical aspects of human and environmental overload with fluorine, Chem. Rev. 121 (8) (2021) 4678–4742.

[167] Y. Cao, Y. Fang, X. Lei, B. Tan, X. Hu, B. Liu, Q. Chen, Fabrication of novel CuFe2O4/MXene hierarchical heterostructures for enhanced photocatalytic degradation of sulfonamides under visible light, J. Hazard. Mater. 387 (2020) 122021.

[168] W. Mu, S. Du, Q. Yu, X. Li, H. Wei, Y. Yang, Improving barium ion adsorption on two-dimensional titanium carbide by surface modification, Dalton Trans. 47 (25) (2018) 8375–8381.

[169] S. Lim, J.H. Kim, H. Park, C. Kwak, J. Yang, J. Kim, S.Y. Ryu, J. Lee, Role of electrostatic interactions in the adsorption of dye molecules by Ti 3 C 2-MXenes, RSC Adv. 11 (11) (2021) 6201–6211.

[170] P. Zhang, M. Xiang, H. Liu, C. Yang, S. Deng, Novel two-dimensional magnetic titanium carbide for methylene blue removal over a wide pH range: insight into removal performance and mechanism, ACS Appl. Mater. Interfaces 11 (27) (2019) 24027–24036.

[171] V.V. Dev, G. Baburaj, S. Antony, V. Arun, K.A. Krishnan, Zwitterion-chitosan bed for the simultaneous immobilization of Zn (II), Cd (II), Pb (II) and Cu (II) from multi-metal aqueous systems, J. Clean. Prod. 255 (2020) 120309.

[172] P. Gu, J. Xing, T. Wen, R. Zhang, J. Wang, G. Zhao, T. Hayat, Y. Ai, Z. Lin, X. Wang, Experimental and theoretical calculation investigation on efficient Pb (II) adsorption on etched Ti 3 AlC 2 nanofibers and nanosheets, Environ. Sci. Nano 5 (4) (2018) 946–955.

[173] S. Li, L. Wang, J. Peng, M. Zhai, W. Shi, Efficient thorium (IV) removal by two-dimensional Ti2CTx MXene from aqueous solution, Chem. Eng. J. 366 (2019) 192–199.

[174] A.R. Khan, S.M. Husnain, F. Shahzad, S. Mujtaba-ul-Hassan, M. Mehmood, J. Ahmad, M.T. Mehran, S. Rahman, Two-dimensional transition metal carbide (Ti 3 C 2 T x) as an efficient adsorbent to remove cesium (Cs+), Dalton Trans. 48 (31) (2019) 11803–11812.

[175] W. Mu, S. Du, X. Li, Q. Yu, H. Wei, Y. Yang, S. Peng, Removal of radioactive palladium based on novel 2D titanium carbides, Chem. Eng. J. 358 (2019) 283–290.

[176] S. Shankar, B.B. Murphy, N. Driscoll, M. Shekhirev, G. Valurouthu, K. Shevchuk, M. Anayee, F. Cimino, Y. Gogotsi, F. Vitale, Effect of the deposition process on the stability of $Ti_3C_2T_x$ MXene films for bioelectronics, 2D, Materials 10 (4) (2023) 044001.

[177] N. Khandelwal, G.K. Darbha, A decade of exploring MXenes as aquatic cleaners: Covering a broad range of contaminants, current challenges and future trends, Chemosphere 279 (2021) 130587.

[178] G.P. Lim, C.F. Soon, N.L. Ma, M. Morsin, N. Nayan, M.K. Ahmad, K.S. Tee, Cytotoxicity of MXene-based nanomaterials for biomedical applications: A mini review, Environ. Res. 201 (2021) 111592.

[179] A. Arabi Shamsabadi, M. Sharifian Gh, B. Anasori, M. Soroush, Antimicrobial mode-of-action of colloidal Ti_3C_2T x MXene nanosheets, ACS Sustain. Chem. Eng. 6 (12) (2018) 16586–16596.

[180] K. Rasool, R.P. Pandey, P.A. Rasheed, S. Buczek, Y. Gogotsi, K.A. Mahmoud, Water treatment and environmental remediation applications of two-dimensional metal carbides (MXenes), Mater. Today 30 (2019) 80–102.

[181] E.A. Mayerberger, R.M. Street, R.M. McDaniel, M.W. Barsoum, C.L. Schauer, Antibacterial properties of electrospun Ti 3 C 2 T z (MXene)/chitosan nanofibers, RSC Adv. 8 (62) (2018) 35386–35394.

[182] A.S. Prabha, R. Dorothy, S. Jancirani, S. Rajendran, G. Singh, S.S. Kumaran, Recent advances in the study of toxicity of polymer-based nanomaterials, Nanotoxicity (2020) 143–165.

[183] M. Bilal, I. Ihsanullah, What makes MXenes emergent materials for the adsorption of heavy metals from water? A Critical Review, J. Water Process Eng. 49 (2022) 103010.

[184] A.A. Ghani, A. Shahzad, M. Moztahida, K. Tahir, H. Jeon, B. Kim, D.S. Lee, Adsorption and electrochemical regeneration of intercalated $Ti_3C_2T_x$ MXene for the removal of ciprofloxacin from wastewater, Chem. Eng. J. 421 (2021) 127780.

[185] H. Ghassemi, W. Harlow, O. Mashtalir, M. Beidaghi, M. Lukatskaya, Y. Gogotsi, M.L. Taheri, In situ environmental transmission electron microscopy study of oxidation of two-dimensional Ti_3C_2 and formation of carbon-supported TiO_2, J. Mater. Chem. A 2 (35) (2014) 14339–14343.

[186] T. Habib, X. Zhao, S.A. Shah, Y. Chen, W. Sun, H. An, J.L. Lutkenhaus, M. Radovic, M.J. Green, Oxidation stability of $Ti_3C_2T_x$ MXene nanosheets in solvents and composite films, npj 2D Mater. Appl. 3 (1) (2019) 8.

[187] X. Zhao, A. Vashisth, E. Prehn, W. Sun, S.A. Shah, T. Habib, Y. Chen, Z. Tan, J. L. Lutkenhaus, M. Radovic, Antioxidants unlock shelf-stable Ti3C2Tx (MXene) nanosheet dispersions, Matter 1 (2) (2019) 513–526.

[188] G. Zeng, Z. He, T. Wan, T. Wang, Z. Yang, Y. Liu, Q. Lin, Y. Wang, A. Sengupta, S. Pu, A self-cleaning photocatalytic composite membrane based on g-C3N4@ MXene nanosheets for the removal of dyes and antibiotics from wastewater, Sep. Purif. Technol. 292 (2022) 121037.

[189] Z. Yang, Q. Lin, G. Zeng, S. Zhao, G. Yan, M.B.M.Y. Ang, Y.-H. Chiao, S. Pu, Ternary hetero-structured BiOBr/Bi2MoO6@ MXene composite membrane: Construction and enhanced removal of antibiotics and dyes from water, J. Membr. Sci. 669 (2023) 121329.

[190] L. Yang, X. Cao, J. Cui, Y. Wang, Z. Zhu, H. Sun, W. Liang, J. Li, A. Li, Holey Ti_3C_2 nanosheets based membranes for efficient separation and removal of microplastics from water, J. Colloid Interface Sci. 617 (2022) 673–682.

[191] K. H. J. Buschow, R. W. Cahn, M. C. Flemings, B. Ilschner, E. J. Kramer and S. Mahajan, Eds., ―Encyclopedia of Materials—Science and Technology, Vol. 1-11, Elsevier, New York, 2001.

[192] Yuan, W., Cheng, L., An, Y., Wu, H., Yao, N., Fan, X., & Guo, X. (2018). MXene nanofibers as highly active catalysts for hydrogen evolution reaction. ACS sustainable chemistry & engineering, 6(7), 8976-8982.

[193] Tsyganov, A., Shindrov, A., Vikulova, M., Zheleznov, D., Gorokhovsky, A., & Gorshkov, N. (2023). Effect of LiCl Electrolyte Concentration on Energy Storage of Supercapacitor with Multilayered Ti3C2Tx MXene Electrodes Synthesized by Hydrothermal Etching. Processes, 11(9), 2528.